M.Tech (Geoinformatics)

Badal Mohanty

2022

PREPARING COASTAL EROSION VULNERABILITY INDEX IN ODISHA APPLYING GEOSPATIAL AND MACHINE LEARNING TECHNIQUES

A DISSERTATION

SUBMITTED IN PARTIAL FULFILMENT OF THE REQUIREMENTS
FOR THE AWARD OF THE DEGREE
OF

MASTER OF TECHNOLOGY
IN

CIVIL ENGINEERING
(With Specialization in Geoinformatics Engineering)

Submitted By:

BADAL MOHANTY
(2K20/GEO/05)

Under the supervision of

DR. RAJU SARKAR, PROFESSOR

MULTIDISCIPLINARY CENTRE FOR GEOINFORMATICS
DEPARTMENT OF CIVIL ENGINEERING
DELHI TECHNOLOGICAL UNIVERSITY
(Formerly Delhi College of Engineering)
Bawana Road, Delhi – 110042

MAY 2022

PREPARING COASTAL EROSION VULNERABILITY INDEX IN ODISHA APPLYING GEOSPATIAL AND MACHINE LEARNING TECHNIQUES

A DISSERTATION

SUBMITTED IN PARTIAL FULFILMENT OF THE REQUIREMENTS
FOR THE AWARD OF THE DEGREE
OF

MASTER OF TECHNOLOGY
IN

CIVIL ENGINEERING
(With Specialization in Geoinformatics Engineering)

Submitted By:

BADAL MOHANTY
(2K20/GEO/05)

Under the supervision of

DR. RAJU SARKAR, PROFESSOR

MULTIDISCIPLINARY CENTRE FOR GEOINFORMATICS
DEPARTMENT OF CIVIL ENGINEERING
DELHI TECHNOLOGICAL UNIVERSITY
(Formerly Delhi College of Engineering)
Bawana Road, Delhi – 110042

MAY 2022

DELHI TECHNOLOGICAL UNIVERSITY

(Formerly Delhi College of Engineering)

Bawana Road, Delhi – 110042

CANDIDATE'S DECLARATION

I, **Badal Mohanty**, Roll No. 2K20/GEO/05 of M.Tech Geoinformatics, hereby declare that the project dissertation titled "**Preparing Coastal Erosion Vulnerability Index in Odisha Applying Geospatial and Machine Learning Techniques**" which is submitted by me to the Department of Civil Engineering, Delhi Technological University, Delhi in partial fulfillment of the requirement for the award of the degree of Master of Technology, is original and not copied from any source without proper citation. This work has not previously formed the basis for the award of any Degree, Diploma, Associateship, Fellowship, or other similar title or recognition.

Place: Delhi **BADAL MOHANTY**

Date:

CIVIL ENGINEERING DEPARTMENT
DELHI TECHNOLOGICAL UNIVERSITY
(Formerly Delhi College of Engineering)
Bawana Road, Delhi – 110042

CERTIFICATE

I hereby declare that the Project Dissertation titled "**Preparing Coastal Erosion Vulnerability Index in Odisha Applying Geospatial and Machine Learning Techniques**" which is submitted by **Badal Mohanty**, Roll No 2K20/GEO/05 [Civil Engineering] Delhi Technological University, Delhi in partial fulfillment of the requirement for the award of the degree of Master in Technology, is a record of the project work carried by the student under my supervision. To the best of my knowledge this work has not been submitted in part or full for any Degree or Diploma to this university or elsewhere.

Place: Delhi
Date:

PROF. RAJU SARKAR

SUPERVISOR

Department of Civil Engineering
Delhi Technological University
(Formerly Delhi College of Engineering)
Bawana Road, Delhi – 110042

ABSTRACT

With the changing climatic and anthropogenic conditions, the natural ecosystem especially the coastal zones is at great risk. The ocean is engulfing the land through the process of coastal erosion and this is becoming a great threat to coastal communities by forcing them to relocate from their homes and destroying their livelihoods. To understand the severity of the coastal erosion by keeping the usability aspect in mind, this study has considered the whole Odisha coast as the area of interest and has studied the effect of coastal erosion as a statistical analysis to evaluate the Net Shoreline Movement (NSM), End Point Rate (EPR), Linear Regression Rate (LRR) with the help of Digital Shoreline Analysis Tool (DSAS) at the blocks level for all the 22 coastal blocks of the 6 coastal districts. The area that has altered in the past has been determined to better comprehend the impact of the erosion process in the state. The future trend for the coastline position for 2030 and 2040 has been forecasted which showed the estuary positions are going to be affected most. Considering the Landsat satellite data to manually delineate the shoreline position from 1973 to 2020, the analysis showed average NSM, EPR, and LRR values of -84.95m, -1.81 m/year, and -0.36 m/year respectively with 72.47 sq. km of the eroded coastal area against 42.83 sq. km of newly formed landmass by the coastal dynamic process. Furthermore, this study has tried to use machine learning algorithms for the first time to find the probability of the vulnerability associated with this hazard along the coast of Odisha state of India using a total of 32 factors involving environmental and socio-economic conditions. A total of 2500 locations have been used to create Support Vector Machine (SVM), Random Forest (RF), Shallow Neural Network (SNN), Deep Neural Network (DNN), and Convolutional Neural Network (CNN) models. Various accuracy metrics have been calculated which showed the RF model outperformed all with an accuracy score of 0.96.

This is followed by CNN (0.93), DNN (0.91), SVM (0.88), and SNN (0.88). Further, factor importance analysis by RF has been performed at state, district, and block levels to understand the influence of various parameters in this disaster. The study showed that mitigation and preventive measures are of utmost importance for the coast. This novel method will broaden the approach which we use to analyze this calamity and serve as an aid in the decision-making process of the concerned authorities.

ACKNOWLEDGEMENTS

First and foremost, I would like to convey my heartfelt appreciation to **Prof. Raju Sarkar**, Department of Civil Engineering, for his continual advice, guidance, motivation, and encouragement during the duration of this effort. Their constant availability for advice, educational remarks, concern, and support have been essential.

I also want to thank **Dr. Sunil Saha** (Assistant Professor, University of Gour Banga) for their support and help in the work.

I would like to thank **Prof. K C Tiwari** (Professor, Delhi Technological University) and **Prof. Vijay K. Minocha** (HOD, Delhi Technological University) for their support.

BADAL MOHANTY

CONTENTS

Candidate's Declaration i

Certificate ii

Abstract iii

Acknowledgements v

Contents vii

List of Tables viiiii

List of Figures ix

List of Abbreviations x

CHAPTER 1 INTRODUCTION 1

1.1 Problem Statement 1

1.2 Literature Review 2

1.2.1 Shoreline Change Detection Techniques 2

1.2.2 Shoreline Forecast 5

1.2.3 Vulnerability due to Coastal Erosion 5

1.3 Research Gaps 11

1.4 Objectives 11

1.5 Thesis Overview 12

CHAPTER 2 STUDY AREA 13

CHAPTER 3 MATERIALS AND METHODS 17

3.1 Data Used 17

3.1.1 Satellite Images 17

3.1.2 Coastal Erosion Vulnerability Factors (CEVFs) 17

3.1.2.1 Environmental Factors 19

3.1.2.2 Socio-economic Factors 20

3.2 Methodology 31

3.2.1 Shoreline Change Analysis 32

3.2.1.1 Shoreline Extraction 32

3.2.1.2 Shoreline Change Statistics 32

3.2.1.3 Change in Area due to Coastal Dynamic Process 34

3.2.2 Shoreline Forecast 35

3.2.3 Preparation of CEM 35

3.2.4 Applied ML models for CEV mapping 37
3.2.4.1 Support Vector Machine (SVM) 37
3.2.4.2 Random Forest (RF) 37
3.2.4.3 Shallow Neural Network (SNN) 38
3.2.4.4 Deep Neural Network (DNN) 38
3.2.4.5 Convolutional Neural Network (CNN) 39
3.2.5 Accuracy Assessment of ML Models 40
3.2.6 Factor Importance Analysis 41
CHAPTER 4 RESULTS AND DISCUSSIONS 43
4.1 Shoreline Change Statistics 42
4.2 Change in Area Due to Coastal Dynamic Process 46
4.3 Shoreline Forecast 51
4.4 Accuracy Assessment of Machine Learning Models 52
4.5 Coastal Erosion Vulnerability Maps 55
4.6 Factor Importance (FI) Analysis 59
CHAPTER 5 CONCLUSIONS 66
REFERENCES 68
Appendix 1: Research Contributions 75
Appendix 2: Map Submitted to IITB-AICTE Mapathon 2022 76
Appendix 3: Photographs 77

LIST OF TABLES

Table 1.1 Details of adopted methods and considered factors in various literature 8
Table 2.1 Details of the study area 15
Table 3.1 Satellite image data used 18
Table 3.2 Importance of various factors in the analysis 21
Table 3.3 Classification of DSAS statistics 34
Table 4.1 Rate of change in area for different districts 48
Table 4.2 Change in the area at block level from 1973 to 2020 49
Table 4.3 Result of accuracy assessments 55
Table 4.4 Length (%) under different vulnerability categories of various districts by each model 58

LIST OF FIGURES

Figure 1.1 Tree map of the considered factors in the literature 10
Figure 2.1 Study Area 14
Figure 2.2 LULC map of 1985 and 2020 16
Figure 3.1 Coastal erosion vulnerability factors 27
Figure 3.2 Flowchart of the adopted methodology 31
Figure 3.3 Change in area calculation process 35
Figure 3.4 LRR at different locations 36
Figure 3.5 Diagrammatical representation of DNN model architecture 39
Figure 3.6 Diagrammatical representation of CNN model architecture 40
Figure 4.1 NSM, EPR, LRR classified values of a. Baleshwar, b. Bhadrak, c. Kendrapara, d. Jagatsinghpur, e. Puri, and f. Ganjam 45
Figure 4.2 % coastline at district level under different classes of NSM, EPR, and LRR 46
Figure 4.3 Change in area of different district from 1973 to 2020 49
Figure 4.4 a. The breakwater structures, b. the concrete sea walls, c. at the Siali beach of Ersama block 49
Figure 4.5 NSM of a. 2030 and b. 2040 51
Figure 4.6 Predicted shoreline positions for 2030 and 2040 at a. estuary of Devi River, b. the border of Kendrapara district and Jagatsinghpur district c. coastline near the Bhitarakanika national park or mangrove wetland, and d. estuary of Subarnarekha 52
Figure 4.7 ROC curves for (a) training, (b) validation, and (c) testing 53
Figure 4.8 Area under each vulnerability class by different models 55
Figure 4.9 Coastal Erosion Vulnerability maps 56
Figure 4.10 FI at the state level 59
Figure 4.11 FI at the district level 60
Figure 4.12 FI at the district level 61
Figure 4.13 Coastal erosion at (a) Siali beach of Jagatsinghpur, (b) Chandrabhaga beach of Puri, (c) and (d) Podampeta village of Ganjam [Photo credit (c) and (d): Aarthi Sridhar, Dakshin Foundation] 63

LIST OF ABBREVIATIONS

ANN	Artificial Neural Networks
AUC	Area Under The Curve
BVI	Beach Vulnerability Index
CEVF	Coastal Erosion Vulnerability Factor
CHIRPS	Climate Hazards Group Infrared Precipitation With Station Data
CNN	Convolutional Neural Network
CVI	Coastal Vulnerability Index
DEM	Digital Elevation Model
DNN	Deep Neural Network
DSAS	Digital Shoreline Analysis System
DT	Decision Tree
EPR	End Point Rate
ESRI	Environmental Systems Research Institute
ETM	Enhanced Thematic Mapper
FAO	Food And Agriculture Organization
FI	Factor Importance
FNR	False Negative Rate
FPR	False Positive Rate
FY	Financial Year
GEBCO	General Bathymetric Chart Of The Oceans
GeoTIFF	Geographic Tagged Image File Format
GP	Gaussian Process
GWA	Global Wind Atlas
LR	Linear Regression
LRR	Linear Regression Rate
LSTM	Long Short-Term Memory
LULC	Land Use And Land Cover
MCC	Matthews Correlation Coefficient
MDim-CVI	Multi-Dimensional Coastal Vulnerability Index
ML	Machine Learning
MLP	Multilayer Perceptron

MNDWI	Modified Normalized Difference Index
MSS	Multi-Spectral Scanner
NDVI	Normalize Difference Vegetation Index
NIR	Near Infrared
NNAR	Neural Network Auto-Regression
NSM	Net Shoreline Movement
OLI	Operational Land Imager
PCI	Per Capita Income
PSMSL	Permanent Service For Mean Sea Level
PVI	Physical Vulnerability Index
QGIS	Quantum Geographic Information System
RBF	Radial Basis Function
RF	Random Forest
SARIMA	Seasonal Auto-Regressive Integrated Moving Average
SNN	Shallow Neural Network
SPOT	Systeme Pour l'Observation De La Terre
SRTM	Shuttle Radar Topography Mission
SSP	Shared Socioeconomic Pathways
SVM	Support Vector Machine
SWH	Significant Wave Height
SWIR	Short-Wave Infrared
TM	Thematic Mapper
TNR	True Negative Rate
TPR	True Positive Rate
UNESCO	United Nations Educational, Scientific And Cultural Organization
WLR	Weighted Linear Regression

CHAPTER 1

INTRODUCTION

1.1 PROBLEM STATEMENT

Coastal regions have always been an essential part of human life. It is used as a major trading route across countries, as a zone to construct monumental structures, or as a recreational place. The coastal zones around the world are also a major source of income through developmental activities, sea production, port establishments, etc. It is a general trend to observe coastal areas to be more populated than other areas worldwide. On a global scale, 20% of the land can be categorized as the coastal area which is inhabited by 41% of the global population as of the year 2003. The distribution of population is not uniform but rather depends on the weather condition, availability of opportunities for economic growth, etc. Also, among the 33 megacities with a population greater than 8 million, 21 are present in and within a distance of 100 km from the seashore [1]. Along with the adverse effect of climatic changes, the increase in these numbers is creating pressure on the coastal zones and changing the coastal dynamic actions [2].

The coastal dynamic action implies the process of erosion of landmass and the deposition or accretion of the same as a cyclic process of sediment circulation. But, the global trends are suggesting the depletion of the accretion process which is causing severe erosion [2]. The coast can undergo temporary or permanent changes with the movement of sediment which is known as the short-term or long-term coastal erosion process respectively. The permanent loss of land is a concerning problem and is generally termed coastal erosion. Erosion is the result of many natural and anthropogenic causes. These natural causes can be the presence of any type of sediment or soil near the shore or being supplied to the shore through the river or runoff processes, amount of rainfall, speed of wind flow, the rise of sea level, and so forth [3]. Another salient natural factor for erosion is the melting of ice sheets that expose the soil present underneath. This is a major issue for the seas present in temperate climate zones [4]. Tropical storms and extreme events can also cause erosion [5]. Among the

anthropogenic factors are the creation of dams on the river upstream, degradation of mangrove forest resources [3], etc. The loss of mangrove forests is a trend seen worldwide and is estimated to be 35% between 1980 and 2001 [6]. Other similar factors include the construction of roads or railways near the coast or sand mining activities [7]. Climatic conditions, geological features, sediment flow, human activities, sea level, geomorphological characteristics, etc. all influence the coastal erosion process, and the fractional importance of these factors shows a spatial variation [8]. Due to these stated causes, about 28,000 sq. km of land have been eroded while the figure for gained land is 50% less than the loss i.e. 14,000 sq. km from the year 1984 to 2015 [3]. As reported by the IPCC 6th Assessment Report [9], by the year 2150 following the SSP1 pathway the sea level will rise by 0.59 ± 0.28m whereas by following the SSP5 pathway it will be 1.32 ± 0.56m. SSP stands for shared socioeconomic pathways which describe different scenarios or changes that may happen in the future. SSP1 represents the most sustainable way of development and SSP5 represents the maximum use of fossil fuels causing different climate crises [10]. With the sea-level change, the process of coastal erosion is bound to increase.

1.2 LITERATURE REVIEW

1.2.1 Shoreline Change Detection Techniques

Ghosh, et al. (2015) [11] used GIS techniques to track coastal changes on Hatiya Island, Bangladesh, from 1989 to 2010. Satellite imagery from Thematic Mapper (TM) and Enhanced Thematic Mapper (ETM) was utilized in this work to quantify the temporal variations on Hatiya Island's coastline zone over the stipulated timeframe. The modified normalized difference index (MNDWI) technique was utilized to differentiate the land–water interface in TM (1989 and 2010) and ETM (2000) pictures, and the on-screen digitizing approach was employed for coastline delineation in 1989, 2000, and 2010. Following that, the number of changes in the shoreline was calculated by superimposing Hatiya Island's digitized maps from all three years. The coastal positions were marked to deduce the erosion/accretion sectors along the coast, and the coastline changes were determined. This offshore island eroded 64.76 sq. km throughout the study years (1989–2010). In comparison, it grew by 99.16 sq. km.

El-Asmar and Hereher (2011) [12] used four aerial photographs from the multi-spectral scanner (MSS), the thematic mapper (TM), and Systeme Pour

l'Observation de la Terre (SPOT) sensors to quantify the spatiotemporal variations in the coastal zone in a portion of the Nile delta between 1973 and 2007. On-screen shoreline digitization of the 1973 (MSS) and 2007 (SPOT) photographs were undertaken, as well as a water index technique for assessing lagoon surface area change using 1973 (MSS), 1984 (TM), and 2003 (TM) images. According to the findings, approximately 50% of the coastal strip was eroding and 13% was accreting. Furthermore, a 34.5 percent decrease in the total area of the Manzala lagoon was projected. The authors ascribed these effects to anthropogenic land-use changes and the management of River Nile floods.

Mishra, et al. (2021) [13] used Landsat satellite data and the Digital Shoreline Analysis System (DSAS) tool to examine short- and long-term shoreline trends in the Ganjam district of Odisha from 1990 to 2019. They have also forecasted the expected coastline for the 2030–2040 timeframe. In this study, endpoint rate (EPR) analysis, weighted linear regression (WLR) analysis, and trigonometric functions have been used to assess and forecast the coastline from 1990 to 2019. The mean erosion, as well as accretion rates in the Ganjam coastline, were found to be -2.58 m/year and 11.63 m/year, respectively. The rate of coastal erosion was shown to be faster during cyclone years.

Digital Earth Australia Coastlines, covering three decades of shoreline evolution in Australia, was proposed by Bishop-Taylor, et al. (2021) [14]. From 1988 to 2019, they used sub-pixel shoreline extraction and a novel pixel-based tidal modeling approach to record over 2 million km of tide-datum shorelines throughout the entire Australian coast. The proposed median composite technique, which suppresses the short-term impact of tides and sub-annual shoreline fluctuation, depicts the dominating yearly location of the coastline at 0 m Above Mean Sea Level each year. Long-term coastal change rates over the previous three decades were reliably estimated and plotted at the continental scale by using a strong mid-term shoreline proxy. The authors discovered that 22% of Australia's non-rocky coastline has retreated considerably since 1988, with 16% altering at a rate greater than 0.5 m per year. Even though patterns of retreat and expansion were nearly balanced across the Australian continent, findings reveal substantial regional heterogeneity and dramatic small hotspots of coastal change.

Mondal, et al. (2020) [15] used the Digital Shoreline Analysis System (DSAS) tool on the ArcGIS platform to explore and analyze the shoreline dynamics of Sagar Island for 40 years (1975–2015). End Point Rate (EPR) and Linear Regression (LR) models were used to analyze coastline change trends and estimate future shoreline positions. It was discovered that the whole southern section of Sagar Island is prone to rapid coastline erosion. The island's entire coastline change rate was 4.94 m/year, while the uncertainty of the total shoreline change rate was 4.4 m/year.

Jana, et al. (2014) [16] showed how remote sensing, geospatial, and statistical tools may be used to monitor shoreline changes and sea-level rise along the Digha coast in eastern India. Landsat multi-resolution and multi-temporal satellite photos were used in this work to demarcate coastline locations in 1972, 1980, 1990, 2000, and 2010. Statistical approaches such as linear regression, end-point rate, and regression coefficient (R^2) were used to determine the trends of shoreline alteration and sea-level change from 1972 to 2010. From 1972 to 2006, monthly and yearly mean sea level data from three neighboring stations, Haldia, Paradip, and Gangra, were used in this study. The results of the present study show that the combined use of satellite imagery, sea level data, and statistical methods can be a reliable method in correlating shoreline changes with sea-level rise.

Mentaschi, et al. (2018) [3] conducted a worldwide assessment of coastal morphodynamics analysis of satellite measurements for 32 years (1984–2015). The variations in water level along more than 2 million virtual transects were used to assess land losses and gains. They discovered that the total surface of degraded land is approximately 28,000 sq. km, which is double the amount of acquired land. Anthropogenic factors emerge as the dominant driver of change, both as planned exploitation of coastal resources, such as the construction of coastal structures, and as unanticipated side effects of human activities, such as the construction of dams, irrigation projects, and structures that alter the flux of sediments, or the clearing of coastal habitats, such as mangrove forests. The incidence of natural disasters such as tsunamis and severe storms is another key cause.

1.2.2 Shoreline Forecast

Kupilik, et al. (2019) [17] projected Arctic coastal erosion in the Beaufort Sea in the United States using Gaussian process (GP) models. The GP regression approach was utilized, which is a data-driven modeling tool capable of identifying patterns and trends from data-poor situations such as isolated Arctic coasts. To train the model, the authors employed yearly coastal locations and near-shore summer temperature averages from existing data sets, as well as new coasts extracted from satellite images. To develop a range of realistic future erosion scenarios, the validated models were integrated with future climate models. The results demonstrate that the GP technique outperforms linear and nonlinear least-squares methods for yearly predictions and can generate comprehensive forecasts.

To predict shoreline variations from surveillance camera images along the Nha Trang Coast in South Central Vietnam, Yin, et al. (2021) [18] used a statistical forecasting model, Seasonal Auto-regressive Integrated Moving Average (SARIMA), and two Machine Learning (ML) models, Neural Network Auto-Regression (NNAR) and Long Short-Term Memory (LSTM). In terms of prediction accuracy, the SARIMA, NNAR, and LSTM models greatly exceed the Empirical Orthogonal Function (EOF) model, which is the most often used approach for forecasting shoreline changes from cameras. The long and short-term forecasting performances of the SARIMA model, NNAR model, and LSTM model are comparable. The findings indicate that these models are quite good at identifying shoreline changes from video cameras in harsh weather situations.

1.2.3 Vulnerability due to Coastal Erosion

Mujabar and Chandrasekar (2013) [19] investigated erosion risk and susceptibility along Tamil Nadu's southern coast. Different portions of the area's erosion and deposition were measured. The relative susceptibility along the research region was mapped using the coastal vulnerability index (CVI). The susceptibility was discovered to be caused by a complex blend of natural as well as human-induced processes. Geology and geomorphology, the combined action of waves and currents, fluctuations in sea level, tectonics, and storms are examples of natural processes. Human activities include the development of houses along beaches, coastal constructions such as harbors,

beach protection structures and jetties, exploitation of beach sand, and the loss of coastal dune systems.

Sahoo and Bhaskaran (2018) [20] attempted to explore the physical, ecological, social, and economic implications of tropical cyclones on coastal vulnerability along the Odisha shore. The study also looks at the future projections of coastal vulnerability in this region under changing climate conditions. The Physical Vulnerability Index (PVI) was calculated using eight fair weather characteristics, as well as storm surge height and onshore flooding. Following that, the PVI, as well as social, economic, and environmental vulnerability, were utilized to calculate the overall CVI using a GIS-based technique.

Peponi, et al. (2019) [21] created a model that estimates erosion changes along the coast of Lisbon, Portugal, using GIS and artificial neural networks (ANN). The GIS–ANN model proved to be an effective tool, analyzing and providing the "where" with "why" that had occurred or would occur in the future. The authors stated that ANNs have significant benefits over other approaches utilized for prediction and decision-making in urban coastal environments. Two kinds of ANNs with radial basis function (RBF) and multilayer perceptron (MLP) were evaluated on a GIS platform to perform a sensitivity analysis on natural and societal influences, along with dynamic relations in the research area's dune–beach structure.

Islam, et al. (2016) [22] sought to create a coastal vulnerability index (CVI) for the Ganges deltaic coast using seven physical characteristics. The factors were regarded as relative risk characteristics and were combined using geospatial approaches before being ranked to assess the degree of shoreline vulnerability to sea-level rise. The whole coastline is assessed in terms of multi-hazard vulnerability, and the results show that 20.1 percent of the shoreline was extremely highly susceptible, whereas 21.2 percent of the total shorelines were classified as low vulnerability.

Alexandrakis and Poulos (2014) [23] introduced the Beach Vulnerability Index (BVI), a novel indicator that combines mathematical simplicity, freely accessible data, and minimal processing capacity. This method yields findings not just for various beaches, but also for different areas of the same beach, allowing the relative importance of the processes involved to be determined. It works by numerically approximating indicators linked to the processes that drive beach development, such as silt availability,

wave climate, beach morphodynamics, and sea-level rise. The BVI is also meant to be used as a management tool for beach sustainability, including resilience to the effects of climate change on coastal erosion.

Rangel-Buitrago, et al. (2020) [24] assessed 32.6 km of Cartagena city's waterfront of Colombia for coastal erosion management, producing the Hazard and Vulnerability Indexes, which combined comprised the Coastal Erosion Risk Index and gave a single numerical estimate of risk. The computations made use of a variety of variables. The authors stated that coastal forcing, as well as susceptibility, were the foundation for determining the Hazard, with induced susceptibility resulting primarily from 60 years of over-reliance on shore-hardening structures, interruption/reduction of sediment supply, and over-development in terms of urbanization. Furthermore, the authors acknowledged that the buffer zone between the coastline and development should be expanded with no new construction or planned retreat, building rules should be modified, and further shore-hardening must be avoided.

Murali, et al. (2018) [25] analyzed the coastal risk of a portion of the Odisha coast, comprising the districts of Kendrapara and Jagatsinghpur, on a finer scale. AHP was utilized to infer vulnerability from a collection of physical–geological elements and socioeconomic variables, and vulnerability maps were created to demarcate regions with varying levels of risk. For the final coastal vulnerability map, the Coastal Vulnerability Index (CVI) was eventually divided into three vulnerability groups. According to this categorization, approximately 35% of the coastline was classified as high vulnerability and 26% as low vulnerability.

Table 1.1 shows the factors taken and the method followed by some of the existing literature on coastal vulnerability assessment. Fig. 1.1 shows the treemap of the factors taken in previous research. Sea level change, tidal range, coastal slope, wave height, geomorphology, shoreline change, population, and LULC are some of the most used factors in the research.

Table 1.1 Details of adopted methods and considered factors in various literature

Sl No	Author	Method followed	Factors Taken
1	[19]	CVI	geomorphology, shoreline change rate, coastal slope, relative sea-level change, mean wave height, mean tide range
2	[23]	BVI	width of beach profile, beach slope, subaerial profile width, maximum beach profile elevation, drainage basin maximum elevation, river catchment area, river run-off, grain fall velocity, breaking zone grain size, subaerial beach grain size, wind speed, wind direction, mean air temperature, temperature range, wave breaking height, wave breaking angle, significant wave height, wavelength, wave period, sea-level rise, closure depth, mean sea level
3	[22]	CVI	geomorphology, coastal slope, shoreline change rate, rate of sea-level change, mean tide range, bathymetry, storm surge height
4	[20]	CVI	coastal slope, relative sea-level change, shoreline change, mean tidal range, mean sig. wave height, geomorphology, rainfall, storm surge, inundation, cyclone intensity
5	[25]	AHP	coastal slope, geomorphology, elevation, shoreline change, sea-level change, significant wave height, tidal range, population, land-use/land-cover, road network, tourist places
6	[26]	CVI	rate of sea-level rise, mean tidal range, significant wave height, shoreline change rate, geomorphology, regional coastal slope, land use and coverage, population, coastal settlements, and economic activities,
7	[21]	Machine learning	resident population, land cover, no of households, area of erosion, area of vegetated and non-vegetated lands

Table 1.1 (Continued)

Sl No	Author	Method followed	Factors Taken
8	[27]	AHP	Population, Infrastructure, Heritage importance, Coastal elevation, Shoreline change, Proximity to sea, Tidal range, Sea level rise
9	[24]	Risk assessment	wave height, storm surge, littoral exposure, tidal range, dune height, percent wash overs, beach width, beach slope, rock types, Lithology, Weathering, land use, percent urbanized area, population density, road, Conservation designation, Number of infrastructure services, Tourism, Economic activities
10	[28]	CVI	shoreline change, altitude, slope, geomorphology, coastal bathymetry, sea-level rise, wave height, mean tidal range, LULC, population density, tourist density, fisher folk density
11	[29]	CVI	Geomorphology, Coastal slope, Shoreline change, Land use/Land cover, Tidal data, Wave height data
12	[30]	Multi-dimensional Coastal Vulnerability Index (MDim-CVI)	Extreme sea level, Digital elevation model, Artificial Protection, coastline, Administrative boundaries, Geomorphology, Shoreline evolution trend, Land use/land cover, Protected areas, GDP, Population projections, Population < 5 years, Population > 65 years

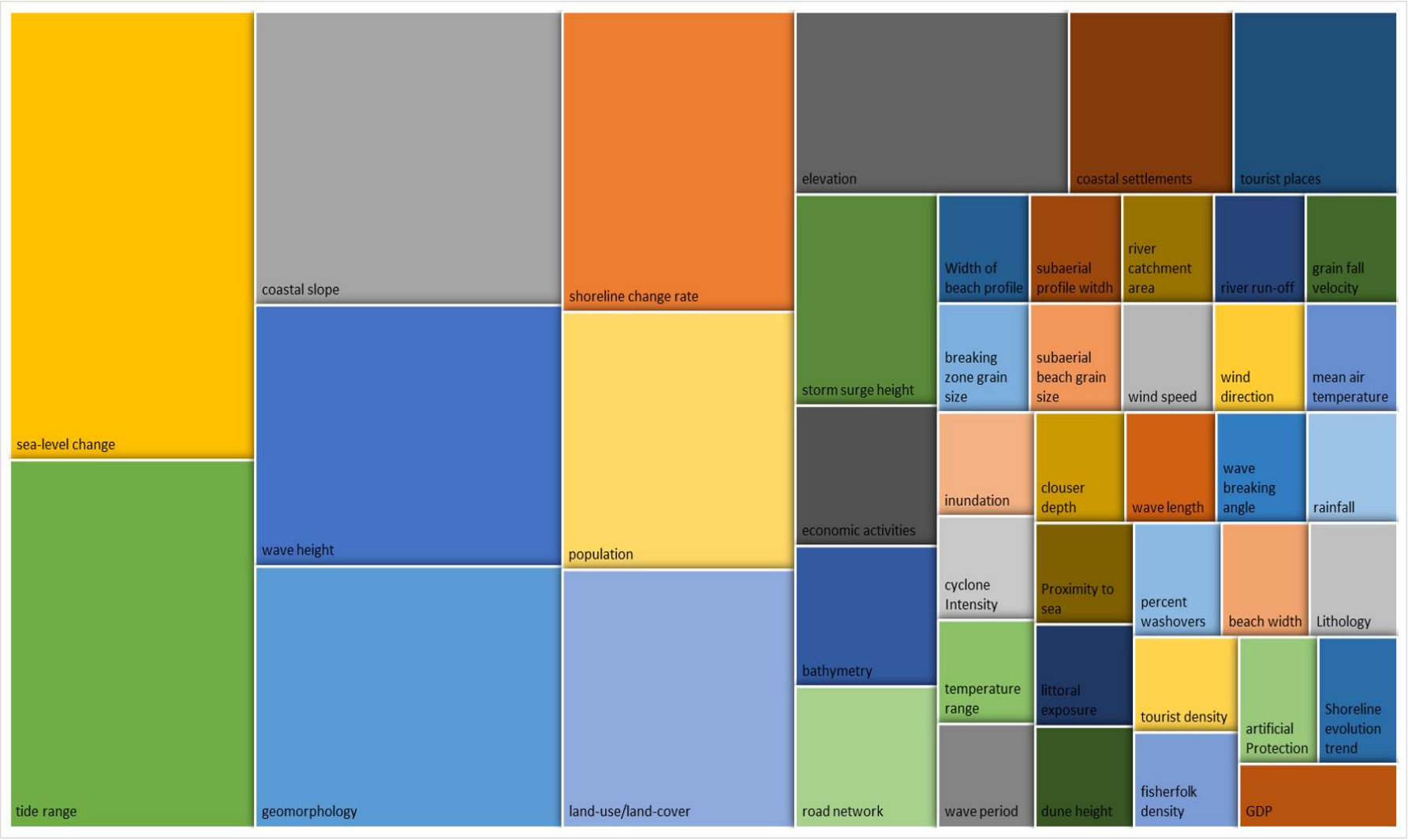

Figure 1.1 Tree map of the considered factors in the literature

1.3 RESEARCH GAPS

The reviewed studies mainly focus on a relatively smaller part of the coastal length and generally don't cover any state entirely [31] [32]. Also, these study usually focuses on the district as the smallest individual unit [33] while neglecting the variation in the dynamic effect at even smaller administrative units. This is especially the case for the state of Odisha which is the study area of this research work where the preventive and protective measures taken against the horrific effect of this dynamic action by sea are minimal as compared to its magnitude. Many studies have been conducted to address this issue but failed at its usability as they have concentrated on a small region for their investigation and have rarely considered areas below the district level to make their analysis.

The machine learning approach to map the relationship among the independent and dependent variables makes no assumption and can be adjusted to fit the data. Though the applications of machine learning or ML are present in numerous non-computer science domains including studying the effect of other types of natural disasters, the same to address the issue of coastal erosion is not widely evident in the available literature. Goldstein et al. (2019) [34] have pointed out the scarcity of research work using various ML algorithms in a coastal erosion assessment setting. ML can be used to predict erosion by using its classified dependent variables [21].

1.4 OBJECTIVES

Considering the research gaps, this work has been based on the following objectives.

Objective 1. Shoreline change analysis considering the entire coast of Odisha state of India.

Objective 2. The projection or forecasting of the coastline for the next 20 years for the coastline of Odisha.

Objective 3. Finding the coastal erosion vulnerability probability using various widely-known ML algorithms for the coast of Odisha.

Objective 4. Conducting a factor importance (FI) analysis to understand the influence of various factors in the coastal erosion process.

1.5 THESIS OVERVIEW

This manuscript provides an introduction of the subject field in chapter 2, then goes on to detail the resources used and the methods followed in chapter 3, and the obtained results with commentary in chapter 4. Finally, in Chapter 5, there are concluding notes on the study's effort as well as its findings.

CHAPTER 2

STUDY AREA

The taken study area in this research is the coastal region of Odisha (Fig. 2.1). Situated at the coast of the Bay of Bengal, Odisha is the Eastern state of India with 588 km of coastline with a share of 11% in the water resource at the country level. As of 2012, around 36% of the rural population of the state lived below the poverty line. The agricultural sector is the backbone of the state as the livelihood of 60% of the population is dependent on the same. In the year 2019-20, 51.33% of the cultivable land of the state was used to produce cereals and a crop loan of INR 20,432.69 Cores had been given to the farmers. In the 2019-20 financial year (FY), the Per Capita Income (PCI) of the state is registered to be INR 1.045 Lakhs. In the same FY, INR 109.64 Cores have been generated by the 3 major ports of the state which are situated at Paradeep, Dhamra, and Gopalpur. Notably, the state is the source of 96% of Chromite, 92% of Nickel, and 51% of Bauxite of the country. It is also the largest Steel and Aluminium producer. Different natural calamities are recurrent in the state. Specifically, the South and West Odisha fall under drought-prone regions whereas the coastal Odisha is vulnerable to cyclones and floods (Odisha Economic Survey, 2020-21).

Spanning from 87.48 E – 21.61 N to 84.76 E – 19.08 N, the 588 km long coastline of the state is shared among the 22 coastal blocks of the 6 districts of Odisha namely, Baleshwar, Bhadrak, Kendrapara, Jagatsinghpur, Puri, and Ganjam (table 2.1). At the block level, a total of 22 blocks with an area of 8189 sq. km of these six districts are home to 3.61 million people. This population translates to a density of 441 people in sq. km of land in the study area which is 64% higher than the population density of 270 for the state (the 2011 census report). The population density of coastal areas is high whereas these areas have comparably low forest cover. The coastal blocks show the highest surface elevation of 716 m and agricultural land is the dominant land-use class. The principal soil type in the area is Eutric Nitosols with the prevalence of clay-loamy soil texture. The cumulative rainfall over the area is recorded to be 1,551 mm for the year 2020.

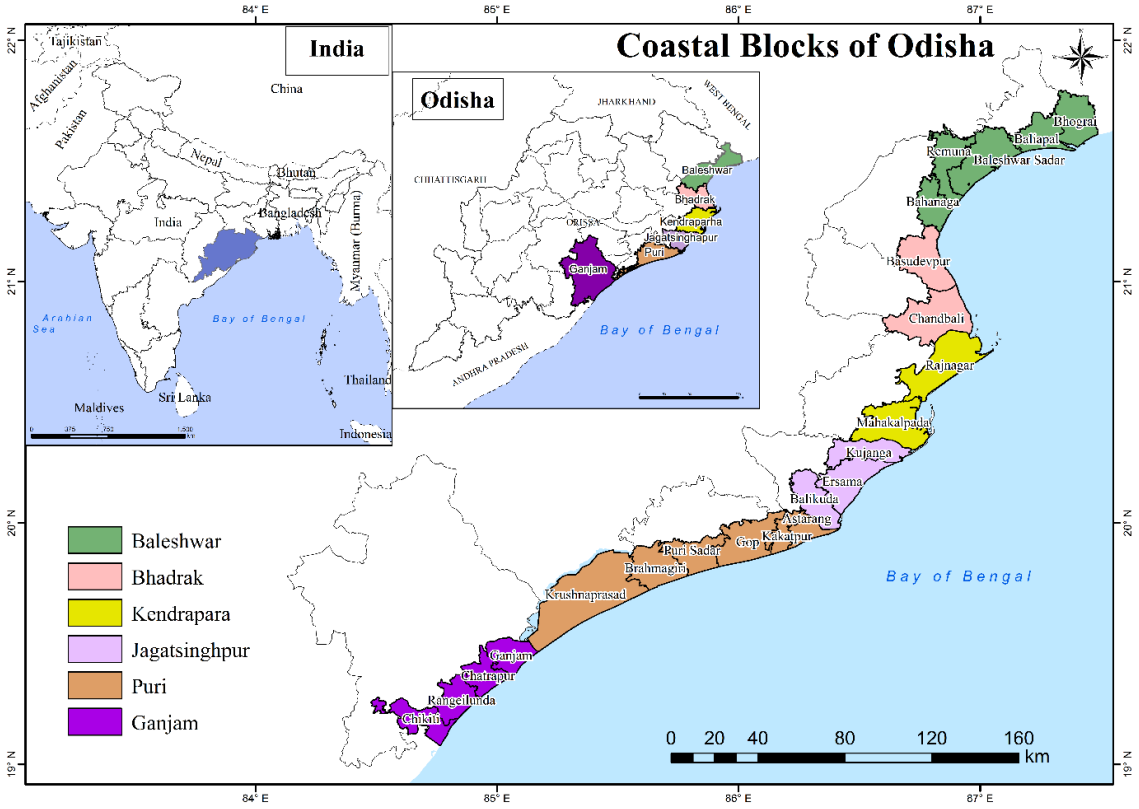

Figure 2.1 Study Area

Rajanagar block of Kendrapara district has the longest coast, Krushnaprasad block of Puri district has the maximum land area, and Chandbali block of Kendrapara district has the maximum population. The details about the coastal length, area, and population have been presented in table 2.1. There are three ports in the state which are all in the study area. One port is managed by the national government at Paradeep of Jagatsinghpur district, the other two at Gopalpur of Ganjam district and Dhamra of Bhadrak district are under state government jurisdiction. Six major rivers form estuaries in the coastal districts namely, Budhabalanga and Subarnarekha River at Baleswar, Brahmani and Baitarani Rivers at Bhadrak, Mahanadi River at Jagatsinghpur, and the Rushikulya River at Ganjam. The Chilika Lake which is the largest brackish lake in Asia is also present in the Puri district. Further, all the district of the study area comes under the cyclone-prone region [35]. Fig. 2.2 shows the LULC map of 1985 and 2020 of the study area.

Table 2.1 Details of the study area

Sl No.	Block	Coast length (km)	Area (sq. km)	Population (2011 census)
		Baleshwar district		
1	Baleshwar Sadar	44.17	471.95	247047
2	Baliapal	35.82	275.40	197259
3	Bhograi	21.80	332.37	283586
4	Remuna	68.06	315.49	180044
5	Bahanaga	17.38	250.51	138369
		Bhadrak district		
6	Basudevpur	36.89	427.28	219108
7	Chandbali	28.41	586.52	250037
		Kendrapara district		
8	Rajnagar	69.83	559.45	170110
9	Mahakalpada	60.95	480.53	212463
		Jagatsinghpur district		
10	Balikuda	8.27	313.68	165275
11	Ersama	35.25	406.91	146273
12	Kujanga	17.95	304	176065
		Puri district		
13	Kakatpur	7.67	163	107406
14	Astarang	24.57	147.93	82176
15	Brahmagiri	17.87	348.54	139449
16	Gop	23.83	425.08	165952
17	Krushnaprasad	56.06	1062.27	89371
18	Puri Sadar	14.36	289.59	150800
		Ganjam district		
19	Chikiti	14.75	295.43	104572
20	Chatrapur	17.16	223.02	135751
21	Rangeilunda	13.16	266.33	161372
22	Ganjam	16.80	243.98	89170

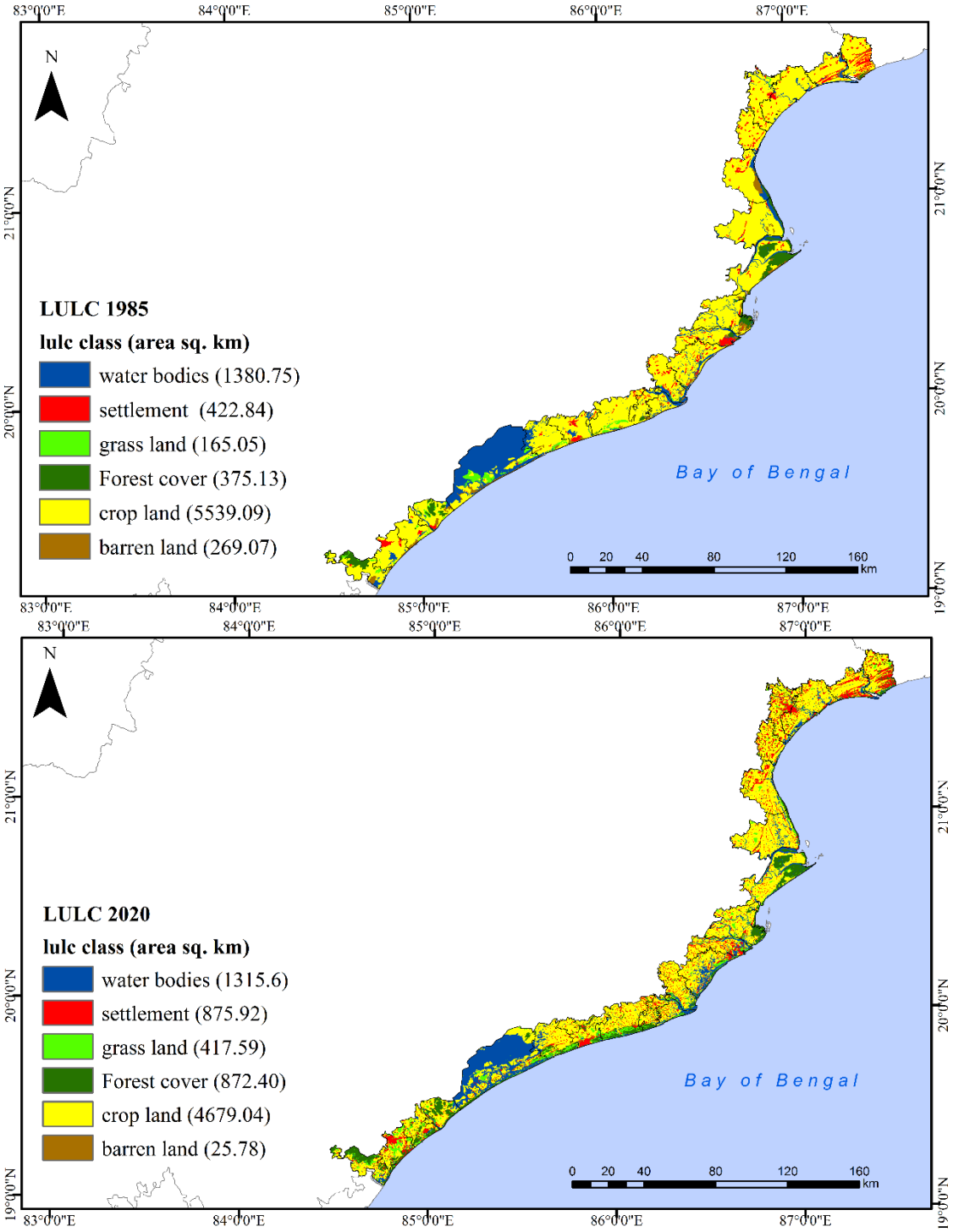

Figure 2.2 LULC map of 1985 and 2020

CHAPTER 3

MATERIALS AND METHODS

3.1 DATA USED

3.1.1 Satellite Images

To detect the shoreline position for the analysis the Landsat series images have been used (Table 3.1). Since the lunch of the Landsat 1 satellite in 1972, the Landsat satellite program is providing continuous temporal coverage of the earth. The Landsat images have been used in studies related to aquatic science, surface water mapping, vegetation phenology, surface temperature, agriculture, forest monitoring, etc. [36]. Previous studies also prove the efficacy of Landsat satellite images with spatial resolution up to 30m to be suitable for the coastal erosion analysis [33] [32]. Images corresponding to different paths/ rows covering the entire study area from the year 1973 to 2020 have been taken keeping the gap of 5 years. This gap could not be maintained in the earlier years due to the absence of cloud-free images. Images of post-monsoon and pre-monsoon periods have been considered for the analysis.

3.1.2 Coastal Erosion Vulnerability Factors (CEVFs)

Total 32 CEVFs (Fig. 3.1) have been taken considering their impact on the coastal erosion process based on the literature survey and field experience. Among these, 21 are related to environmental factors such as land surface elevation, slope, sea surface elevation, sea-level change, significant wave height, wave direction, wave period, tidal range, wind speed, geology, pH, bulk density, and organic carbon content of the soil, clay, sand, and silt percentage of soil, rainfall, geomorphology, land use/ land cover (LULC), NDVI, distance from stream features. In the creation of the data layers for the factors related to different characteristics of the sea, a distance of 30 km from the shoreline has been considered. Other 11 are for socio-economic factors such as distance from the road, population density, settlement density, literacy rate, percentage of agricultural workers, availability of electricity, Drinking water facility, and hospital, agricultural land density, and LULC changed to settlement and agricultural land. All the

layers have been prepared at 30m spatial resolution with resampling or interpolation for homogeneity in analysis with the help of Google Earth Engine and ArcMap. The details about all the factors, with their significance and spatial and temporal coverage have been mentioned in table 3.2.

Table 3.1 Satellite image data used

Year	Date	Path/ row	Satellite/ sensor	Spatial resolution
1973	17th Jan	149/ 46	Landsat 1 MSS	60m
	18th Jan	150/ 46		
1977	5th Jan	149/ 45	Landsat 2 MSS	
		149/ 46		
	6th Jan	150/ 46		
		150/ 47		
1991	30th Apr	139/ 45	Landsat 5 TM	30m
	20th Mar	140/ 46		
		140/ 47		
1995	29th Mar	139/ 46		
	19th Jan	139/ 45		
		139/ 46		
	26th Jan	140/ 46		
		140/ 47		
2000	10th Dec	139/ 45	Landsat 7 ETM+	
		139/ 46		
	17th Dec	140/ 46		
		140/ 47		
2005	15th Feb	139/ 45	Landsat 5 TM	
		139/ 46		
	22nd Feb	140/ 46		
		140/ 47		
2010	28th Jan	139/ 46		
	4th Feb	140/ 46		
		140/ 47		
2015	13th Feb	139/ 45	Landsat 8 OLI	
	10th Jan	139/ 45		
		139/ 46		
	17th Jan	140/ 46		
		140/ 47		
2020	3rd Mar	140/ 46		
		140/ 47		
	28th Mar	139/ 45		
		139/ 46		

3.1.2.1 Environmental Factors

Elevation is one of the prime factors in the process of beach erosion. A low elevation can facilitate a smother propagation of waves which will create significant erosion whereas high elevated coastal areas can act as barriers in reducing the impact of the wave forces on the beach [26]. For the analysis, SRTM DEM and the General Bathymetric Chart of the Oceans (GEBCO) grids have been used for land and sea surface elevation data layers respectively. The area shows a maximum surface height of 716 m and a sea bed depth of 541 m. Data related to dynamic and long term changes of the sea are important for coastal erosion [23]. PSMSL tide gauge data [37, 38] for Haldia, Paradeep, and Vishakhapatnam stations considering the average yearly change from 1970 to 2013 have been interpolated spatially to generate the sea level change rate in mm/ year. In the area, the sea-level change varies from a positive change rate of 6.16 mm/ year to a negative change of 1.35 mm/ year. Similar interpolation methods have been employed to derive the tidal range data from point data of Sagar Island, Shortt Island, Chandbali, Gopalpur, and Vishakhapatnam. The average tidal range in the metre at all the stations was calculated from the daily tidal range data (equation 3.1 [27]) of 2020.

$$\text{Daily tidal range} = \text{Daily maximum tide height} - \text{Daily minimum tide height} \quad (3.1)$$

The average of the biggest one-third of waves that occur within a specified timeframe is defined as significant wave height or SWH [39]. The average SWH, wave direction, and wave period data layers have been derived for 2019 from the Copernicus marine service global reanalysis gridded data. The registered SWH in the area reached up to a value of 1.43 m. The directions of the waves are observed to be in the North-West and West directions with wave period ranging from 7.45 10.91 sec. The wind speed over the area at 10m height have been taken from the Global wind atlas (GWA 3.0) for the analysis. Considering the surface and the sea, the speed of the wind ranges from 0.59 to 6.9 m/ sec. A total of 7 parameters related to soil have been considered in the analysis. The FAO/UNESCO Soil Map has been considered to get the geological properties of the soil. The soil shows higher quantities of Eutric Fluvisols and Dystric Regosols. The pH, bulk density, organic carbon content, percentage of clay, sand, and silt have been derived from the Open Land Map [40]. The pH values were found to be in the slightly acidic (4.4) to neutral (8.19) range. The bulk density of the soil differs in

the range of 581.67 to 1725.05 kg/ cubic m whereas the maximum organic carbon content of the soil is 18%. The clay, sand, and silt percentage of soil in the area vary up to 50-60. Along with the above-stated factors, rainfall can also act as a catalyst for erosion at the beach. The amount of rainfall in an area can make the water level rise temporarily near the shore which can cause erosion [41]. The average rainfall data for 2020 over the area varied from 3.13 to 5.61 mm as derived from the daily values of the same considering the CHIRPS Precipitation Data. The geomorphology layer for the area has been collected from the Geological Survey of India's Bhukosh data repository. The LULC map for the area was extracted from the ESRI Global Land Cover Map of 2020 Sentinel-2 images. The land use was reclassified into 6 classes, those are water bodies, forest cover, grassland, cropland, settlement, and barren land. The NDVI data layer was derived from the Near Infrared (NIR) and red wavelength bands of the Landsat OLI 2020 image. The range of NDVI was observed to be between -0.55 to 0.79. The Euclidean distance method was used to find the distance of each point from the stream network which was previously derived from DEM data.

3.1.2.2 Socio-economic Factors

The road network was collected from the Bhukosh data repository and processed to prepare the distance from the road data layer using the Euclidean distance method. The village-level 2001 census geospatial data have been taken in the preparation of various socio-economic factors. Factors such as population density, literacy rate, availability of electrical facility, hospital, and drinking water can show the development of the region and have been derived from the same. The population density of the area showed the maximum value of 25113 persons in a sq. km of land and the area showed village level literacy rate mostly in the range of 50 to 76%. As of 2001, most of the villages did not have a hospital but had a drinking water facility. The Agricultural land density or percentage of area per village used as agricultural land according to the 2020 LULC map that is found to be varying in the range of 32 to 86% and the percentage of agricultural workers have also been considered as inputs. Taking the settlement of 2020 LULC map the settlement density have been accounted and it varied largely in the range of 0 and 30%. The change in LULC type to settlement and agricultural land have been calculated between the year 1985 and 2020 for the analysis. The decadal LULC map of 1985 and 2020 have been used for this purpose.

Table 3.2 Importance of various factors in the analysis

Sl No	Data	Significance	Reference	Format, unit, spatial, and temporal coverage	Source
1	Sea level elevation	The nearshore sea level elevation has a significant role in the erosion process. The height of storm surge which in turn erode the beach is greatly affected by the sea level elevation	[42]	GeoTIFF, meter, 30m, NA	GEBCO bathymetry tif data
2	Land surface elevation	Elevation of the land surface controls the rate at which the erosion process occurs. High elevation region exhibits lower erosion probability than areas with low elevation.	[26] [19]	GeoTIFF, meter, 30m, NA	SRTM DEM Version 3
3	Slope	Beach with a high degree of steep slope react differently to the coastal erosion process than that with a moderate slope as the area affected by wave action will be more in later.	[29]	GeoTIFF, meter, 30m, NA	SRTM DEM Version 3
4	Sea level change	The vulnerability due to erosion would be high with the rise in sea level. The study suggests that the length of erosion will be 1 m with a 1 mm rise in sea level.	[19]	GeoTIFF, millimetre/ year, 30m, 1970 to 2013	Permanent Service for Mean Sea Level (PSMSL) data
5	Significant wave height	The dynamic effect of waves can change the beach profile. The wave with a comparatively larger height is associated with high energy which creates more erosion.	[29]	GeoTIFF, meter, 30m, 2019	Copernicus marine service
6	Wave direction	Wave direction controls the impact of the waves on the beach. Waves with high energy if get propagated in a certain direction create damage, especially near the estuaries.	[43]	GeoTIFF, degree, 30m, 2019	Copernicus marine service

Table 3.2 (Continued)

Sl No	Data	Significance	Reference	Format, unit, spatial, and temporal coverage	Source
7	Wave period	Waves with a longer duration or period can do more erosion as the sediment eroded will be more.	[44]	GeoTIFF, Sec, 30m, 2019	Copernicus marine service
8	Tidal range	The tidal range is associated with the tidal current. A high tidal range with a high value of tidal current can create more erosion than a low tidal range.	[29]	GeoTIFF, meter, 30m, 2019	WXTide32 program
9	Wind speed	Wind act as a catalyst in fuelling the energy associated with the tide, wave, or storm surge. Wind stress is also responsible for the creation of depression fields or cyclones.	[45]	GeoTIFF, Meter/sec, 30m, Reanalysis product	Global Wind Atlas
10	Geology	The geological characteristics of the beach control sediment transport. The erosion tends to be less in the presence of more resistive materials like rock	[46]	GeoTIFF, NA, 30m, NA	FAO/UNESCO Soil Map
11	pH of soil	The spatial variation of soil pH causes the change in the physical properties of soil. Higher pH can cause the soil particle size to increase which may create favorable conditions for erosion.	[47]	GeoTIFF, NA, 30m, NA	Open Land Map
12	Bulk density of soil	The bulk density of soil which shows the soil compaction level generally has an inverse relationship with erosion. In other words, the erosion rate decrease with an increase in the value of bulk density.	[48]	GeoTIFF, kg/cubic meter, 30m, NA	Open Land Map

Table 3.2 (Continued)

Sl No	Data	Significance	Reference	Format, unit, spatial, and temporal coverage	Source
13	Organic carbon content of the soil	High organic carbon content in soil can decrease the erosion probability by increasing its resistivity against disintegration caused by external forces.	[49]	GeoTIFF, percentage, 30m, NA	Open Land Map
14	Clay percentage of soil	The adhesion property in clayey soil showed a higher value which greatly influence the erosion possibility negatively.	[50]	GeoTIFF, percentage, 30m, NA	Open Land Map
15	Sand percentage of soil	The presence of sand-like coarser soil particles creates a void in the soil which make the soil loose. The loose soil has a high percolation capacity and shows less resistance against erosion.	[51]	GeoTIFF, percentage, 30m, NA	Open Land Map
16	Silt percentage of soil	Silty soil has particle sizes larger than clayey soil and smaller than sandy soil. The erosion likelihood of these types of soil also falls in-between the other two soil types.	[51]	GeoTIFF, percentage, 30m, NA	Open Land Map
17	Rainfall	Rainfall in a coastal area can cause an increase in sediment transport. It also increases the chance of loss of dune or failure of the cliff.	[52] [53]	GeoTIFF, millimeter/ year, 30m, 2020	CHIRPS Precipitation Data
18	Geomorphology	Geomorphology which defined the type of landmass present in an area has important consideration as the type of land affects the resistivity of that area against the process of coastal erosion.	[29]	GeoTIFF, NA, 30m, NA	Bhukosh data repository

Table 3.2 (Continued)

Sl No	Data	Significance	Reference	Format, unit, spatial, and temporal coverage	Source
19	LULC	The land use pattern or the land cover present in an area affect the erosion as different LULC type are affected differently by the process.	[54]	GeoTIFF, NA, 30m, 2020	ESRI Global Land Cover Map
20	NDVI	The presence of vegetation cover on the coast provides support against the wave action as well as storm surges. The root system of live vegetation also holds the soil in place.	[55]	GeoTIFF, NA, 30m, 2020	Landsat OLI images
21	Distance from stream	Streams transport sediments to the coast from inland. The cyclic deposition of sediment affects the erosion process. The area near estuaries shows more may show accretion than other areas along the coast.	[56]	GeoTIFF, kilometre, 30m, NA	SRTM DEM Version 3
22	Distance from road	Road networks near the coast generally receive more traffic as it is a place for tourist attractions. Also, the landmasses present in between the road and the sea coast generally get affected by anthropogenic activities as they serve as major recreational places.	[54] [57]	GeoTIFF, kilometer, 30m, NA	Bhukosh data repository
23	Population density	The population of a particular area can create strain on the coastal zone and act as a catalyst in the erosion process.	[58]	GeoTIFF, people/ square kilometre, 30m, NA	2001 census geospatial data
24	Settlement density	The settlement and its associated built-area can disrupt the geomorphology of the coastal zone and increase the chance of coastal flooding due to high runoff. It also acts as sediment	[59]	GeoTIFF, percentage, 30m, 2020	ESRI Global Land Cover Map

Table 3.2 (Continued)

Sl No	Data	Significance	Reference	Format, unit, spatial, and temporal coverage	Source
25	Literacy rate	The higher literacy rate in an area suggests the presence of awareness about the adverse effect of coastal erosion. This can help in creating an aware coastal community and lessen the human impact of the coastal zone	[54]	GeoTIFF, percentage, 30m, 2001	2001 census geospatial data
26	Percentage agricultural worker	Farmers solely depend on the fertility of the soil. In a coastal environmental setting, the severity of coastal erosion is a constant threat to agricultural land which in turn affects the agricultural workers.	[60]	GeoTIFF, percentage, 30m, 2001	2001 census geospatial data
27	Availability of electricity	The availability of electricity shows the development condition of any society. Comparatively, a developed society would show more resistance to coastal erosion than a less developed society.	[61] [62]	GeoTIFF, percentage, 30m, 2001	2001 census geospatial data
28	Availability of drinking water facility	Drinking water availability is a basic need and a socio-economic development indicator. It also shows the preparedness of a coastal community against flooding as the people with limited access to proper drinking water suffer more.	[61] [63]	GeoTIFF, percentage, 30m, 2001	2001 census geospatial data
29	Availability of hospital	The availability of hospitals at community level is important for the maintenance of social fairness. Its need becomes paramount in the coastal areas during storm surge or cyclone as the effect of these disasters along with coastal erosion can make the rural population of the area vulnerable.	[61] [63]	GeoTIFF, NA, 30m, 2001	2001 census geospatial data

Table 3.2 (Continued)

Sl No	Data	Significance	Reference	Format, unit, spatial, and temporal coverage	Source
30	Agricultural land density	The presence of agricultural land in excess quantity in an area can cause land degradation over some time. In a coastal ecosystem, agricultural practices can make the soil loose and disrupt the sediment supply to the coast.	[64]	GeoTIFF, percentage, 30m, 2020	ESRI Global Land Cover Map
31	LULC Changed to Settlement	The change in the LULC pattern to the built-up area increases the impervious land and disrupts the ecological and geomorphological process of the coastal ecosystem. The stress on the ecosystem increases the probability of erosion or coastal changes.	[65]	GeoTIFF, NA, 30m, 1985 to 2020	Decadal LULC map (1985) and ESRI LULC Map (2020)
32	LULC Changed to Agriculture	With the increase in food demand, the agricultural land area is increasing. Intensive tillage along with unsustainable agricultural practices intensify the erosion process.	[64]	GeoTIFF, NA, 30m, 1985 to 2020	Decadal LULC map (1985) and ESRI LULC Map (2020)

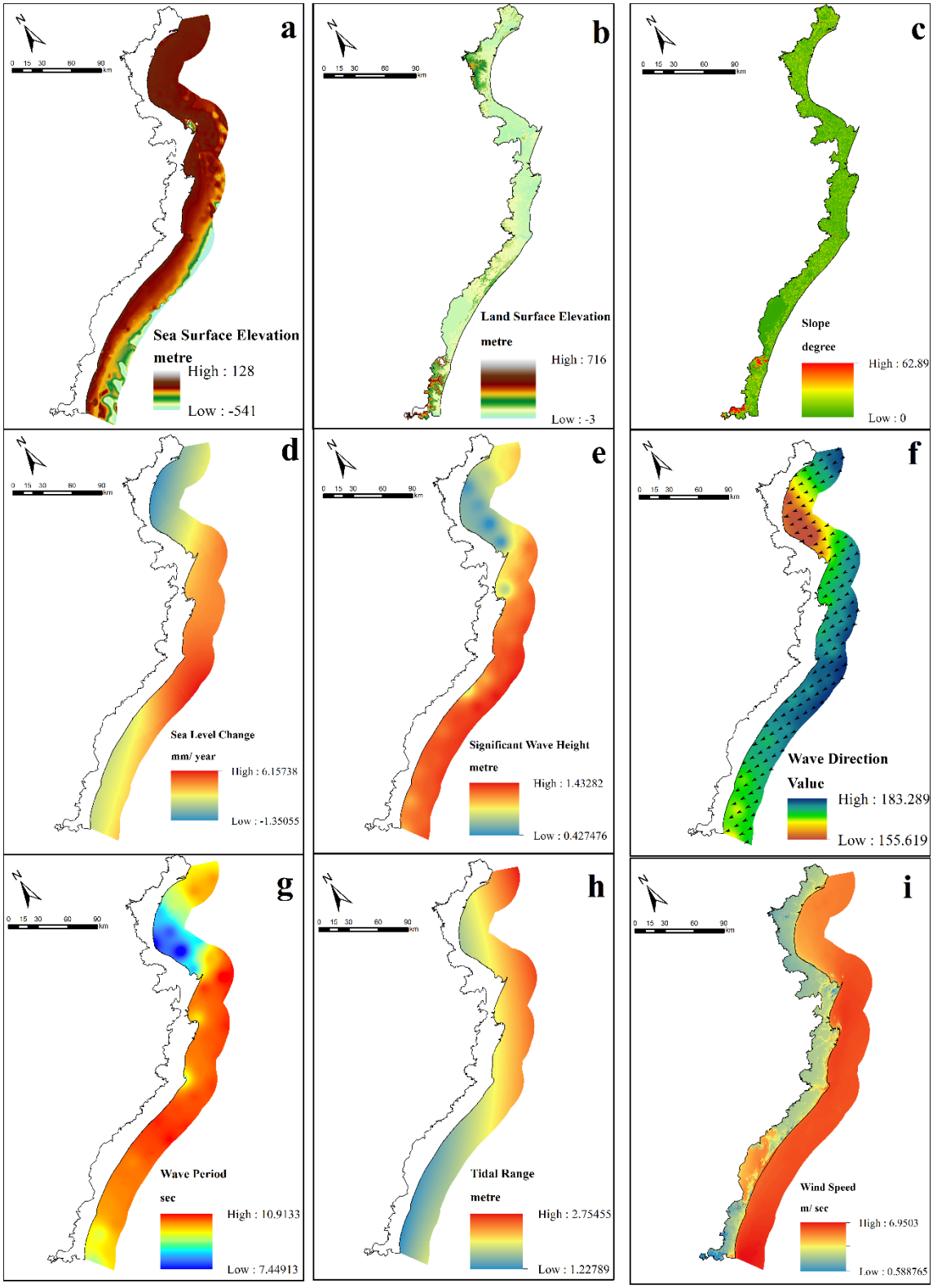

Figure. 3.1 Coastal erosion vulnerability factors: (a) Land surface elevation, (b) sea surface elevation, (c) slope, (d) Sea level change, (e) Significant wave height, (f) wave direction, (g) wave period, (h) tidal range, and (i) wind speed.

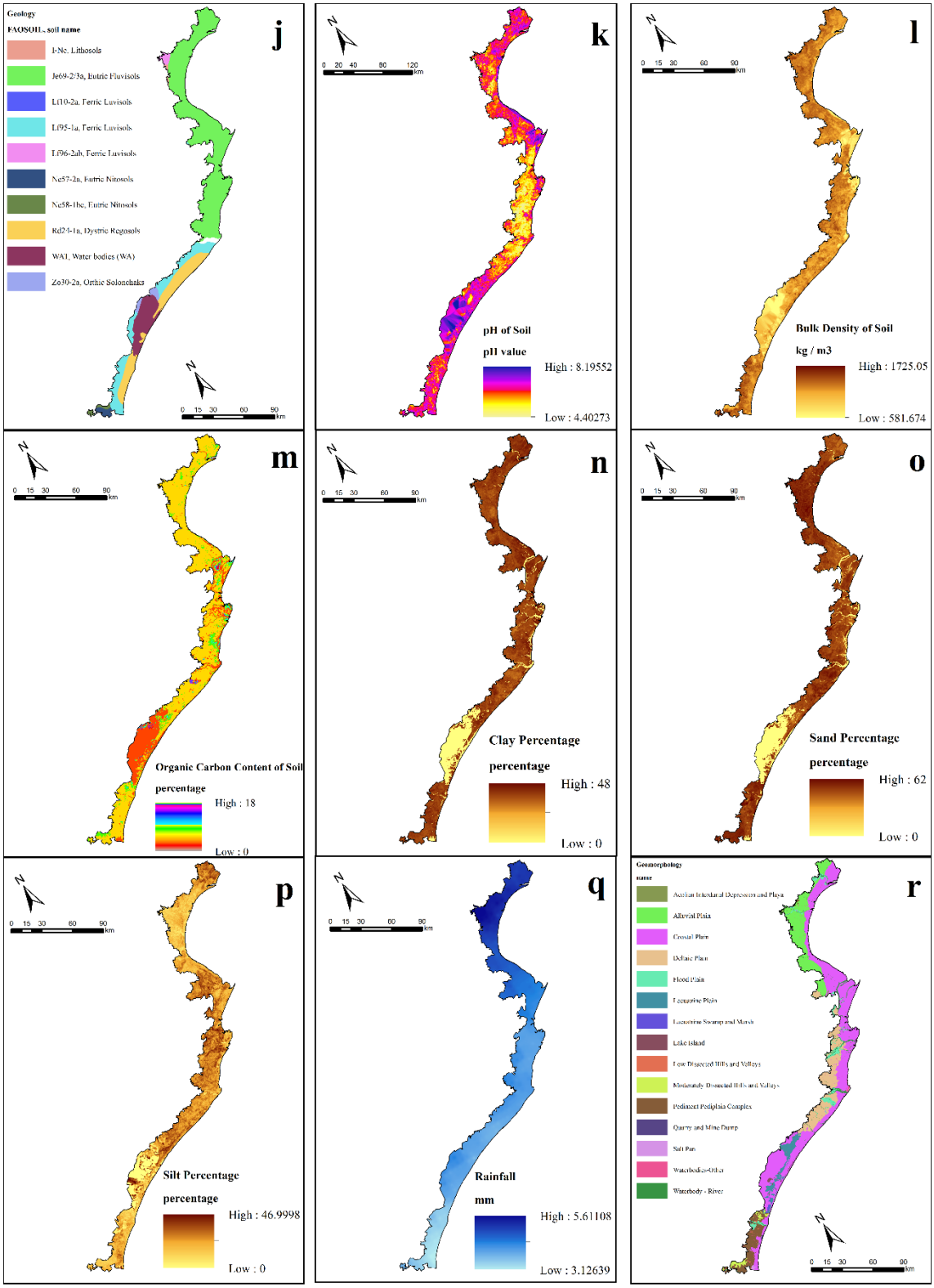

Figure. 3.1 (Continued) (j) geology, (k) pH of the soil, (l) bulk density of soil, (m) organic carbon content of soil, (n) clay percentage, (o) sand percentage, (p) silt percentage, (q) rainfall, and (r) geomorphology.

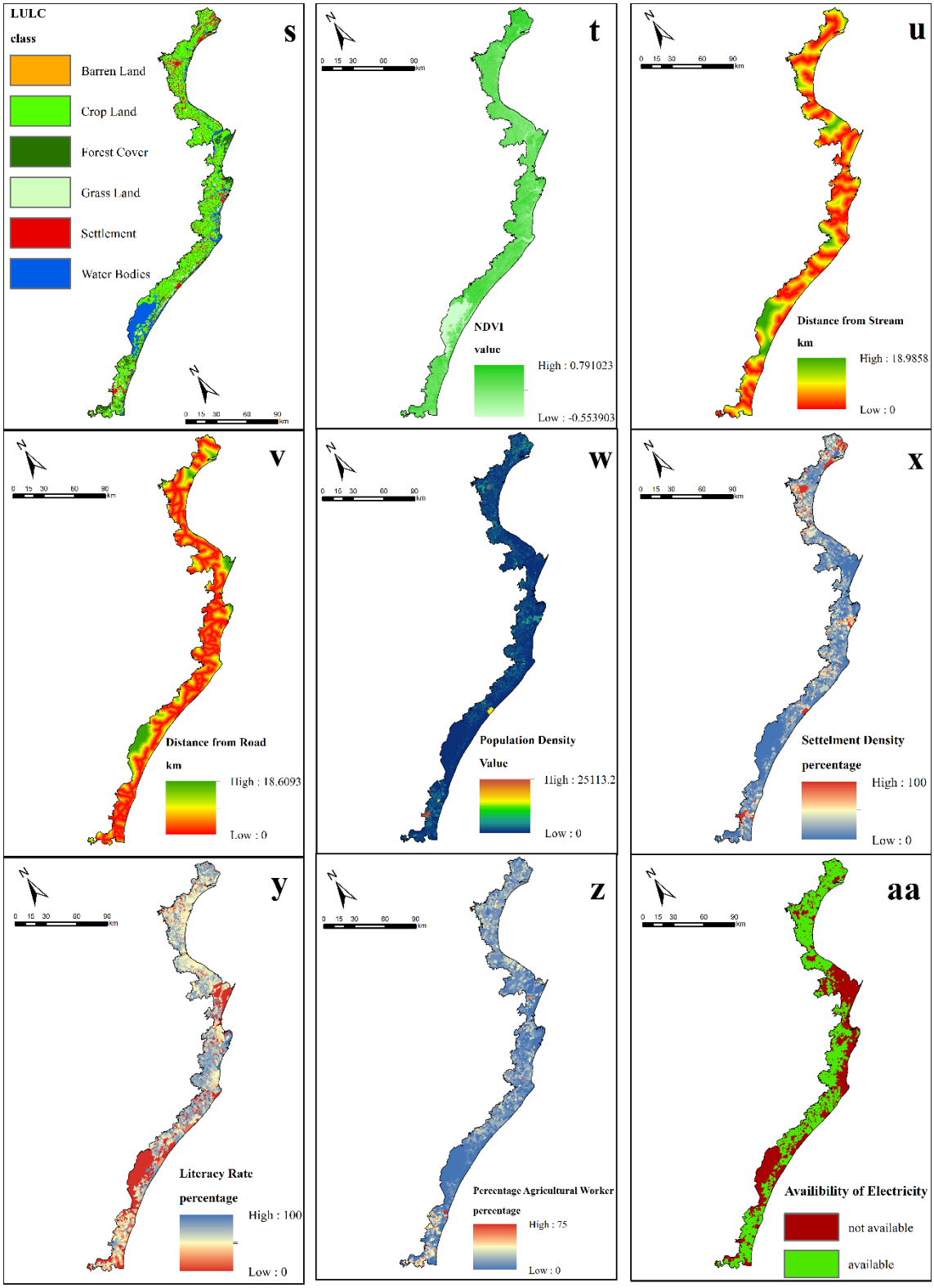

Figure. 3.1 (Continued) (s) LULC, and (t) NDVI, (u) distance from stream, (v) distance from the road, (w) population density, (x) settlement density, (y) literacy rate, (z) percentage of the agricultural population, and (aa) availability of electricity.

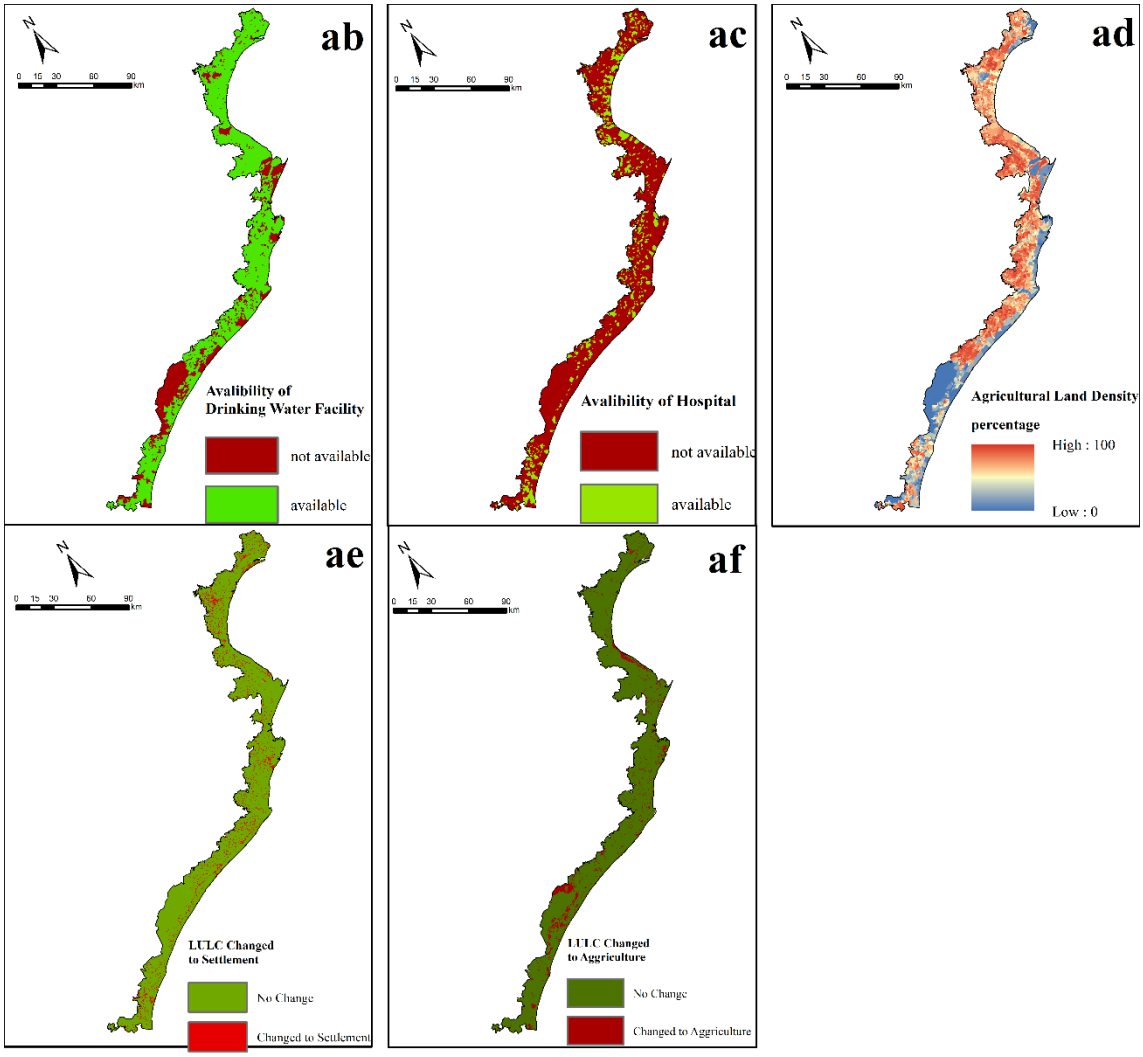

Figure. 3.1 (Continued) (ab) Availability of drinking water facility, (ac) availability of hospital, (ad) agricultural land density, (ae) LULC changed to settlement, and (af) LULC changed to agriculture.

3.2 METHODOLOGY

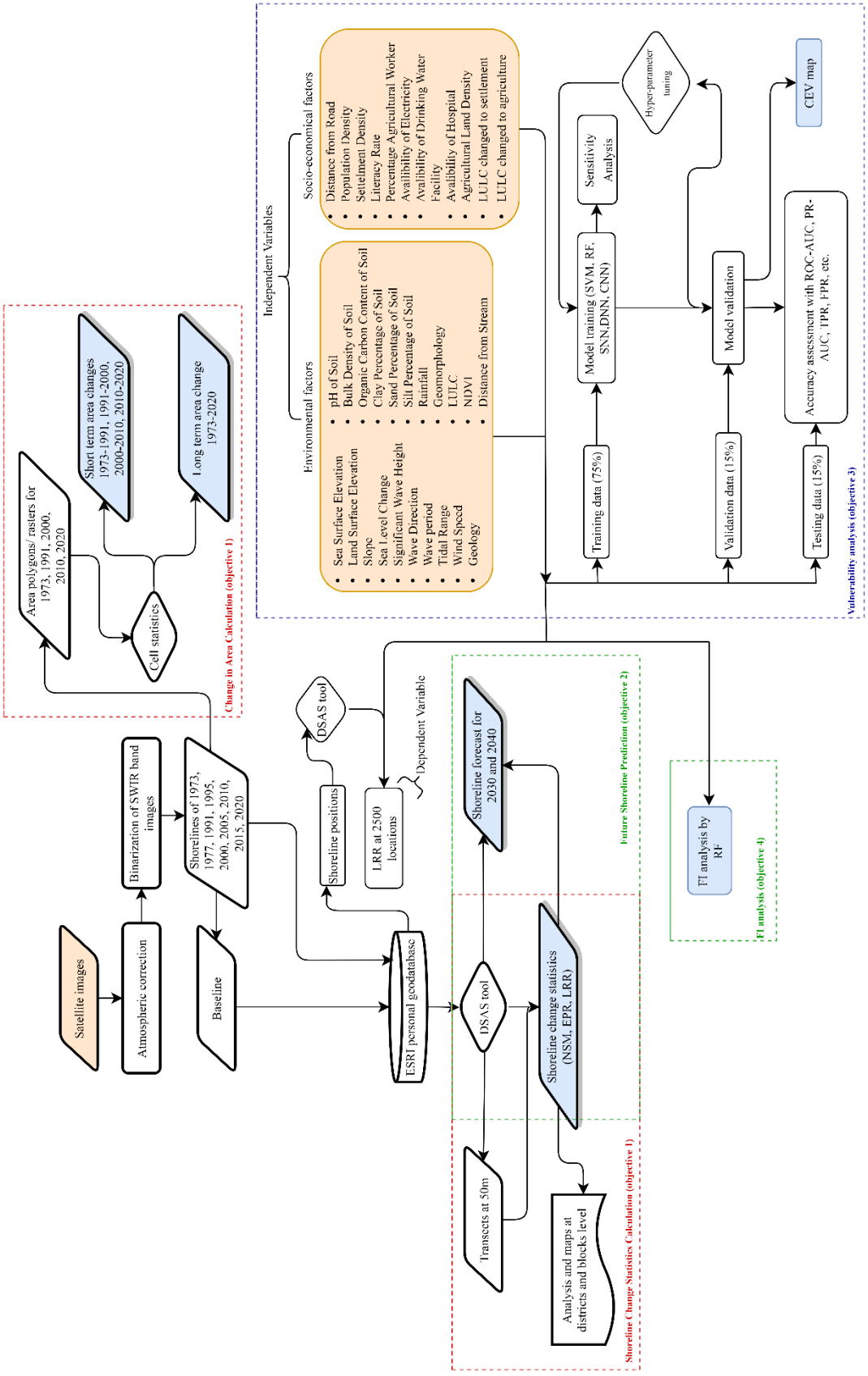

Figure 3.2 Flowchart of the adopted methodology

3.2.1 Shoreline Change Analysis

3.2.1.1 Shoreline Extraction

The absorption spectra of water in infra-red wavelength bands are very low as compared to visible wavelength bands. So, the Near Infrared (NIR) and Shortwave Infrared (SWIR) bands of the Landsat satellites are most useful for differentiating land from the sea. Further, the presence of sediments in water can cause the seawater to have slightly higher reflectance in the NIR band which can create problems in the differentiation process. But, turbid water generally does not cause the same problem for the SWIR band [66]. So for the shoreline extraction task, SWIR band images have been chosen. Before this, the satellite images have been atmospherically corrected. The satellite images are subjected to some errors due to the absorption and scattering of particles in the atmosphere while the images were collected by the sensor. Atmospheric correction is a necessary task that is done before any analysis of the images [67]. In this case, the atmospheric corrections were done using the Semi-Automated Classification Plugin of QGIS [68]. Along with the SWIR band, other optical band images for each year were also corrected to facilitate a better understanding of the study area by creating color composites. After the correction, the image tiles were mosaicked to cover the entire study area. Then the SWIR band image was binaries by visual interpretation of the image to make the demarcation of the land and sea better. The shorelines for every considered year were digitized by the heads-up digitization method at a constant map scale of 1:100000 in ArcMap 10.7. False-color composites with NIR, red, and green bands in RGB channels were created to help in better visualization of the process. To maintain a similar scale while digitizing the coastline, the Landsat 1 and 2 MSS images have been resampled from 60 m to 30 m with the cubic convolution resampling technique as done by Barik, et al. (2021) [33].

3.2.1.2 Shoreline Change Statistics

The Digital Shoreline Analysis System (DSAS) tool is free software that works as an extension to ArcGIS or ArcMap and helps in calculating the change statistics from the time series data of the shoreline positions [69]. This tool required two inputs, one is the shoreline line feature layer which has to contain all the shorelines as the feature vector. The second one is the baseline. These two have to be stored in an

ESRI personal geodatabase file. The shorelines change rates are calculated at the transect intersections along the shoreline. The transects are the lines drawn at a regular user-defined interval on the baseline and cross the shorelines. The attribute field of the shorelines contains the date information and the uncertainty value for each shoreline to facilitate the calculations of change statistics [16]. For this analysis, the shoreline position for 2020 was buffered at some distance landward and reconstructed as the baseline. A total of 9645 transects were drawn at 50m intervals with a default uncertainty of 10m and smoothening distance of 2500m. High smoothening distance has been taken to make the transects close to parallel to each other [70]. Afterward, change statistics such as Net Shoreline Movement (NSM), End Point Rate (EPR), and Linear Regression Rate (LRR) have been calculated at each transect location.

The NSM depicts the separation between the youngest or newest coastline and the oldest. A positive NSM number indicates accretion, whereas a negative value indicates erosion. Considering $d_{2020}$and d_{1972} as the distances of the shorelines from the baseline in 2020 and 1972 respectively, NSM in meters is calculated as equation 3.2 [32],

$$NSM = d_{2020} - d_{1973} \tag{3.2}$$

Further, the EPR in m/year is calculated from the NSM as equation 3.3. EPR shows the rate of change of the shoreline and like NSM, the Positive value shows accretion and the negative value shows erosion [32].

$$EPR = \frac{NSM}{\text{Number of years between the oldest and youngest shoreline}} \tag{3.3}$$

The LRR is calculated by considering the shoreline positions of all the years unlike that of NSM and EPR which are derived with only the youngest and the oldest shoreline positions. The regression rate is calculated with the Ordinary Least Square (OLS) method [70]. OLS finds a linear fit line by minimizing the residual sum of squares [71]. The slope of this line is represented by the LRR value.

The NSM, EPR, and LRR values were also categorized into 5 classes as shown in table 3.3. The geographical coastline of the study area was split into smaller

segments and all 3 categorized values (NSM, EPR, and LRR) were extracted to those lines at the blocks level.

Table 3.3 Classification of DSAS statistics

Sl No	Class	NSM values (m)	EPR and LRR rates (m/ yr)
1	High erosion	≤ -100	≤ -10
2	Moderate erosion	> -100 and ≤ -1	> -10 and ≤ -1
3	Almost no change	> -1 and ≤ 1	> -1 and ≤ 1
4	Moderate accretion	> 1 and < 100	> 1 and < 10
5	High accretion	≥ 100	≥ 10

3.2.1.3 Change in Area due to Coastal Dynamic Process

The rate of change in land area in sq. km/ year due to coastal erosion or accretion has been derived for all the blocks in the study area. This change has been calculated starting from 1973 as both short term change considering years as 1973-1991, 1991-2000, 2000-2010, 2010-2020 and long term change taking years as 1973-2020.

For the calculation, first, the area polygon for any particular year was created by considering the coastline of that year as the seaward boundary and the geographic separation of the block line as the landward boundary. This process is done for all the years. In different years, as the geographic separation line remains constant, the change in the coastal area would be only due to the change in the coastline. Then the polygons were converted to raster of constant cell size and cell values of 1 or 2. For example, considering the short-term area change between 1991 and 2000, the area raster was created with a cell value of 1 for 1991 and 2 for 2000. Further, these two rasters were combined with the sum operation of cell statistics. The process is shown in fig 3.3. The raster produced from this operation got three values, 1 2, and 3 which implied erosion, accretion, and no change respectively. Then the portion of the raster with cell values of 1 and 2 was converted to feature or polygon layer and separated at the block level to quantify the rate of changes in the area.

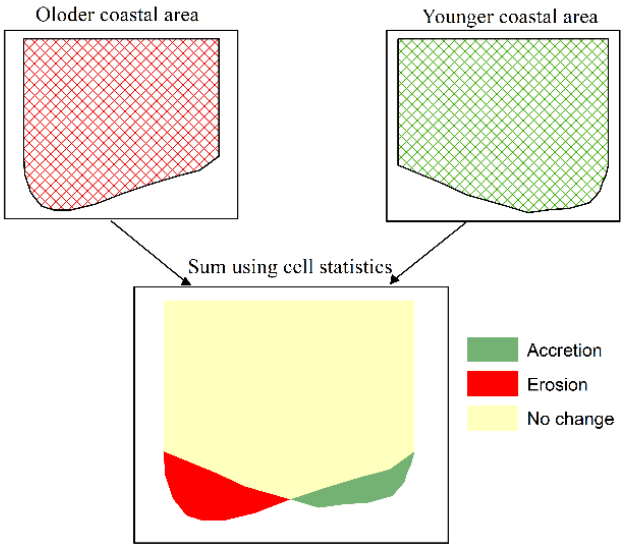

Figure 3.3 Change in area calculation process

3.2.2 Shoreline Forecast

The DSAS tool provides a shoreline forecasting option for 10 and 20 years in the future. This method is an abstract form of the Kalman Filtering which was derived as a linear filtering and prediction solution [72], moreover uses the concept of shoreline forecasting incorporating both long-term and short-term shoreline positions [73]. This model requires at least four previous shoreline positions and calculate in a successive approach [70]. Along with the future shoreline position, this tool also calculates an uncertainty layer for every forecasted year showing the reliability of the prediction at each transect location.

Using this process the shoreline positions for 2030 and 2040 have been derived. The quantitative measure for the movement of the shorelines in both the predicted years has been derived individually. For this, a feature layer with the shoreline of 2020 and a predicted year has been designed and using the DSAS tool, the statistics on NSM have been calculated with transects drawn at 500m intervals along with other inputs as before.

3.2.3 Preparation of CEM

To prepare the CEM, the Digital Shoreline Analysis System (DSAS) tool have been used. This tool takes the historical positions of the shoreline and generates statistics based on the erosion condition of the coast [70]. Shoreline positions for 1973, 1977, 1991, 1995, 2000, 2005, 2010, 2015, and 2020 were derived from the

atmospherically corrected binaries Short-Wave Infrared (SWIR) images for the Landsat series satellites by manual digitization. The shorelines were stored in an ESRI file geodatabase along with the baseline. A baseline is a line parallel to the shoreline that is required to draw the transects [69]. The transects lines were generated at a spacing of 250 m perpendicular to the baseline. The DSAS tool calculates different statistics such as Net Shoreline Movement (NSM), End Point Rate (EPR), Linear Regression Rate (LRR), and Weighted Linear Regression Rate (WLR) at these transect locations. NSM is the distance in metres between the earliest and latest shoreline position. The EPR is derived by dividing the number of years elapsed between the earliest and latest years with the NSM value. The LRR is the regression rate calculated by taking the position of the shoreline for all the years into account. Similar to LRR, WLR is the weighted regression rate. The weights are allocated to different shorelines based on their uncertainty [70]. In this case, as all the shorelines are derived using the same type of data source, the uncertainties for those are also the same. This makes the rate derived from LRR and WLR be same. The negative rate shows erosion and the positive rate shows accretion in the corresponding location.

In this analysis, the LRR rate (Fig 3.4) was considered in the creation of CEM. The negative rates were reclassified as 1 to show erosion whereas positive and zero rates were reclassified as 0 to show accretion or not-erosion which made the work as a binary classification problem. A total of 2,500 points along the coastline with a spacing of 250m were derived this way from which 1,530 locations are of erosion (negative values of LRR) and 970 locations are of accretion (0 or values positive LRR).

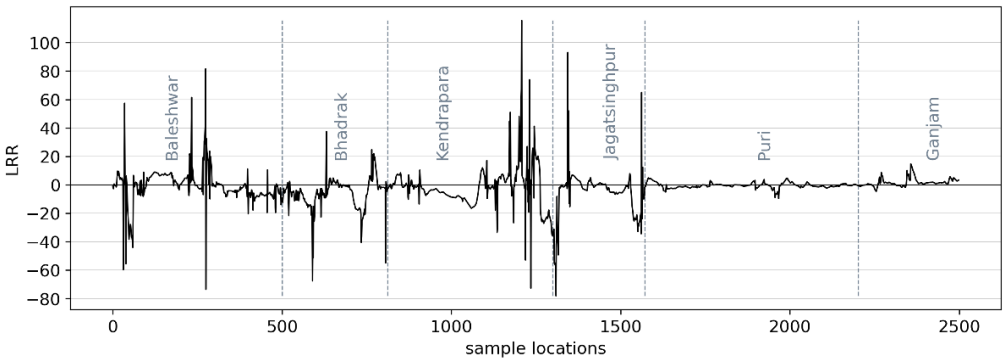

Figure 3.4 LRR at different locations

3.2.4 Applied ML models for CEV mapping

Total 5 widely used ML models comprising 2 classical algorithms and 3 deep learning (DL) algorithms have been applied in the study as binary supervised classification problems. For the classification, 70:15:15% random split has been performed to make the training, validation, and test set. The models have been prepared in the Python programming interface and tuning of various hyper-parameters have been done with 10 fold cross-validation grid search technique.

3.2.4.1 Support Vector Machine (SVM)

It is one of the ML algorithms that finds a line or plane also called a hyperplane that can be of n dimension which can separate all the data classes based on the inputs. The name support vector comes from the fact that this algorithm finds the margins on each side of the hyperplane which are called support vectors. The important concept with this algorithm is its method to handle the non-linear relationship among the training variable which cannot be separated by any hyperplane. This is done by transforming the inputs from the input space to feature space with the help of kernel function [74]. Commonly used kernel functions are, sigmoid, RBF or Radial Basis Function, linear, and polynomial.

The RBF kernel has been applied in this algorithm which is calculated as per equation 3.4 where K is the kernel function and two hyper-parameters, ɣ and C. ɣ is the kernel coefficient and C is the regularization parameter [75] which have been taken as 10-6 and 106 respectively.

$$K(X_n, X_i) = \exp(-\gamma \,||\, X_n - X_i \,||^2 + C) \tag{3.4}$$

3.2.4.2 Random Forest (RF)

Tree-based classification algorithm or decision tree (DT) predict by splitting the dataset based on decision and arriving at the result. This type of model performs with good accuracy on the testing data while may prove to be less efficient in testing. But considering many models like this for the classification can mitigate this problem. Based on this premise RF algorithm uses many DTs as a group of ensemble and produce the output by majority voting. This eliminates the over-fitting issue of the DT [76]. The implemented RF model has considered all the samples in the creation of each of the 220 DTs. The maximum depth of each tree has been restricted to 25 while

considering a minimum of 2 samples for splitting the nodes and to be taken as leaf nodes.

3.2.4.3 Shallow Neural Network (SNN)

The motivation behind the neural network concept is based on the working of the human brain. The inputs are transformed to the output classes with the help of the forward and backwards propagation with the weight adjustments for the hidden units. The SNN model comprises only one hidden layer with a user-defined number of neural units (U). At the hidden layer, the calculation is done in two steps. First using the weights (w_u) and bias (b), the input x_u is transformed as Z (equation 3.5) which is further converted to A with the activation function g (equation 3.6) [77].

$$Z = \sum_{u=1}^{U} W_u X_u + b \tag{3.5}$$

$$A = g(Z) \tag{3.6}$$

At the start of the learning, the weights are allocated randomly by following any statistical distribution and readjustments of the weights are done throughout the learning till the cost of learning or the loss between the actual value and the prediction can reach minima. The process of learning is done as an iterative process by taking a learning rate [77]. The ReLu function (equation 3.7) has been used as the activation for the hidden layer with 34 units in the tuned model. The weights initialization are done by considering the Glorot uniform initializer [78]. A total of 1227 parameters have been trained for 600 iterations with a batch size of 64 and a learning rate of 0.005 considering Adam optimization.

$$g(y) = \max(0, y) \tag{3.7}$$

3.2.4.4 Deep Neural Network (DNN)

A neural network is said to be deep if it contains more than one hidden layer. Both SNN and DNN are suitable for application based on the task. The DNN can be applied to scenarios where the complexity and non-linearity of the problem are high [79]. 5 Hidden layers with varying hidden units of 55, 45, 35, 25, and 15 have been taken in the implemented model (fig. 3.5). Softplus activation function as described in equation 3.8 have been used along with uniform weight initialization and optimization

have been done with Adam optimizer with a learning rate of 0.005. 400 iterations have been performed with a batch size of 32 to train 7955 parameters.

$$h(y) = \log(\exp(y) + 1) \tag{3.8}$$

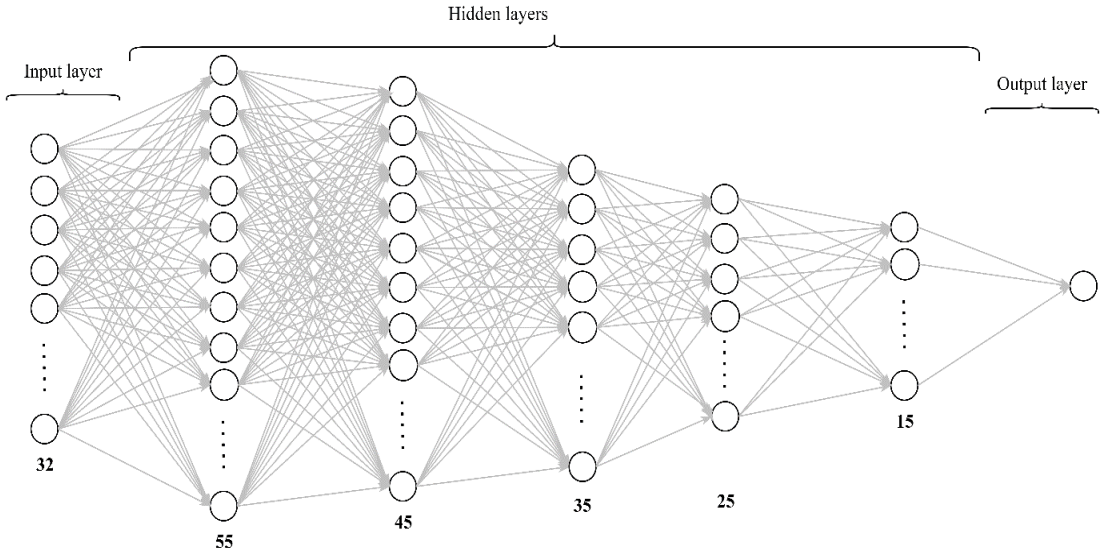

Figure 3.5 Diagrammatical representation of DNN model architecture

3.2.4.5 Convolutional Neural Network (CNN)

A typical design of CNN comprises a convolutional layer, pooling layer, and fully connected layer. Depending on the input shape or dimension, the CNN can be termed as 1D or 2D CNN. The implementation of 1D CNN with row vector as input layer is comparatively recent but numerous due to the appreciable decrease in complexity and computational cost over 2D CNN (Kiranyaz, et al. 2021). In this study, 1D CNN has been implemented (Fig 3.6) as the inputs can be segregated as row vectors with a dimension of 32 representing all the 32 CEVFs. 2 convolutional layers each using 64 filters with size 3 followed by a maximum pool layer with size 2 have been used. The output of the pooling operation has been flattened and connected with a fully connected layer with 100 neural units by considering 20% dropout regularization. Uniform weight initialization along with ReLu activation have been used to tune 102409 parameters using Adam optimizer and a learning rate of 0.005. In this, a batch size of 32 has been considered to perform 250 iterations.

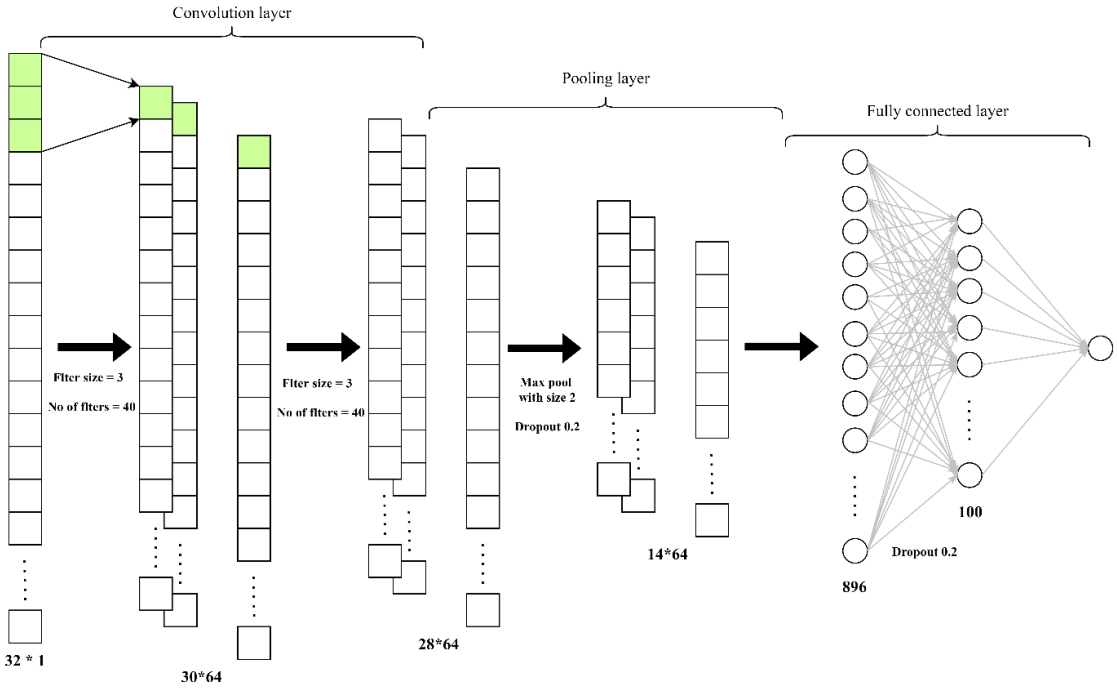

Figure 3.6 Diagrammatical representation of CNN model architecture

3.2.5 Accuracy Assessment of ML Models

Several accuracy metrics have been calculated to access the accuracy of the prepared models. The ROC or Receiver Operating Characteristic plots have been drawn by taking false positive rate (FPR) on the x-axis and corresponding true positive rate (TPR) on the y-axis by gradually changing the threshold to classify the prediction probability for training, testing, and validation data separately. The area under the curve (AUC) of the ROC has been calculated which shows how well the model has performed. Similarly, TPR, FPR, TNR, FNR have been calculated considering an optimum threshold using the following equations [80].

$$\text{True positive rate (TPR) or Recall} = \frac{\text{Correctly classified positive class or TP}}{\text{Total positive class}} \tag{3.9}$$

$$\text{False positive rate (FPR)} = \frac{\text{Incorrectly classified negative class or FP}}{\text{Total negative class}} \tag{3.10}$$

$$\text{True negative rate (TNR)} = \frac{\text{Correctly classified negative class or TN}}{\text{Total negative class}} \tag{3.11}$$

$$\text{False negative rate (FNR)} = \frac{\text{Incorrectly classified positive class or FN}}{\text{Total positive class}} \tag{3.12}$$

The AUC for PR or precision-recall curve has been calculated. Again taking an optimum value for threshold, precision score and from the precision-recall, the F1

score has been measured. The accuracy scores have been calculated as equation 3.15 [80].

$$Precision = \frac{TP}{\text{Total data classified as positive class}} \tag{3.13}$$

$$\text{F1 score} = \frac{2}{\frac{1}{\text{Pr}ecision} + \frac{1}{\text{Re}call}} \tag{3.14}$$

$$\text{Accuracy score} = \frac{TP + TN}{\text{Total positive class} + \text{Total negative class}} \tag{3.15}$$

All the aforementioned metrics range from 0 to 1 whereas the MCC or Matthews Correlation Coefficient varies from -1 to 1 with 1 for a perfect classifier [81]. Also, the binary cross-entropy loss or log losses for all the classifiers have been derived. The MCC and log loss have been calculated using equations 3.16 [81] and 3.17 [82] where y is the true class and p is the probability for that class.

$$MCC = \frac{TP.TN - FP.FN}{\sqrt{(TP + FP).(TP + FN).(TN + FP).(TN + FN)}} \tag{3.16}$$

$$\text{Log loss(y, p)} = -(y \log(p) + (1 - y) \log(1 - p)) \tag{3.17}$$

3.2.6 Factor Importance Analysis

The interpretability of the prediction and understanding of the impact of the various features or factors on the process of erosion can be explained by the factor importance (FI) analysis. The FI by the Gini impurity of the RF model at state, districts, and block-level have been determined for the same.

At a particular node n of any particular tree t of the RF model, the Gini impurity i(n, t) is determined as equation 3.18 where the f_1 and f_0 are the fractions of a sample belonging to class 0 and 1 considering the total sample at node n. The node n gets split into two nodes, left node (n_l) and right node (n_r). Due to this, a decrease in the impurity occurs which is denoted as $\Delta i(n, t)$ and defined as equation 3.19 where the f_l and f_r are the fractions of sample allocated to left and right node considering total sample at node n [83].

$$i(n,t) = 1 - f_1^2 - f_0^2 \tag{3.18}$$

$$\Delta i(n,t) = i(n,t) - f_l i(n_l,t) - f_r i(n_r,t) \tag{3.19}$$

The maximum value of Δi(n, t) corresponding to factor m is taken as the optimum value and denoted as $\Delta i_m(n)$. With this value, considering all the similar nodes (N) and all the trees (T) of the RF, the FI by Gini impurity for factor m or $I_g(m)$ is determined as equation 3.20 [83].

$$I_g(m) = \sum_{t=1}^{T} \sum_{n=1}^{N} \Delta i_m(n,t) \tag{3.20}$$

CHAPTER 4

RESULTS AND DISCUSSIONS

4.1 SHORELINE CHANGE STATISTICS

On the entire coastline of Odisha, among the 9645 transects, 5866 (60.82%) and 5549 (39.18%) transects registered land retreat and deposition respectively. The average change in shoreline position or mean NSM is -84.95 m with a maximum negative change of -3508.4 m and a maximum positive change of 4042.9 m. The calculated EPR and LRR showed corresponding average values of -1.81 m/year and -0.36 m/year. The transects have the maximum EPR values for erosion as -74.45 m/year with an average of -5.34 m/year and accretion as 85.79 m/year with an average of 3.67 m/year. Also, the maximum erosion rate is -36.54 m/year with an average rate of -4.74m/year and the maximum accretion rate is 72.83 m/year with an average rate of 4.32 m/year for LRR.

1810 number of transects for the Baleshwar district showed depletion of coastal length by an average of -53.6 m with the maximum retreat of -2382.25 m and the maximum deposition of 1291.44 m. The average EPR value is -1.14 m/year with maximum erosion and accretion rates of -50.55 and 27.41 respectively. Similarly, the average LRR value for this district is 2.46 m/year with a rate of -36.54 m/year and 25.95 m/year concerning the maximum erosion and accretion. The south side shoreline covering the Bahanaga, Remuna, and part of Baleshwar Sadar blocks showed higher erosion rates in all three measured statistics as compared to the north-east side shoreline.

For the Bhadrak district, the average NSM length is observed to be -257.4 m from the 1089 transects. The maximum erosion length is -1206.33 m and that of accretion is 1039.42 m. -5.46 m/year of average EPR is measured along with the maximum erosion rate of -25.6 m/year and maximum accretion rate of 22.06 m/year. The maximum erosion rate is -14.52 m/year and the maximum accretion rate of 19.06 m/year for LRR with an average rate of 1.26 m/year. Along the coastal stretch of this

district, the two sides show a high erosion rate in comparison with the middle part covering both blocks.

A total 1504 number of transects have been generated in the Kendrapara district which showed an average NSM value of -224.99 m with a maximum retreat of -3508.4 m and a maximum deposition of 4042.9 m. The average EPR is -4.77 m/year for the districts in addition to the maximum erosion rate is -74.45 m/year and the maximum accretion rate of 85.79 m/year. By considering the LRR, the maximum erosion rate and maximum accretion rate are found to be -33.65 m/year and 72.83 m/year. The average LRR value is 4.33 m/year. Between the two blocks, almost the whole coastal length of the Rajnagar block is found to be under erosion along with the south part of the Mahakalpada block.

The average change in shoreline position is -206.26 m for the Jagatsinghpur district calculated by 1168 numbers of transects. The maximum withdraws of -1628.88 m and maximum accumulation of 662.29 m are observed in the area. The average EPR value is -4.37 m/year and the average LRR value is -4.19 m/year. The maximum erosion rate is -34.57 m/year and the maximum accretion rate of 14.05 m/year for the EPR. Further, by taking LRR into account, the maximum erosion rate is -33.65 m/year, and the maximum accretion rate of 18.31 m/year. The erosion rate is found to be higher on the southeast side of the Ersama block and the Balikuda block of the district.

For the Puri district, a total 2876 number of transects have been used to calculate the DSAS statistics. The average change in coastal line position is found to be -32.09 m which is the lowest among all the districts on the negative side i.e. for average shoreline retreat. As derived from the NSM, the maximum retreat is -634.89 m and the maximum deposition is 262.24 m. Both EPR and LRR showed an average value of -0.68 m/year and -0.61 m/year respectively. Also, from the EPR and LRR values, the maximum erosion rates are -13.47 m/year and -17.67 m/year. Further, the maximum accretion rates are 5.56 m/year and 10.46 m/year. Among the 6 blocks of the district, the Kakatpur, Gop, and parts of Krushnaprasad block fell on transects showing erosion.

A total of 1263 transects for the Ganjam district showed an average change in coastal distance of 71.92 m as NSM. This is the only district to show the average outward movement of the shoreline as derived from the NSM. The maximum shoreline retreat length is -226.51 m and that for accretion is 695.9 m. 1.52 m/year of average

EPR is measured along with the maximum erosion rate of -4.81 m/year and maximum accretion rate of 14.77 m/year. The maximum erosion rate is -4.02 m/year and the maximum accretion rate of 9.9 m/year for LRR with an average rate of 0.93 m/year. The southeast coastline of the Ganjam block and the middle part of the coastline of the Chatrapur block showed erosion.

The areas near the estuary of Subarnarekha River which is present towards the north-east side of the Baleshwar district and the estuary of Devi River which is present at the border of the Jagatsinghpur and the Puri district are found to be under erosion. Also, the area near the Dhamra Port of the Bhadrak district and the northeast side of the Paradeep Port is under erosion condition.

The DSAS statistics were categorized into five classes based on their values and transferred to the geographical coastal line of the study area as described in the methodology section (Fig. 4.1). Also, the length of each class at the district level in percentage has been calculated to give an estimate of the severity of the erosion (Fig. 4.2).

Taking the class division as per the NSM, for the Baleshwar district about 37% of coastal length is under high erosion (less than -100 m) which is balanced by almost the same (40%) amount of high accretion (more than 100 m) length. The EPR classes also show a similar trend for this district with 6.28% length under high erosion (-10 m/year) and 6.89% under high accretion (10 m/year) unlike the class division by LRR, in which 3.27% length under high erosion (10 m/year) and 19.21% length under high accretion (10 m/year). In the Bhadrak district, about 60% of the coastline has been retreated by less than -100m and 50% of the coastline shows an EPR rate in the moderate erosion class (between -10 m/year and -1 m/year). About 43-44% of the coastline of both the Kendrapara and Jagatsinghpur districts have retreated by less than -100m. For the Puri district, 52.88% of coastal length has witnessed moderate erosion (between -100 m/year and -1 m/year) as per NSM values, and considering the LRR classes almost similar percentage of length shows no change (between -1 m/year to 1 m/year). Ganjam is the only district for which the accretion and almost no change classes have higher values considering all three statistical measures in comparison with the erosion classes.

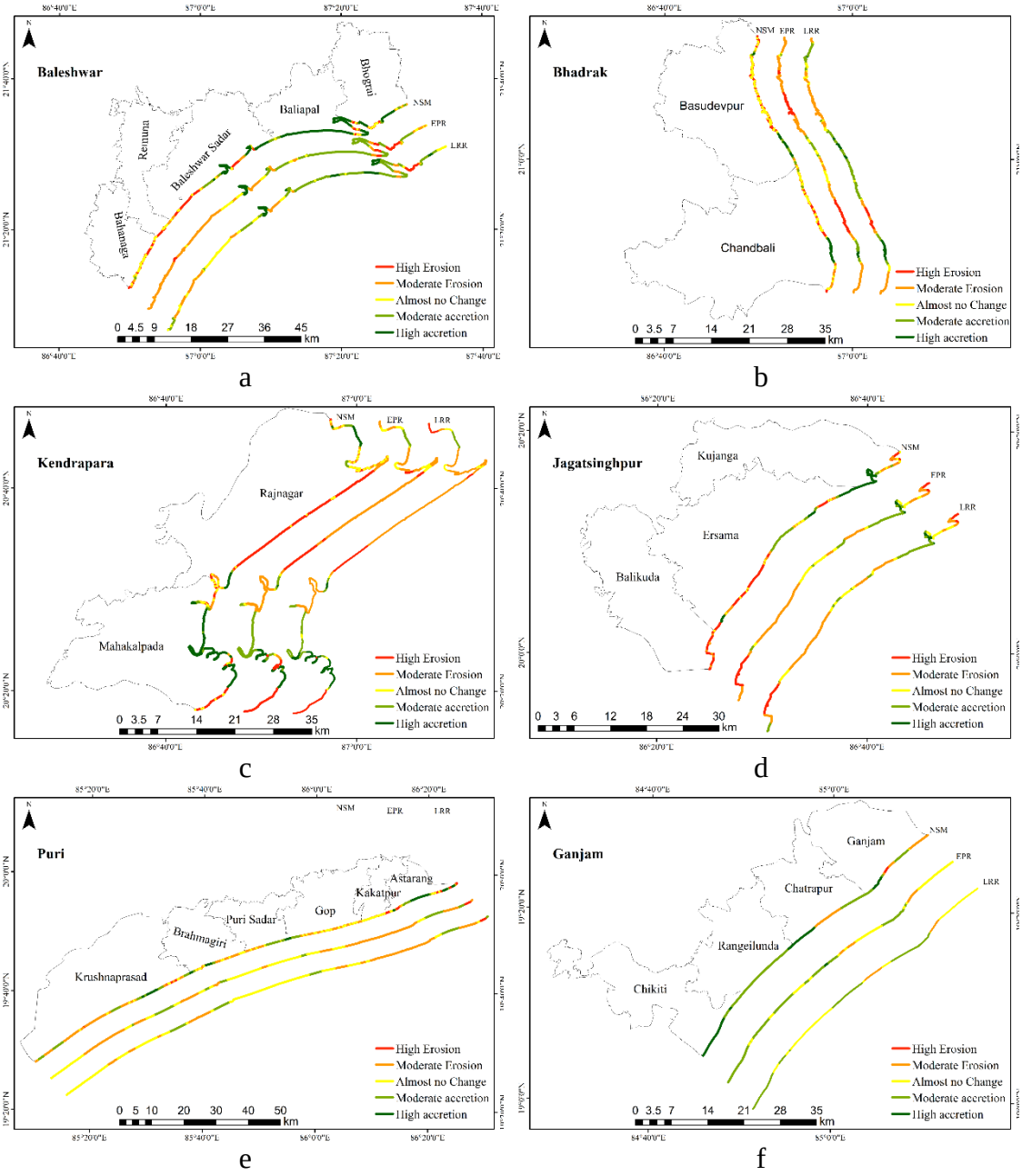

Figure 4.1 NSM, EPR, LRR classified values of a. Baleshwar, b. Bhadrak, c. Kendrapara, d. Jagatsinghpur, e. Puri, and f. Ganjam

The contrast in the percentage lengths under different categories considering both EPR and LRR values can be attributed to the calculation considerations of both. Calculation of the EPR uses only the oldest and the youngest shoreline whereas, for the LRR, shorelines of all the years under investigation are taken into account. So in this study, EPR has been calculated from the shoreline of 1973 and 2020 however in the calculation of the LRR, the shorelines of all nine years have been considered. Considering all three statistics and all six districts, around 50% of the shorelines of the Bhadrak, Kendrapara, and Jagatsinghpur [33] districts are either under high or moderate

erosion categories. Both the Baleshwar [16] and Ganjam [13] districts are showing more accretion.

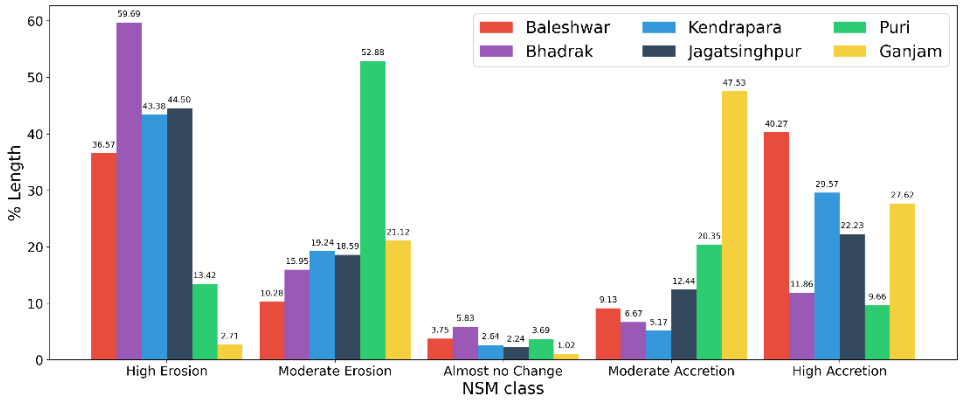

a

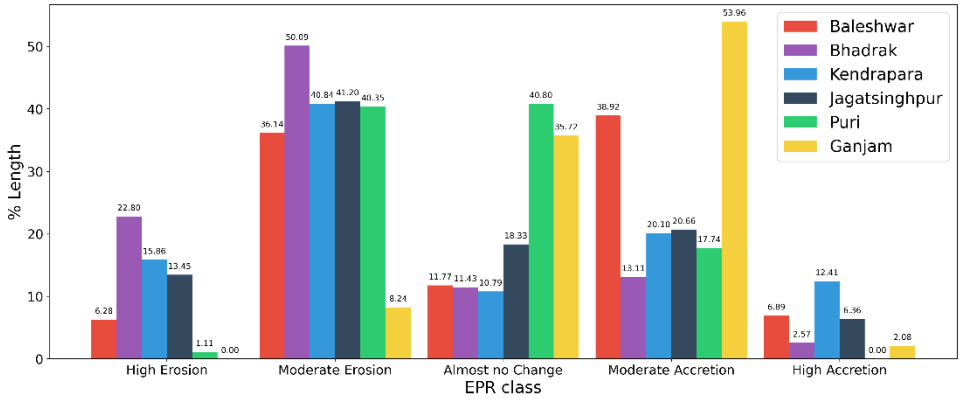

b

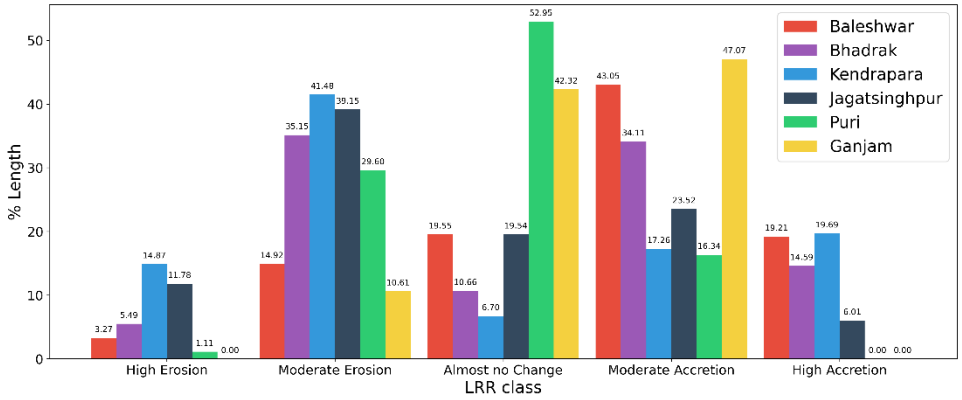

c

Figure 4.2 % coastline at district level under different classes of NSM, EPR, and LRR

4.2 CHANGE IN AREA DUE TO COASTAL DYNAMIC PROCESS

Both the short-term and long-term area change rates due to both erosion and accretion processes in sq. km/ year have been calculated at the block level and aggregated at the district level (table 4.1). Considering short term changes, the Baleshwar has the maximum rate of change in area for erosion in the year range of

1973-1991 (2.04 sq. km/year) and 2000-2010 (0.578 sq. km/year) but the same district is found to has the maximum rate of change in area for accretion in the year range of 1991-2000 (2.993 sq. km/year) and 2010-2020 (0.558 sq. km/year). For the year interval of 2010-2020, Puri district also shared the same area change due to accretion as with Baleshwar. For the earlier year interval of 1991-2000, Puri was found to have the maximum rate of change in the area considering erosion conditions (0.601 sq. km/year). For a consecutive year span of 2000-2010 and 2010-2020, Jagatsinghpur district showed the maximum area change due to accretion (1.059 sq. km/year) and erosion (1.017 sq. km/year) respectively. In long term, i.e. from 1973 to 2020, Kendrapara district has both maximum area change by erosion (0.516 sq. km/year) as well as accretion (0.415 sq. km/year).

Table 4.1 Rate of change in area for different districts

	Baleshwar		**Bhadrak**		**Kendrapara**	
Year range	Er*	Ac#	Er	Ac	Er	Ac
	Short term change rate (sq. km/ year)					
1973-1991	2.04	0.034	1.715	0	1.121	0.327
1991-2000	0.094	2.993	0.062	1.351	0.494	1.64
2000-2010	0.578	0.743	0.022	0.744	0.518	0.857
2010-2020	0.49	0.558	0.194	0.352	0.707	0.404
	Long term change rate (sq. km/ year)					
1973-2020	0.317	0.212	0.283	0.055	0.516	0.415
	Jagatsinghpur		**Puri**		**Ganjam**	
Year range	Er	Ac	Er	Ac	Er	Ac
	Short term change rate (sq. km/ year)					
1973-1991	0.437	0.163	0.323	0.218	0.4	0.239
1991-2000	0.472	0.149	0.601	0.304	0.122	0.14
2000-2010	0.173	1.059	0.164	0.639	0.091	0.174
2010-2020	1.017	0.092	0.558	0.212	0.157	0.2
	Long term change rate (sq. km/ year)					
1973-2020	0.242	0.055	0.167	0.058	0.018	0.117

*Erosion
#Accretion

Only for Ganjam district, the net change in area is positive, in other words, only this district has witnessed a gain in the landmass of 4.63 sq. km whereas the other five districts have lost land area (fig. 4.3) between 1973 and 2020. The loss of land is maximum for Bhadrak district (10.69 sq. km) which is followed by Jagatsinghpur (8.78 sq. km) and Puri (5.12 sq. km). Both Baleshwar and Kendrapara districts have lost a similar amount of area (4.8 sq. km). For the entire study area and at large of the coastal area of Odisha, the eroded and gained land masses area amount to be 72.47 sq. km and 42.83 sq. km making the net area have been lost due to coastal erosion to be 29.64 sq.

km. The Odisha coast has experienced about 60% more erosion than accretion which is higher than the 50% mark for the same at the global level [3].

Table 4.2 Change in the area at block level from 1973 to 2020

Block name	Area lost	Area gained	Net area changed
Baleshwar district			
Baleshwar Sadar	3.138	3.353	0.215
Baliapal	0.602	5.304	4.702
Bhograi	5.694	1.276	-4.418
Remuna	1.048	0.013	-1.035
Bahanaga	4.414	0.004	-4.41
Bhadrak district			
Basudevpur	6.35	0.638	-5.712
Chandbali	6.929	1.953	-4.976
Kendrapara district			
Rajnagar	13.588	3.399	-10.189
Mahakalpada	10.657	16.106	5.449
Jagatsinghpur district			
Balikuda	5.019	0.189	-4.83
Ersama	4.709	1.1	-3.609
Kujanga	1.643	1.301	-0.342
Puri district			
Kakatpur	0.777	0	-0.777
Astarang	2.09	1.158	-0.932
Brahmagiri	0.502	0.318	-0.184
Gop	1.268	0.15	-1.118
Krushnaprasad	2.874	0.996	-1.878
Puri Sadar	0.333	0.097	-0.236
Ganjam district			
Chikiti	0.001	1.799	1.798
Chatrapur	0.307	2.072	1.765
Rangeilunda	0	0.852	0.852
Ganjam	0.539	0.754	0.215

At the block level (table 4.2), the Rajnagar block of Kendrapara has lost 10.189 sq. km of land which is 34% of the entire land lost whereas the other block of the same district, Mahakalapada has gained 5.449 sq. km of land. Other blocks which have lost major land area are, the Bhograi block (-4.418 sq. km) of Baleshwar district, Basudevpur (-5.712 sq. km) and Chandbali (-4.976 sq. km) blocks of Bhadrak district, and Balikuda (-4.83), and the Ersma (-3.609) blocks of Jagatsinghpur district. All four blocks of the Ganjam district have gained land by the coastal dynamic actions.

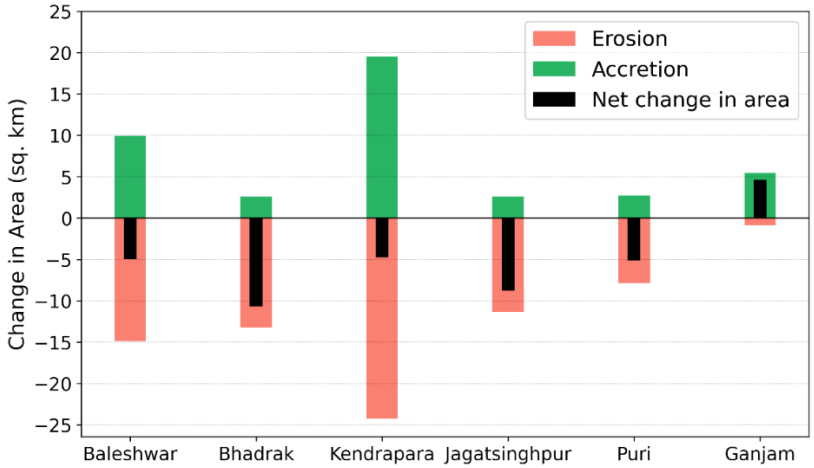

Figure 4.3 Change in area of different district from 1973 to 2020

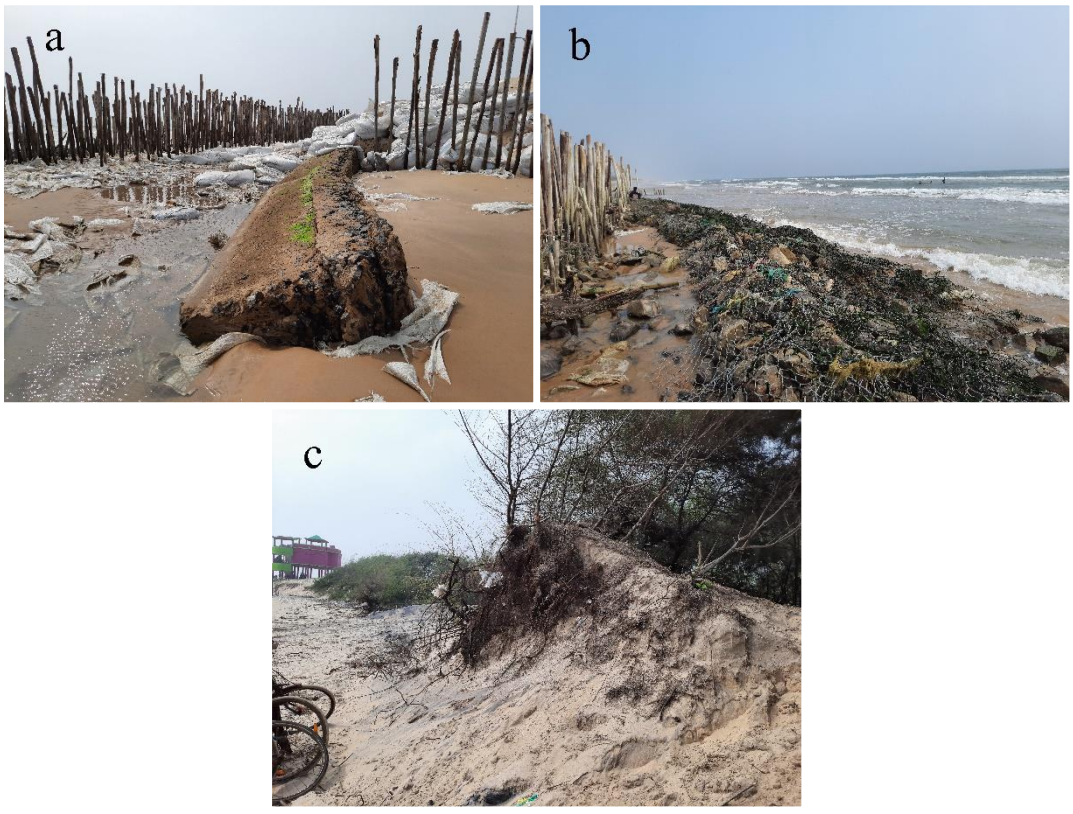

Figure 4.4 a. The breakwater structures, b. the concrete sea walls, c. at the Siali beach of Ersama block

Considering the combined effect of coastal erosion and the accretion process, the coastline gets changed due to the compound outcome of several natural or geographical as well as anthropogenic factors [84]. The constant effect of wave energy that shapes the coast can affect it as the wave pattern or height increases or changes periodically. The effect of sea-level rise, storm surges, and tsunamis also influence the coastline position [85]. The geological features or properties of the coastal soil present

can control the process of erosion as the sandy beach tends to be eroded more than that rocky or clayey beaches [46]. Similarly, various anthropogenic contributors such as spatial distribution of population, the developmental activities like the creation of roads or ports near the coast, construction of dams at rivers upstream, cutting down coastal vegetation, etc. are escalating the coastal erosion conditions [84]. Analogous reasons for the change in coastal zones have also been found in various studies conducted on the Indian coastline. A study done for the coastline along south Gujarat [86] showed that changing land use and land cover patterns are major factors. Furthermore, for the eastern coastline of India, the cyclonic storm surge plays a major role in the erosion process [87].

The data shows, that the prevention, as well as mitigation of the erosion process, is very important in the study area. There are numerous methods available and have been adopted in different parts of the world to mitigate this problem. Many fixed coastal protection structures such as seawalls made up of stone or concrete, groyne created with stone or wood or breakwater structures have been used [88]. Some coastal protection is present in a few parts of the study area. For instance, in the Siali beach of the Ersama block. But these brittle structures don't always withstand the constant dynamic force created by the waves [88]. The breakwater structures (Fig. 4.4a) and the concrete sea walls (Fig. 4.4b) used at the Siali beach have failed due to the same. This shows that even if the same methods have been applied successfully to some other coastal areas, these failed to be translated in practice to this particular area. Also, hard or fixed protection like these creates erosion in the nearby areas where these protections are absent [89]. Another possible solution includes more sustainable approaches such as the creation of artificial dunes, nourishment of eroded beaches, and restoration of vegetation near the coastal areas [88]. Fig. 4.4c shows that sand erosion has exposed the roots of the trees near the Siali beach. Decreasing the anthropogenic activities by different restrictions in constructions or excessive movement or activities by people [88] and/or adopting strategies to do effective coastal retreats [90] may prove effective solutions in this case. Further, the river mouths in the study area are showing signs of excessive erosion, the causes of this need to be further analyzed and managed.

4.3 SHORELINE FORECAST

By using the forecasting option of the DSAS tool, the shoreline positions of 2030 and 2040 have been identified. The shoreline movement (NSM) for 2030- 2020 and 2040-2020 for the entire study area have been derived using the DSAS tool with 885 numbers of transects drawn at 500m intervals. For 2030, 41% of the transects showed retreat in the shoreline distance with an average change in distance of 22.8m. The predicted maximum retreat is -3534m and the maximum deposition is 2421 m. By 2040, the maximum retreat and maximum deposition are forecasted to be -3176m and 2573 m respectively. Also, the average change for this year is 17.9m. The plot of the NSM values at different transects in fig. 4.5 shows, that comparatively the change is low for the Ganjam and Puri districts.

Fig. 4.6 shows the locations with high erosion or accretion as predicted by the tool along with their uncertainty level. Notably, the changes in shoreline positions are higher near the estuary positions. The estuary of Devi River (fig. 4.6a), the east side of Subarnarekha River (fig. 4.6d), and the coastline near the Bhitarakanika national park or mangrove wetland of the Kendrapara district (fig. 4.6c) are predicted to show the erosion of the sand deposits. The south-east side of Kendrapara district near the border of Jagatsinghpur district (fig. 4.6b) will show erosion as well as the shift in sand deposit position which is predicted to cause accretion. The area towards the north side of the Bhitarakanika national park (fig. 4.6c), as well as the west side of Subarnarekha River (fig. 4.6d), are predicted to be under erosion in the coming 20 years.

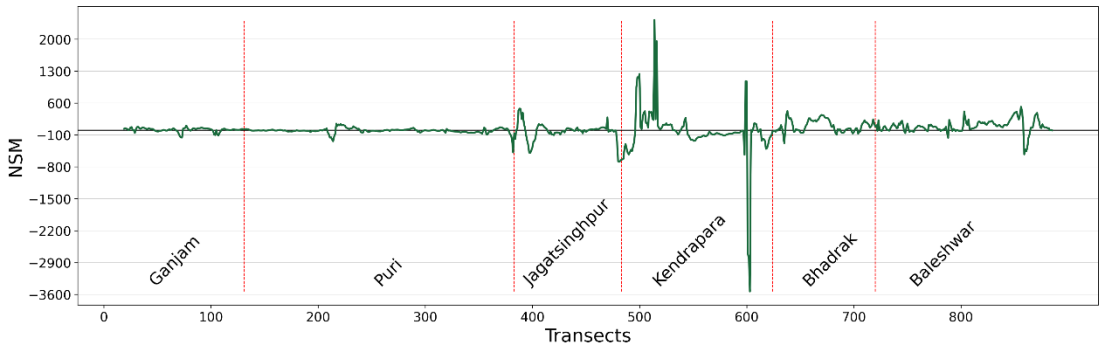

a

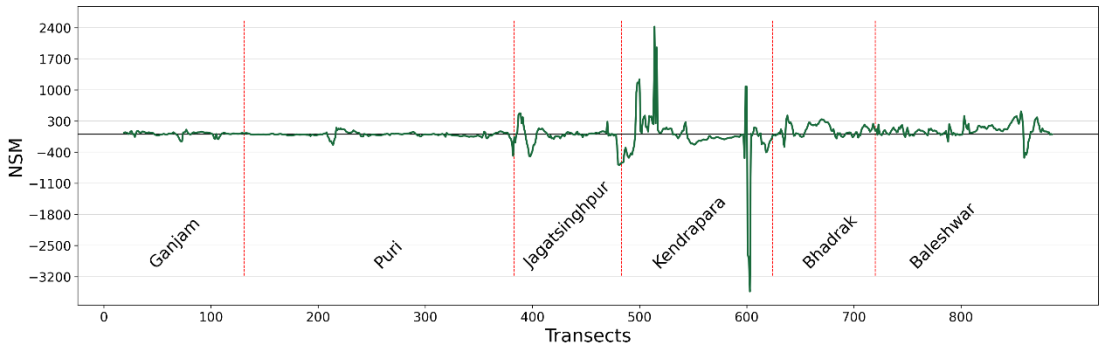

b

Figure 4.5 NSM of a. 2030 and b. 2040

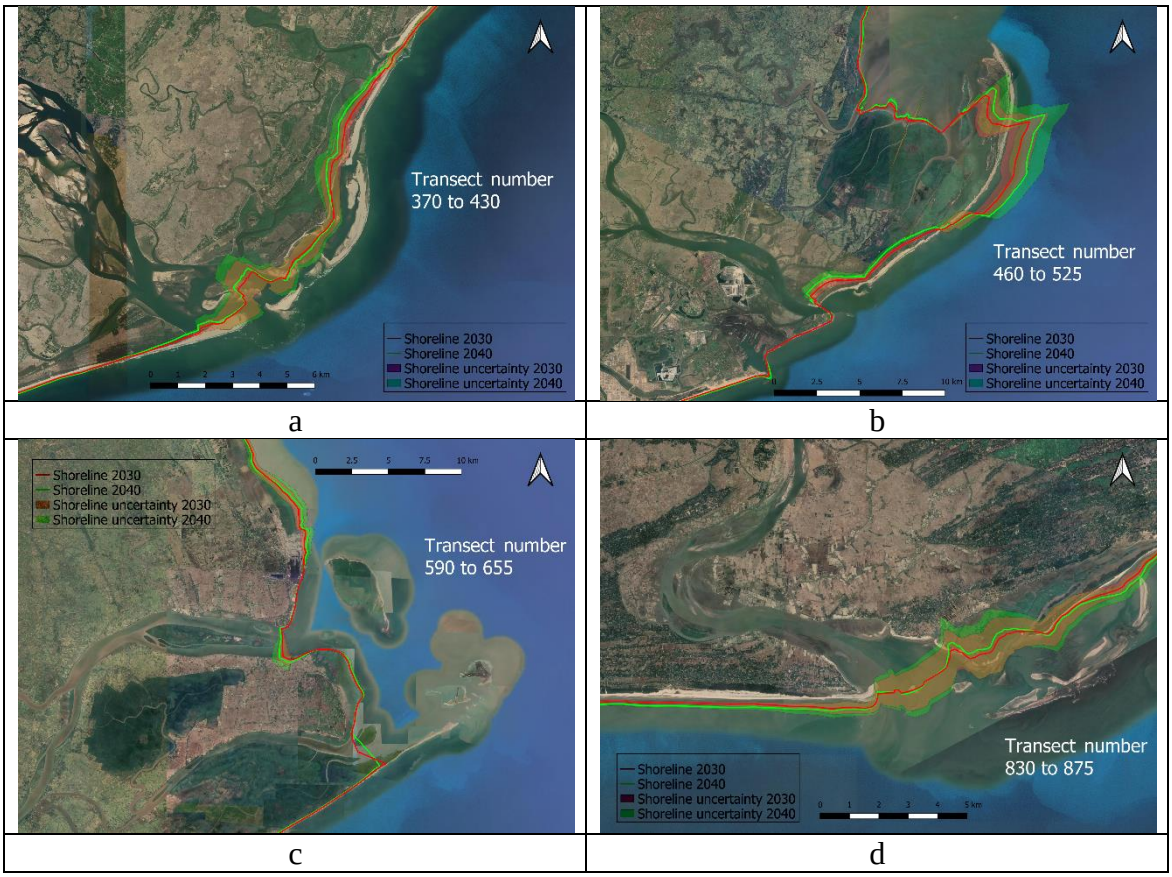

Figure 4.6 Predicted shoreline positions for 2030 and 2040 at a. estuary of Devi River, b. the border of Kendrapara district and Jagatsinghpur district c. coastline near the Bhitarakanika national park or mangrove wetland, and d. estuary of Subarnarekha

4.4 ACCURACY ASSESSMENT OF MACHINE LEARNING MODELS

A total of 11 metrics have been accessed to estimate the accuracy and efficiency of the prepared models. ROC curves as shown in fig. 4.7 have been drawn for all the models with training, validation, and testing data. At the training and validation phase, RF showed a maximum ROC-AUC score (1, 0.96), following this, excellent accuracies have also been shown by DNN (1, 0.94), CNN (1, 0.92), SVM (0.97, 0.92),

and SNN (0.97, 0.91). Similar trend has been observed for TPR with (1, 0.93) for RF, (0.98, 0.92) for DNN, (0.98, 0.87) for CNN, (0.95, 0.89) for SVM, and (0.92, 0.89) for SNN. The accuracy score is the highest for RF (1, 0.93) followed by CNN (0.98, 0.88), DNN (0.97, 0.90), SVM (0.92, 0.87), and SNN (0.92, 0.86). Table 4.3 shows the scores of all the metrics with all 3 datasets. In the testing phase, the RF model showed a maximum ROC-AUC score of 0.99 that is followed by CNN (0.97), DNN (0.97), SNN (0.95), and SVM (0.94). To represent the level of performance of all the models the training, accuracy score has been considered as it uses both true positive and true negative in the calculation. The best model for the task is found to be RF (0.96) followed by CNN (0.93), DNN (0.91), SNN (0.88), and SVM (0.88).

Among all the applied models, the RF model is proved to be the most efficient and accurate in the prediction of coastal erosion vulnerability. Though the use of RF is entirely new to this topic, it has been successfully applied to other problems of natural disasters and climatic crises such as floods [91] or landslides [92]. Also, all the models showed alarming results as the vulnerability probability because almost half of the coastal length comes under the very high vulnerability category with a probability of more than 0.8.

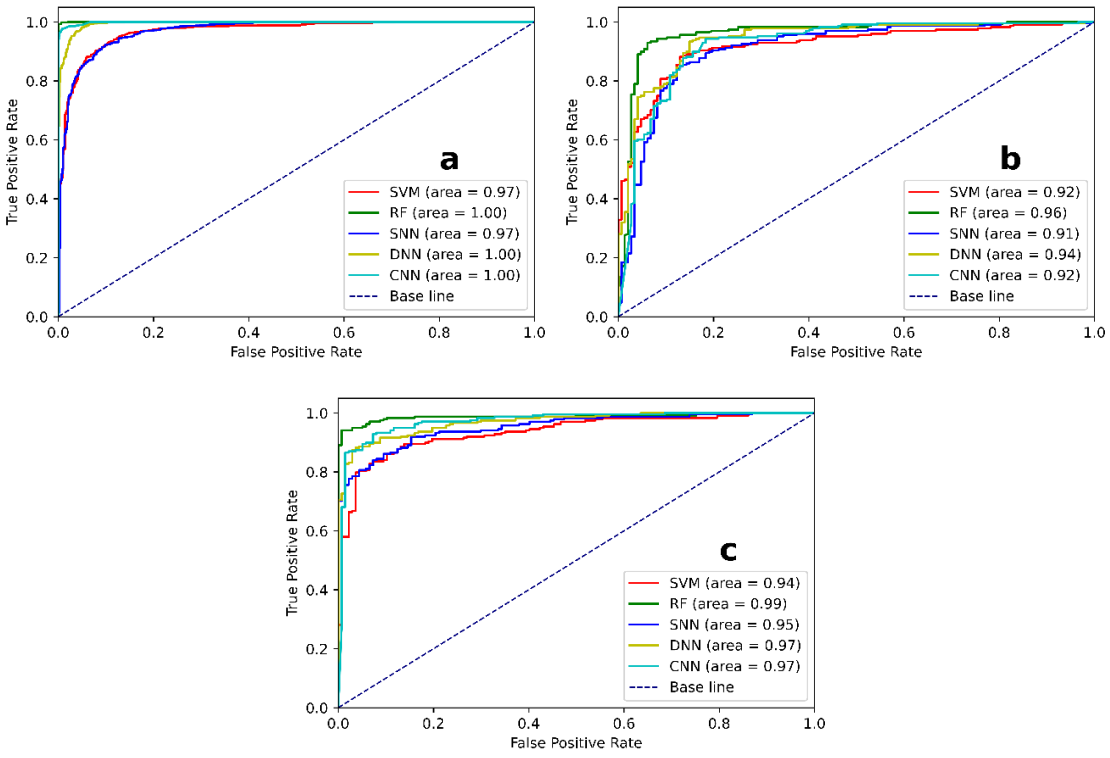

Figure 4.7 ROC curves for (a) training, (b) validation, and (c) testing

Table 4.3 Result of accuracy assessments

			Training (70%)		
Metrics	**SVM**	**RF**	**SNN**	**DNN**	**CNN**
ROC-AUC	0.91	1	0.97	1	1
PR-AUC	0.95	1	0.97	1	1
TPR	0.95	1	0.92	0.98	0.98
FPR	0.13	0.01	0.1	0.08	0.01
TNR	0.87	0.99	0.9	0.95	0.99
FNR	0.05	0	0.08	0.02	0.02
Precision	0.92	1	0.92	0.96	0.99
F1-score	0.93	1	0.93	0.98	0.99
Accuracy score	0.92	1	0.92	0.97	0.98
Log loss	0.3	0.04	0.25	0.24	0.04
MCC	0.83	0.99	0.82	0.94	0.96
			Validation (15%)		
	SVM	**RF**	**SNN**	**DNN**	**CNN**
ROC-AUC	0.87	0.93	0.91	0.94	0.92
PR-AUC	0.93	0.96	0.92	0.96	0.94
TPR	0.89	0.93	0.86	0.92	0.87
FPR	0.16	0.07	0.17	0.15	0.14
TNR	0.84	0.93	0.83	0.85	0.86
FNR	0.11	0.07	0.14	0.08	0.13
Precision	0.9	0.95	0.88	0.9	0.9
F1-score	0.9	0.94	0.89	0.92	0.9
Accuracy score	0.87	0.93	0.86	0.9	0.88
Log loss	0.44	0.45	0.43	0.82	0.15
MCC	0.74	0.86	0.71	0.79	0.74
			Testing (15%)		
	SVM	**RF**	**SNN**	**DNN**	**CNN**
ROC-AUC	0.94	0.99	0.95	0.97	0.97
PR-AUC	0.96	0.99	0.98	0.98	0.98
TPR	0.89	0.95	0.88	0.92	0.93
FPR	0.15	0.03	0.12	0.1	0.08
TNR	0.85	0.97	0.88	0.9	0.92
FNR	0.11	0.05	0.12	0.08	0.07
Precision	0.91	0.98	0.92	0.94	0.95
F1-score	0.9	0.97	0.9	0.93	0.94
Accuracy score	0.88	**0.96**	0.88	0.91	0.93
Log loss	0.32	0.16	0.29	0.74	0.42
MCC	0.74	0.91	0.74	0.81	0.84

4.5 COASTAL EROSION VULNERABILITY MAPS

The CEV maps have been prepared from all the models separately. The vulnerability probability was categorized into 5 classes, namely very high, high, moderate, low, and very low with the equal interval reclassification method. The values are transferred to the geographical coastal polyline with approx. 30 m segments to aid in the calculation of length under each vulnerability class. 56.01% of coastal length are found to be under the high vulnerability category by CNN which is followed by SNN (48.47%), SVM (41.71%), RF (41.4%), and DNN (40.43%). On the other hand, the RF model predicts 41.39% of coastal length to be under very low vulnerability. This is followed by DNN (39.84%), CNN (32.26%), SNN (25.11%), and SVM (16.75%). The % length for all the vulnerability classes have been shown in fig. 4.8.

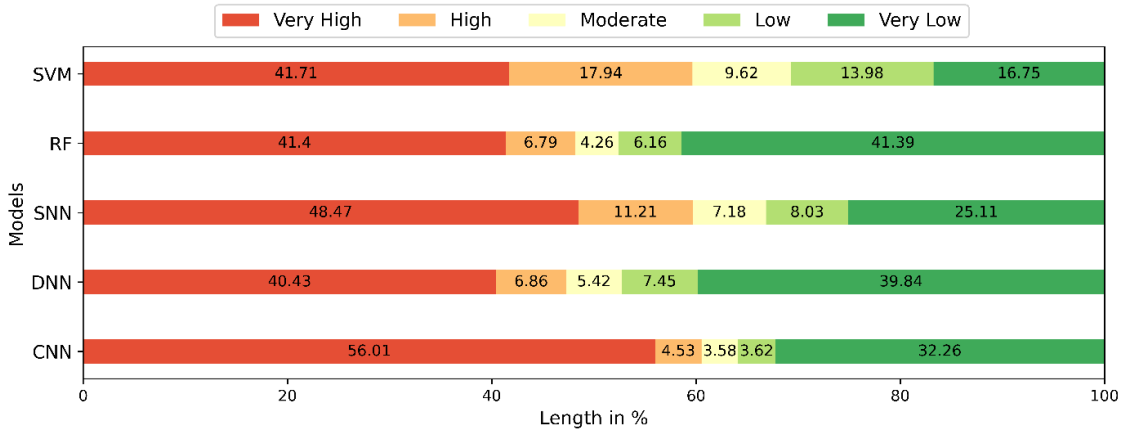

Figure 4.8 Area under each vulnerability class by different models

The CEV map as depicted in fig. 4.9 shows the distribution of vulnerability classes in various areas. The length under each class for the coastline of different districts has been tabulated in table 4.4. As a maximum value in the very high vulnerability class, 76.29% of the coastline of Bhadrak district by RF is closely followed by 75.24% of the coastline of Jagatsinghpur district by CNN. Only Bhadrak district by SVM (68.77%) as well as by SNN (74.41%), Jagatsinghpur (72.74%) and Puri (68.19%) districts by RF, Bhadrak (73.12%) and Jagatsinghpur (62.37%) districts by DNN, and Bhadrak (73.6%) and Puri (70.31%) districts by CNN, and Jagatsinghpur (73.67%) by SNN predicted more than 60% length under very high vulnerability category. The length under the very low vulnerability category for the Ganjam district is found to be 81.45% by DNN, 74.89% by RF, 74.83% by SNN, 74.2% by CNN, and 58.46% by SVM.

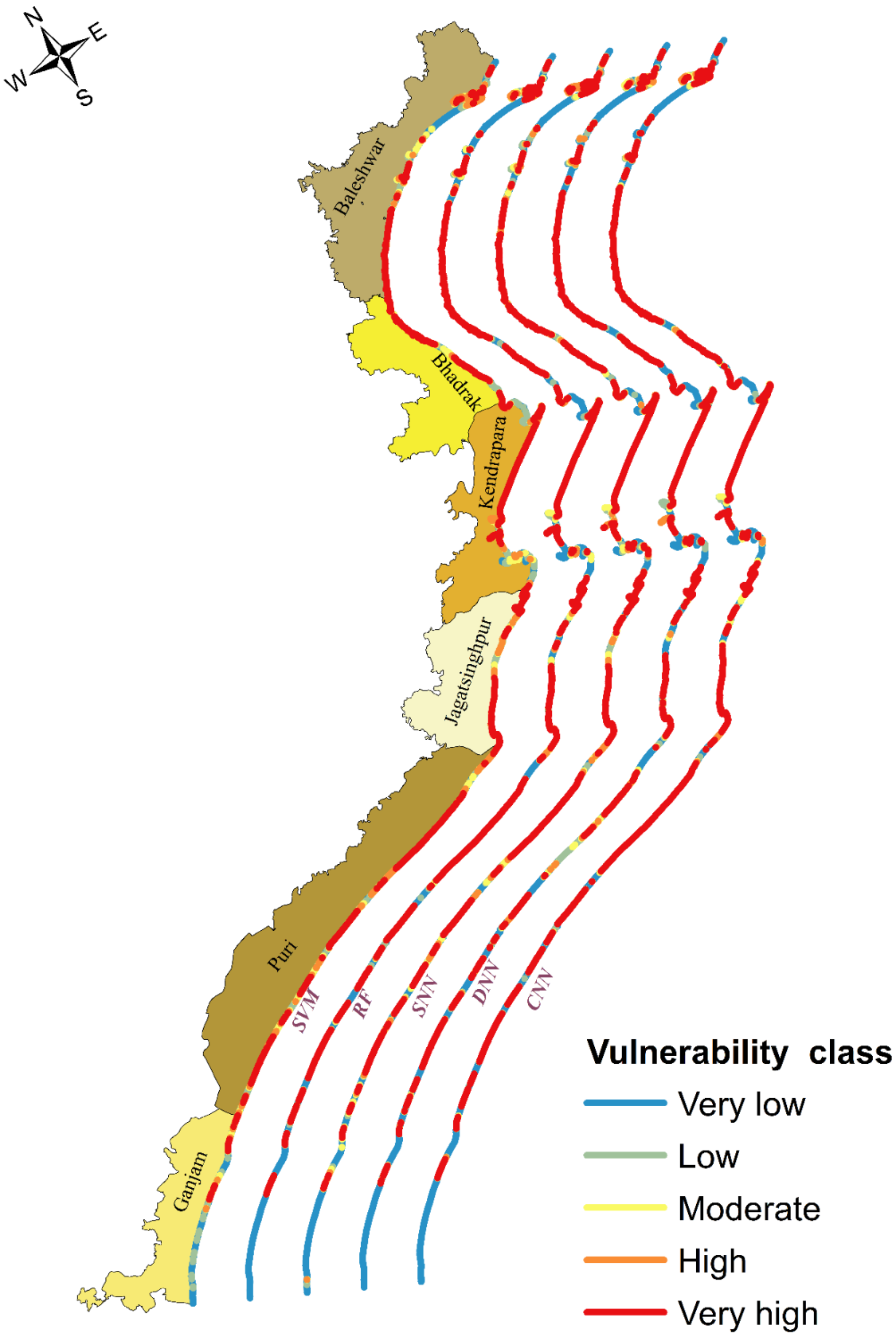

Figure 4.9 Coastal Erosion Vulnerability map

Table 4.4 Length (%) under different vulnerability categories of various districts by each model

Model	District	Very high	high	moderate	low	very low
SVM	Baleshwar	32.94	21.87	11.24	14.07	19.88
	Bhadrak	68.77	9.41	6.11	9.69	6.02
	Kendrapara	38.24	14.11	12.27	17.37	18.01
	Jagatsinghpur	59.29	15.46	8.66	13.8	2.79
	Puri	45.83	26.55	9.81	12.05	5.76
	Ganjam	11.33	9.44	4.97	15.8	58.46
RF	Baleshwar	44.95	8.33	5.06	6.43	35.23
	Bhadrak	76.29	2.39	1.29	3.82	16.21
	Kendrapara	44.36	8.01	4.75	8.33	34.55
	Jagatsinghpur	72.74	4.01	4.01	4.4	14.84
	Puri	68.19	3.35	2.39	2.33	23.74
	Ganjam	21.5	2.11	0.34	1.16	74.89
SNN	Baleshwar	40.74	13.17	8.58	10.91	26.6
	Bhadrak	74.41	7.49	2.76	5.39	9.95
	Kendrapara	41.8	15.61	7.87	8.39	26.33
	Jagatsinghpur	73.67	5.92	6.41	9.59	4.41
	Puri	55.45	12.05	8.21	7.25	17.04
	Ganjam	9.64	5.13	5.96	4.44	74.83
DNN	Baleshwar	33.21	9.42	8.18	6.75	42.44
	Bhadrak	73.12	2.57	2.66	1.75	19.9
	Kendrapara	38.83	9.75	3.99	7.89	39.54
	Jagatsinghpur	62.37	4.26	3.72	6.17	23.48
	Puri	36.61	6.86	7.81	12.76	35.98
	Ganjam	11.19	2.66	1.84	2.86	81.45
CNN	Baleshwar	45	8.68	4.74	6.52	35.06
	Bhadrak	73.6	4.99	3.45	2.48	15.48
	Kendrapara	48.6	3.97	5.53	4.94	36.96
	Jagatsinghpur	75.24	2.89	4.55	3.77	13.55
	Puri	70.31	3.47	1.6	1.5	23.12
	Ganjam	23.04	0.92	0.87	0.97	74.2

The distribution of the very high vulnerability zone is uniform for the entire coastal length except for the North-East side of Baleshwar and Ganjam district. Geologically, this very high probability can be linked to a soil bulk density of 1,040 to 1,400 kg/ cubic m, low organic carbon content (~ 1%), and presence of Eutric Fluvisols soil whereas the variation of pH is inconclusive. Similarly, the presence of Ferric Luvisols shows a very low vulnerability probability. This area can also be characterized by lower surface elevation. The moderate to low vulnerability areas can be directly linked to the presence of high vegetation. The North-East side of Baleshwar and

Ganjam district with high NDVI values (> 0.4) showed low vulnerability probability. The presence of Mangrove vegetation on the North and South East side of Kendrapara district also showed the same result. Thampanya et al. (2006) [93] in their study to understand the effect of mangrove deforestation on coastal erosion also found a similar relationship. A study done by Roy et al. (2019) [94] to estimate the condition of mangrove vegetation along the coast of Odisha found an increase of 53 sq. km forest area between 1990 and 2015 but they also warned about the anthropogenic threats to the same. The rainfall varies uniformly from North to South in the coastal area with the highest towards Baleshwar district and lowest towards Ganjam districts. This factor can also be linked directly with coastal erosion. Similar findings have also been documented by Salem et al. (2021) [95] who studied the effect of simulated uniform rainfall over the coastal areas of North-western Egypt.

The role of sea-level change and other oceanographic parameters are well documented in the literature and similar findings have also been established in this work. The sea-level change of more than 3.5 mm/ year strongly suggests the presence of high vulnerability probability but some coastal length of the Baleshwar and Bhadrak district also shows a high probability of vulnerability despite having decreasing trend in shoreline change. Jena et al. (2014) [16] in their study to find a relation between the shoreline and sea-level change along part of the coast of Odisha and West Bengal found a correlation between the two but also have stated the influence of other factors like storm surge and monsoon dynamic. The IPCC report on sea-level rise and its effect on coastal or low-lying areas has projected a rise by 0.43m by 2100 by following the most positive representative concentration pathway of 2.6. Also, the rise in sea level is not uniform and can vary up to ±30% based on local conditions [96]. This will decisively affect the erosion process and its severity. Similar to the sea level rise, the SWH observations show similar trends in vulnerability severity. The North-West facing waves are found to produce high to very high vulnerability whereas the Westward waves are somewhat responsible for moderate to very low vulnerability. The tidal range of 1.5m or higher is observed to be associated with high and very high vulnerability categories in the region. The relation of the tidal cycle with the regional coastal changes in the Guyanas region by Gratiot et al. (2008) [60]proved the role of low tide levels in gentle coastal slope and that 60% of the erosion in the area will be by the tidal effect.

4.6 FACTOR IMPORTANCE (FI) ANALYSIS

The FIs have been calculated for the whole coastal stretch of the study area (fig. 4.10) as well as for each district (fig. 4.11) and block (fig. 4.12) separately. At the state level, among all CEVFs, rainfall is found to be the most influential. The factors related to sea conditions such as wave period, wave direction, sea-level change, SWH, and sea surface elevation also showed significant importance. Together with NDVI, soil factors like bulk density and pH of soil showed noticeable influence as compared to geology, organic carbon content, silt, sand, and clay contents of the soil. Socio-economic factors like agricultural land density, population density, settlement density, and distance from the road also showed high importance whereas literacy rate, percentage of agricultural workers, availability of electricity, LULC changed to settlement or agriculture, drinking water facility, and hospital showed very little to almost no influence.

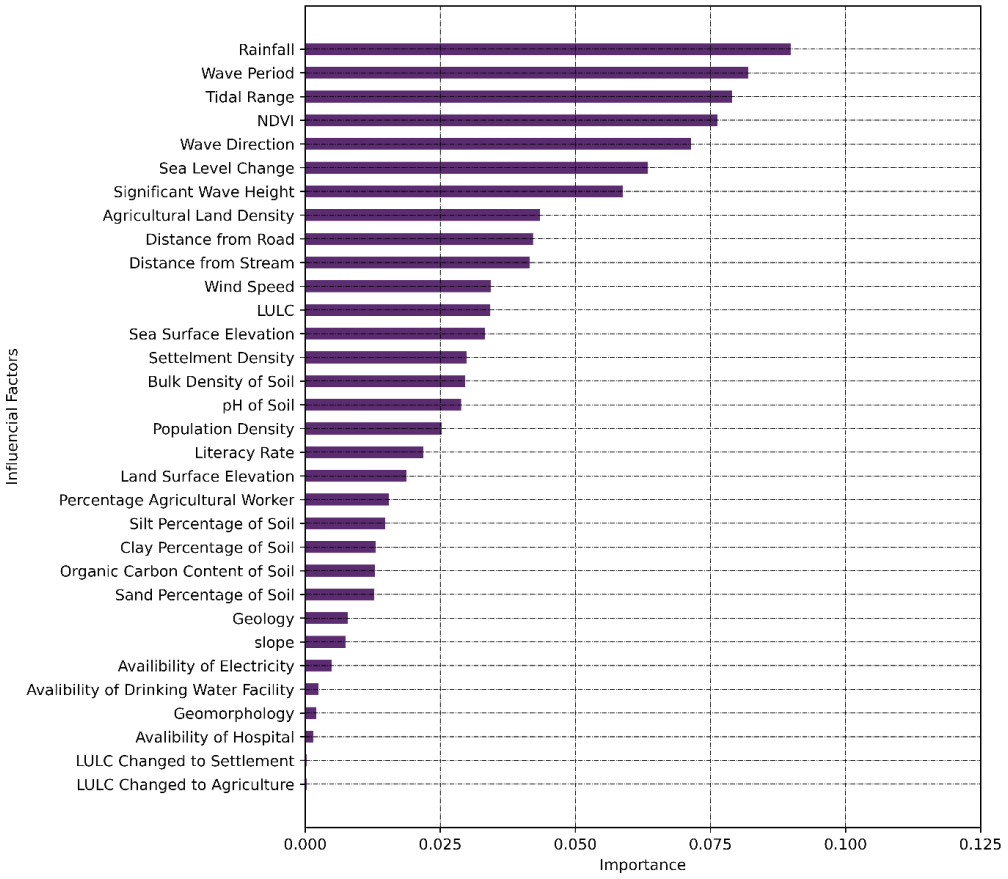

Figure 4.10 FI at the state level

At the district level, the wave direction for Baleshwar, rainfall for Bhadrak, SWH, and wave direction for Kendrapara are most influential. The wave period is the

most important factor for Jagatsinghpur, Puri, and Ganjam. At the block level, sea Surface Elevation, land surface elevation, sea-level change, significant wave height, wave direction, wave period, tidal range, wind speed, pH of the soil, bulk density of soil, sand percentage of soil, silt percentage of soil, rainfall, NDVI, distance from the stream, distance from the road, percentage agricultural worker, and availability of drinking water facility are found to be influential factors.

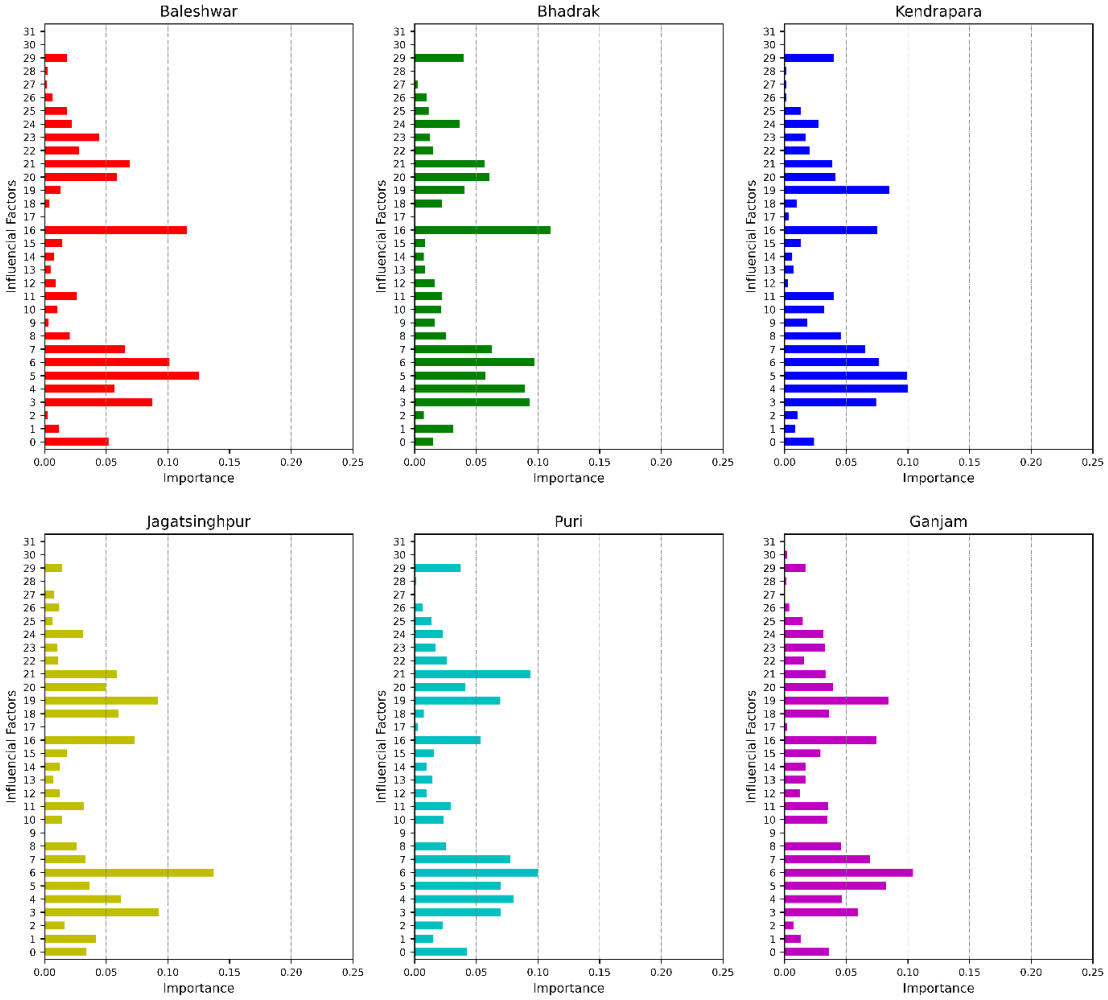

Figure 4.11 FI at the district level. 0 - Sea Surface Elevation, 1 - land surface elevation, 2- slope 3 - sea-level change, 4 - significant wave height, 5 - wave direction, 6 – wave period, 7 – tidal range, 8 - wind speed, 9 - geology, 10 - pH of soil, 11 - bulk density of soil, 12 - organic carbon content of soil, 13 - clay percentage of soil, 14 - sand percentage of soil, 15 - silt percentage of soil, 16 - rainfall, 17 - geomorphology, 18 - LULC, 19 - NDVI, 20 - distance from stream, 21 - distance from road, 22 - population density, 23 - settlement density, 24 - literacy rate, 25 - percentage agricultural worker, 26 - availability of electricity, 27 - availability of drinking water facility, 28 - availability of hospital, 29 - agricultural land density, 30 - LULC changed to settlement, 31 - LULC changed to agriculture

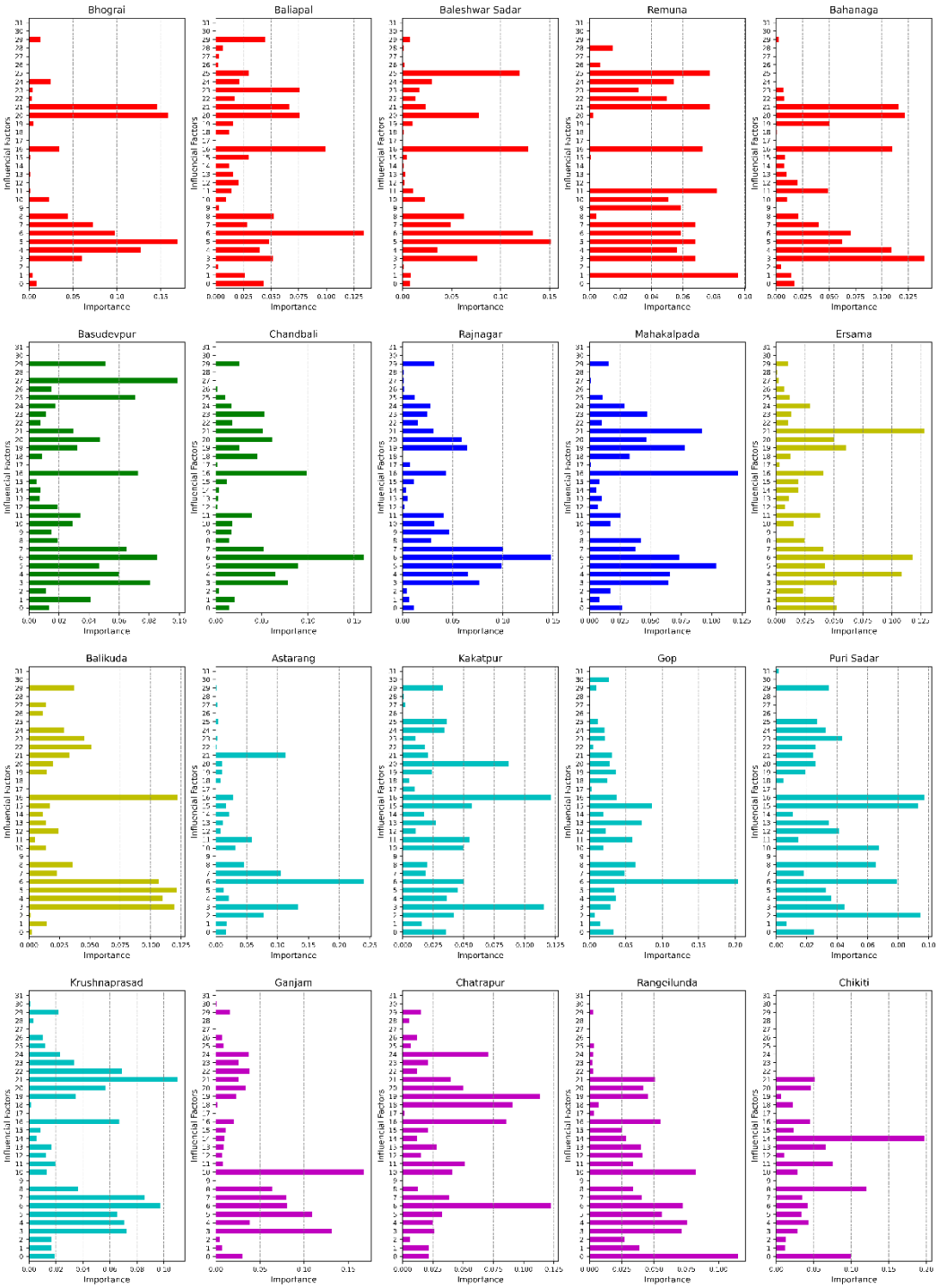

Figure 4.12 FI at the district level. 0 - Sea Surface Elevation, 1 - land surface elevation, 2- slope 3 - sea-level change, 4 - significant wave height, 5 - wave direction, 6 – wave period, 7 – tidal range, 8 - wind speed, 9 - geology, 10 - pH of soil, 11 - bulk density of soil, 12 - organic carbon content of soil, 13 - clay percentage of soil, 14 - sand percentage of soil, 15 - silt percentage of soil, 16 - rainfall, 17 - geomorphology, 18 - LULC, 19 - NDVI, 20 - distance from stream, 21 - distance from road, 22 - population density, 23 - settlement density, 24 - literacy rate, 25 - percentage agricultural worker, 26 - availability of electricity, 27 - availability of drinking water facility, 28 - availability of hospital, 29 - agricultural land density, 30 - LULC changed to settlement, 31 - LULC changed to agriculture

The research also suggests a considerable influence of anthropogenic or socio-economic factors. Though at the state as well as district-level most influential factors are not related to the same, other predominant factors in the process are related to various socio-economic parameters such as density of settlement, agricultural land, and road. Magoon et al. (2020) [96] have done extensive research on the topic of anthropogenic effects on coastal erosion. They have concluded that various human activities throughout the centuries are impacting and disturbing the coastal sediment supply cycle. The uncontrolled construction of harbors, dams, or hard coastal protection as well as the reuse of coastal land to meet the population demand are creating a shortage in supply of the sediments to the coast and increasing coastal erosion.

Concerning coastal erosion, 2 of the 17 sustainable development goals (SDG) laid by the United Nations and supported by 193 countries [97] can be directly linked. SDG 13 on climate change urges to take immediate action to address the climate crisis and its consequences [98] and SDG 15 on life on the land advice safeguarding, preserving, and fostering the responsible use of ecological systems and preventing and restore soil degradation [99] demonstrate the importance of this disaster in the global scale. The analysis suggests that coastal erosion is not a simple process rather it depends on various factors which change intricately. These changes are already impacting the coastal ecosystem and reducing its ability to adapt to the rapid shift in climatic conditions [100]. This problem is causing risk to the coastal communities, their infrastructures, and agricultural sources along with the groundwater quality by the intrusion of seawater. Excessive progression in the seawater intrusion has been discovered along the coastal stretch of the Puri district [101]. Fig. 4.13 shows the ground conditions and severity of erosion in the study region. Admittedly, the issue of coastal erosion has been addressed in many places worldwide and to some extent in the study area. The most common method in this regard is hard coastal protection. Structures like embankments, sea walls, or dykes provide short-term protection but their cost and benefits in longer periods show less satisfactory results [100] and also can accelerate the erosion process in the nearby areas. Also, these hard structures restrict the natural sub-surface flow of groundwater to the sea causing an unfavourable rise in the groundwater table which can create coastal flooding in the long term [102].

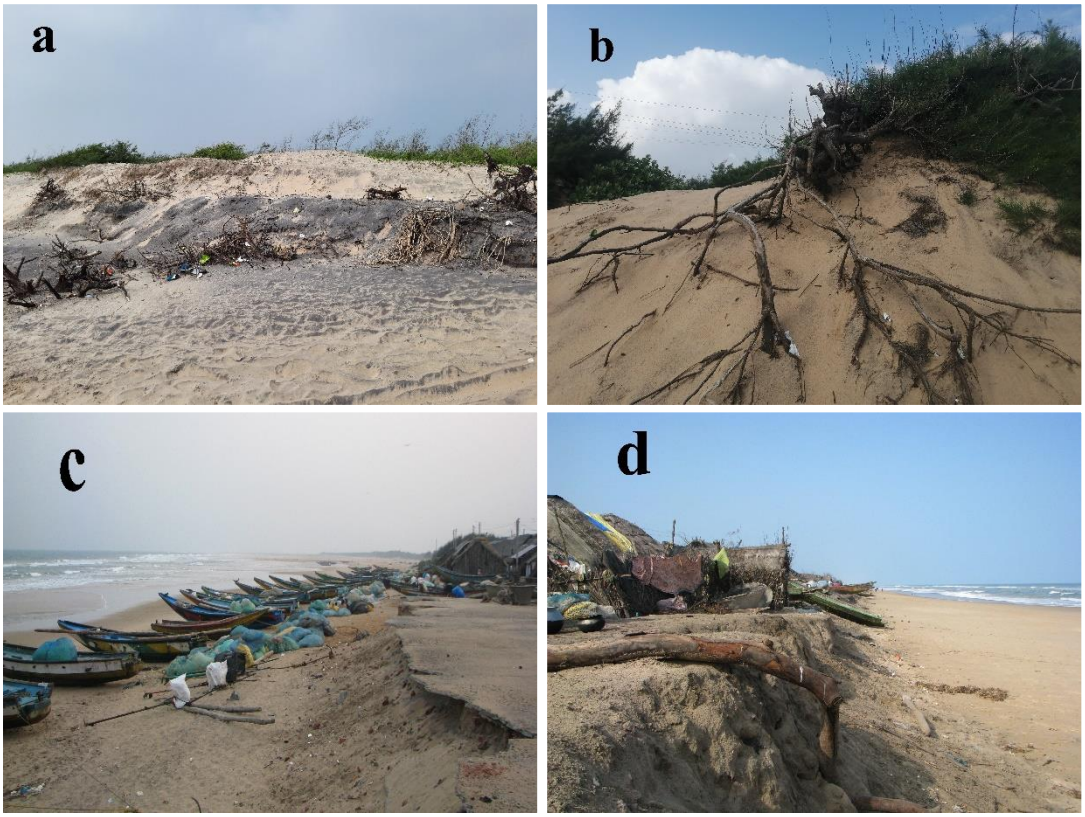

Figure 4.13 Coastal erosion at (a) Siali beach of Jagatsinghpur, (b) Chandrabhaga beach of Puri, (c) and (d) Podampeta village of Ganjam [Photo credit (c) and (d): Aarthi Sridhar, Dakshin Foundation]

Other sophisticated protective measures which can address these issues can prove cost-efficient in highly populated areas but may not be feasible to get adopted by developing or underdeveloped nations [100]. Other methods to tackle this natural disaster is the construction of adoptive advanced building foundations, reestablishments of coastal mangrove cover, or as a final measure coastal retreat [5]. Haasnoot et al. [90] in their discussion on various measures to be taken for coastal retreats have pointed out the need for awareness of the sea level rise and the requirement for the development of satisfactory policies for the retreat process with its proper execution. Correa and Gonzalez [103] have explained the retreat or relocation process of El Choncho island village located on the Colombian Pacific coast by 200m landward in 1997. Similar efforts have been initiated in the Satabhaya village of Kendrapara district to relocate 118 families. As derived from the analysis, the rainfall condition is the most influential factor for coastal erosion in the study area. The change in rainfall pattern can intensify the erosion process, especially if loose soil is present. The remedial measure of such finding should be to handle the loose soil problem. This can be done by revegetation the

coastal zone which will increase the soil stability and protect the coastal land from the adverse effect of erosion [104].

CHAPTER 5

CONCLUSIONS

As of 2003, 41% of the global population lived in the coastal zone and about 28% of this area has been altered by human activities. The numbers are also high for India with 19,300 people living in the 100 sq. km of the coastal zone as of 2015 which is an increase from 16,400 people in 2003 [1]. Due to the coastal erosion, the coastal ecosystem, as well as the human population living near it, are at great risk. Between 1984 and 2015, Mentaschi et al. (2018) [3] found that about 28,000 sq. km land area has been lost.

The shoreline positions derived from the Landsat satellites from the year 1973 to 2020 have been analyzed with the help of the DSAS tool. The NSM, EPR, and LRR values calculated at the district level shows the Bhadrak, Kendrapara, and Jagatsinghpur district are in maximum danger due to erosion. The estuaries of Subarnarekha River and Devi River, also the areas near Paradeep and Dhamra Port are some of the hotspots for erosion. The predicted future shoreline shows except for the Ganjam district; all 5 coastal districts will show the overall landward movement in the next 20 years. Specifically the estuaries will witness the maximum negative change according to the forecast. The whole state has lost 72.47 sq. km of land against the gain of 42.83 sq. km. The Rajnagar block of Kendrapara has lost a maximum of 10.189 sq. km of land area. This study concludes that the Odisha coast is under high erosion and showing signs of escalation in the near future. Also as evident by similar research, it is evident that various natural, as well as anthropogenic conditions, are causing the erosion. The constructed coastal protective structures have failed to fulfill their objective in some places. These statistics or the study can be taken as reference by policymakers or institutions in making a proper and robust work plan for the prevention as well as mitigation of this unfortunate disaster. By a thorough analysis of the locations showing high erosions different protective structures or natural barriers such as plantation of coastal vegetation can be done to control and mitigate the erosion process.

Furthermore the present work has discussed a different and modern approach to estimating the coastal erosion vulnerability with machine learning and deep learning algorithms that have never been adopted to address the issue. Excellent accuracy of all the applied models (SVM, RF, SNN, DNN, CNN) with the highest for RF proved the successful application of machine learning to model and study the effect of coastal erosion. Analysis showed that coastal erosion is a major issue for Odisha with more than 50% of coastal length under the very high vulnerability category. Among the 6 coastal districts, apart from Ganjam, all other 5 districts are being greatly affected by this natural disaster. Models have been created with 21 environmental and 11 socio-economic factors, additionally, factor importance analysis on these, resulted in rainfall being the most influential factor for the coastal erosion in the state. Sea level change, tidal range, SWH, wave period, settlement, and agricultural land densities also showed substantial control over it at the state as well as district level. The analysis showed that the changing climatic conditions related to the variation in rainfall patterns, the altercation of ocean parameters, human-induced variables related to change in land cover patterns, and changes in vegetation cover are prime causes of this disaster. This shows the influence of both environmental and anthropogenic factors in the process of erosion. However this should be studied further to understand the fractional contribution of these two types in the whole progression. A further avenue of research to this approach include a careful selection of variables for this complex coastal dynamic problem to address the issue in other geographical setting or at the global scale, moreover, other ML algorithms can be explored to create a simpler yet sophisticated model. However, the presented work will open new techniques to understand the process and effect of coastal erosion and surely help in the work of officials and government organizations in making efficient decisions.

REFERENCES

[1] M. L. Martínez, A. Intralawan, G. Vázquez, O. Pérez-Maqueo, P. Sutton and R. Landgrave, "The coasts of our world: Ecological, economic and social importance," *Ecological Economics,* vol. 63, pp. 254-272, 2007.

[2] A. Rizzo and G. Anfuso , "Coastal Dynamic and Evolution: Case Studies from Different Sites around the World," *Water,* vol. 12, p. 2829, 2020.

[3] L. Mentaschi, M. I. Vousdoukas, J. F. Pekel, E. Voukouvalas and L. Feyen, "Global long-term observations of coastal erosion and accretion," *Sci Rep,* vol. 8, p. 12876, 2018.

[4] T. A. Łabuz, "Environmental Impacts—Coastal Erosion and Coastline Changes," in *Second Assessment of Climate Change for the Baltic Sea Basin*, Springer, Cham, 2015, pp. 381-396.

[5] P. P. Wong, "Where Have All the Beaches Gone? Coastal Erosion In The Tropics," *Singapore Journal of Tropical Geography,* vol. 24, pp. 111-132, 2003.

[6] I. Valiela, J. L. Bowen and J. K. York, "Mangrove Forests: One of the World's Threatened Major Tropical Environments: At least 35% of the area of mangrove forests has been lost in the past two decades, losses that exceed those for tropical rain forests and coral reefs, two other well-known threa," *BioScience,* vol. 51, p. 807–815, 2001.

[7] R. H. Charlier and C. P. De Meyer, "Chapter I: Coastal erosion," in *Coastal Erosion: Response and Management,* pringer Berlin Heidelberg, 1998, pp. 153-295.

[8] R. Silva, M. L. Martínez, P. A. Hesp, P. Catalan, A. F. Osorio, R. Martell, M. Fossati, G. M. da Silva, I. Mariño-Tapia, P. Pereira, R. Cienguegos, A. Klein and G. Govaere, "Present and future challenges of coastal erosion in Latin America," *Journal of Coastal Research,* vol. 71, pp. 1-16, 2014.

[9] B. Fox-Kemper, H. T. Hewitt, C. Xiao, G. Aðalgeirsdóttir, S. S. Drijfhout, T. L. Edwards, N. R. Golledge, M. Hemer, R. E. Kopp, G. Krinner, A. Mix, D. Notz, S. Nowicki, I. S. Nurhati, L. Ruiz, J. B. Sallée, A. B. A. Slangen and Y. Yu, "Ocean, Cryosphere and Sea Level Change," *Climate Change 2021: The Physical Science Basis. Contribution of Working Group I to the Sixth Assessment Report of the Intergovernmental Panel on Climate Change,* 2021.

[10] B. C. O'Neill, E. Kriegler, K. Riahi, K. L. Ebi, S. Hallegatte, T. R. Carter, R. Mathur and D. P. Vuuren , "A new scenario framework for climate change research: the concept of shared socioeconomic pathways," *Clim. Change,* vol. 122, p. 387–400, 2013.

[11] M. K. Ghosh, L. Kumar and C. Roy, "Monitoring the coastline change of Hatiya Island in Bangladesh using remote sensing techniques," *ISPRS J Photogramm Remote Sens,* vol. 101, pp. 137-144, 2015.

[12] H. M. El-Asmar and M. E. Hereher, "Change detection of the coastal zone east of the Nile Delta using remote sensing," *Environ Earth Sci,* vol. 62, p. 769–777, 2011.

[13] M. Mishra, T. Acharyya, P. Chand, C. A. G. Santos, D. Kar, P. P. Das, N. Pattnaik, R. M. da Silva and T. V. M. do Nascimento, "Analyzing shoreline

dynamicity and the associated socioecological risk along the Southern Odisha Coast of India using remote sensing-based and statistical approaches," *Geocarto Int,* pp. 1-36, 2021.

[14] R. Bishop-Taylor, R. Nanson, S. Sagar and L. Lymburner, "Mapping Australia's dynamic coastline at mean sea level using three decades of Landsat imagery," *Remote Sens Environ,* vol. 267, p. 112734, 2021.

[15] I. Mondal, S. Thakur, M. Juliev, J. Bandyopadhyay and T. K. De, "Spatio-temporal modelling of shoreline migration in Sagar Island, West Bengal, India," *J Coast Conserv,* vol. 24, 2020.

[16] A. Jana, A. Biswas, S. Maiti and A. Bhattacharya, "Shoreline changes in response to sea level rise along Digha Coast, Eastern India: an analytical approach of remote sensing, GIS and statistical techniques," *J Coast Conserv,* vol. 18, p. 145–155, 2014.

[17] M. Kupilik, F. D. W. Witmer, E. A. MacLeod, C. Wang and T. Ravens, "Gaussian Process Regression for Arctic Coastal Erosion Forecasting," *IEEE Trans Geosci Remote Sens,* vol. 57, pp. 1256 - 1264, 2019.

[18] C. Yin, L. T. Binh, D. T. Anh, S. T. Mai, A. Le, V. H. Nguyen, V. C. Nguyen, H. Tanaka and T. Q. Duong, "Advanced Machine Learning Techniques for Predicting Nha Trang Shorelines," *IEEE Access,* vol. 9, pp. 98132 - 98149, 2021.

[19] P. S. Mujabar and N. Chandrasekar, "Coastal erosion hazard and vulnerability assessment for southern coastal Tamil Nadu of India by using remote sensing and GIS," *Natural Hazards,* vol. 69, p. 1295–1314, 2013.

[20] B. Sahoo and P. K. Bhaskaran, "Multi-hazard risk assessment of coastal vulnerability from tropical cyclones – A GIS based approach for the Odisha coast," *J Environ Manage,* vol. 206, pp. 1166-1178, 2018.

[21] A. Peponi, P. Morgado and J. Trindade, "Combining Artificial Neural Networks and GIS Fundamentals for Coastal Erosion Prediction Modeling," *Sustainability,* vol. 11, p. 975, 2019.

[22] M. A. Islam, D. Mitra, A. Dewan and S. H. Akhter, "Coastal multi-hazard vulnerability assessment along the Ganges deltaic coast of Bangladesh–A geospatial approach," *Ocean & Coastal Management,* vol. 127, pp. 1-15, 2016.

[23] G. Alexandrakis and S. E. Poulos , "An holistic approach to beach erosion vulnerability assessment," *Scientific Reports,* vol. 4, p. 6078, 2014.

[24] N. Rangel-Buitrago, W. J. Neal and V. N. de Jonge, "Risk assessment as tool for coastal erosion management," *Ocean Coast Manag,* vol. 186, p. de Jonge, 2020.

[25] M. M. R, A. M and V. P, "A new insight to vulnerability of Central Odisha coast, India using analytical hierarchical process (AHP) based approach," *Journal of Coastal Conservation,* vol. 22, p. 799–819, 2018.

[26] B. E. G. Perez and J. J. Selvaraj, "Evaluation of coastal vulnerability for the District of Buenaventura, Colombia: A geospatial approach," *Remote Sensing Applications: Society and Environment,* vol. 16, p. 100263, 2019.

[27] R. Behera, A. Kar, M. R. Das and P. P. Panda, "GIS-based vulnerability mapping of the coastal stretch from Puri to Konark in Odisha using analytical hierarchy process," *Natural Hazards,* vol. 96, p. 731–751, 2019.

[28] M. K. Pramanik, P. Dash and D. Behal, "Improving outcomes for socioeconomic variables with coastal vulnerability index under significant sea-level rise: an approach from Mumbai coasts," *Environ Dev Sustain,* vol. 23, p. 13819–13853,

2021.

[29] P. Subraelu, M. M. Yagoub, A. Sefelnasr, K. N. Rao, R. Sekhar A, M. Sherif and A. A. Ebraheem, "Sea-level Rise and Coastal Vulnerability: A Preliminary Assessment of UAE Coast through Remote Sensing and GIS," *J Coast Zone Manag,* vol. 24, p. 477, 2021.

[30] E. Furlan, P. D. Pozza, M. Michetti, S. Torresan, A. Critto and A. Marcomini, "Development of a Multi-Dimensional Coastal Vulnerability Index: Assessing vulnerability to inundation scenarios in the Italian coast," *Sci. Total Environ,* vol. 772, p. 144650, 2021.

[31] S. Velsamy, G. Balasubramaniyan, B. Swaminathan and D. Kesavan, "Multi-decadal shoreline change analysis in coast of Thiruchendur Taluk, Thoothukudi district, Tamil Nadu, India, using remote sensing and DSAS techniques," *Arab J Geosci,* vol. 13, p. 838, 2020.

[32] L. Natarajan, N. Sivagnanam, T. Usha, L. Chokkalingam, S. Sundar, M. Gowrappan and P. D. Roy, "Shoreline changes over last five decades and predictions for 2030 and 2040: a case study from Cuddalore, southeast coast of India," *Earth Sci Inform,* vol. 14, 1315–1325 2021.

[33] G. Barik, B. Guru and F. Sangma, "Shoreline Changes Analysis and Forecast Using Digital Shoreline Assessment System 5.0: Evidences from Parts of East Coast of India," *J Indian Soc Remote Sens,* vol. 49, p. 2815–2830, 2021.

[34] E. B. Goldstein, G. Coco and N. G. Plant, "A review of machine learning applications to coastal sediment transport and morphodynamics," *Earth-Science Reviews,* vol. 194, pp. 97-108, 2019.

[35] S. Iwasaki, "Linking disaster management to livelihood security against tropical cyclones: A case study on Odisha state in India," *Int J Disaster Risk Reduct,* vol. 19, pp. 57-63, 2016.

[36] M. A. Wulder, T. R. Loveland, D. P. Roy, C. J. Crawford, J. G. Masek and C. E. Woodcock, "Current status of Landsat program, science, and applications," *Remote Sens Environ,* vol. 225, pp. 127-147, 2019.

[37] S. J. Holgate, A. Matthews, P. L. Woodworth, L. J. Rickards, M. E. Tamisiea, E. Bradshaw, P. R. Foden, K. M. Gordon, S. Jevrejeva and J. Pugh, "New Data Systems and Products at the Permanent Service for Mean Sea Level," *Journal of Coastal Research,* vol. 29, p. 493 – 504, 2013.

[38] "Permanent Service for Mean Sea Level (PSMSL), 2021," 06 Sep 2021. [Online]. Available: http://www.psmsl.org/data/obtaining/.

[39] C. E. Parente, I. C. M. Nogueira, R. P. Martins and E. O. Ribeiro, "Wave climatology," in *Meteorology and Oceanography*, Elsevier, 2017, pp. 55-98.

[40] T. Hengl, J. M. de Jesus, G. B. Heuvelink, M. R. Gonzalez, M. Kilibarda, A. Blagotić, S. Wei, M. N. Wright, X. Geng, B. Bauer-Marschallinger, M. A. Guevara, R. Vargas, R. A. MacMillan, N. H. Batjes, J. G. Leenaars, E. Ribeiro, I. Wheeler, S. Mantel and B. Kempen, "SoilGrids250m: Global gridded soil information based on machine learning," *PLoS one,* vol. 12, p. e0169748, 2017.

[41] E. A. Bryant, Rainfall and beach erosion relationships, Stanwell Park, Australia, 1895 - 1980: worldwide implications for coastal erosion, 1985.

[42] C. Schweiger, N. Koldrack, C. Kaehler and H. Schuettrumpf, "Influence of Nearshore Bathymetry Changes on the Numerical Modelling of Dune Erosion," *J Coast Res,* vol. 36, pp. 545-558, 2020.

[43] S. L. Gallop, A. Vila-Concejo, T. E. Fellowes, M. D. Harley, M. Rahbani and J. L. Largier, "Wave direction shift triggered severe erosion of beaches in estuaries and bays with limited post-storm recovery," *Earth Surf Process Landf,* vol. 45, pp. 3854-3868, 2020.

[44] A. Toimil, P. Camus, I. J. Losada, G. L. Cozannet, R. J. Nicholls, D. Idier and A. Maspataud, "Climate change-driven coastal erosion modelling in temperate sandy beaches: Methods and uncertainty treatment," *Earth Sci Rev,* vol. 202, p. 103110, 2020.

[45] T. R. Healy, "Coastal Wind Effects," in *Encyclopedia of Coastal Science. Encyclopedia of Earth Science Series*, Dordrecht, Science Series. Springer, 2005.

[46] L. M. Valvo, A. B. Murray and A. Ashton, "How does underlying geology affect coastline change? An initial modeling investigation," *J Geophys Res Earth Surf,* vol. 111, 2006.

[47] S. Matsumoto, S. Ogata, H. Shimada, T. Sasaoka, A. Hamanaka and G. J. Kusuma, "Effects of pH-Induced Changes in Soil Physical Characteristics on the Development of Soil Water Erosion," *Geosciences,* vol. 8, p. 134, 2018.

[48] R. Jepsen, J. Roberts and W. Lick, "Effects of Bulk Density on Sediment Erosion Rates," *Water Air Soil Pollut,* vol. 99, p. 21–31, 1997.

[49] S.-H. Jien, M.-H. Lee, Z.-Y. Hseu and H.-H. Wang, "Erosion Potential Estimation by Network Measurement of Soil Properties in Coastal Areas after Clearcutting," *Int J Distrib Sens Netw,* vol. 11, 2015.

[50] A. Mosavi, F. Sajedi-Hosseini, B. Choubin, F. Taromideh, G. Rahi and A. A. Dineva, "Susceptibility Mapping of Soil Water Erosion Using Machine Learning Models," *Water,* vol. 12, p. 1995, 2020.

[51] H. Sahour, V. Gholami, M. Vazifedan and S. Saeedi, "Machine learning applications for water-induced soil erosion modeling and mapping," *Soil Tillage Res,* vol. 211, p. 105032, 2021.

[52] A. P. Young, R. T. Guza, R. E. Flick, W. C. O'Reilly and R. Gutierrez, "Rain, waves, and short-term evolution of composite seacliffs in southern California," *Mar Geol,* vol. 267, pp. 1-7, 2009.

[53] A. P. Young, R. T. Guza, H. Matsumoto, M. A. Merrifield, W. C. O'Reilly and Z. M. Swirad, "Three years of weekly observations of coastal cliff erosion by waves and rainfall," *Geomorphology,* vol. 375, p. 107545, 2021.

[54] N. Ahmed, N. Howlader, M. A. Hoque and B. Pradhan, "Coastal erosion vulnerability assessment along the eastern coast of Bangladesh using geospatial techniques," *Ocean Coast Manag,* vol. 199, p. 105408, 2021.

[55] B. R. Silliman, Q. He, C. Angelini, C. S. Smith, M. L. Kirwan, P. Daleo, J. J. Renzi, J. Butler, T. Z. Osborne, J. C. Nifong and J. V. Koppel, "Field Experiments and Meta-analysis Reveal Wetland Vegetation as a Crucial Element in the Coastal Protection Paradigm," *Curr Biol,* vol. 29, pp. 1800-1806, 2019.

[56] M. K. Layek, P. Sengupta and A. Mukherjee, "Erosional features identification along a recently prograding coastal barrier by ground penetrating radar facies analysis: Paradeep, Odisha, India," *J Coast Conserv,* vol. 23, p. 121–131, 2019.

[57] H. Brandes, O. Doygun, O. Francis, G. Zhang, C. Rossi, L. Yang and H. Togia, "CRESI: A susceptibility index methodology to assess roads threatened by coastal erosion," *Ocean Coast Manag,* vol. 213, p. 105845, 2021.

[58] P. D. Kunte, N. Jauhari, U. Mehrotra, M. Kotha, A. S. Hursthouse and A. S.

Gagnon, “Multi-hazards coastal vulnerability assessment of Goa, India, using geospatial techniques,” *Ocean Coast Manag,* vol. 95, pp. 264-281, 2014.

[59] R. M. Gonçalves, A. Saleem, H. A. A. Queiroz and J. L. Awange, “A fuzzy model integrating shoreline changes, NDVI and settlement influences for coastal zone human impact classification,” *Appl Geogr,* vol. 113, p. 102093, 2019.

[60] M. Z. Hoque, S. Cui, L. Xu, I. Islam , J. Tang and S. Ding, “Assessing Agricultural Livelihood Vulnerability to Climate Change in Coastal Bangladesh,” *Int. J. Environ. Res. Public Health,* vol. 16, p. 4552, 2019.

[61] F. Riva, H. Ahlborg, E. Hartvigsson, S. Pachauri and E. Colombo, “Electricity access and rural development: Review of complex socio-economic dynamics and causal diagrams for more appropriate energy modelling,” *Energy Sustain Dev,* Vols. 203-223, pp. 203-223, 2018.

[62] A. K. Choirunnisa and S. M. Giyarsih, “The Socioeconomic Vulnerability of Coastal Communities to Abrasion In Samas, Bantul Regency, Indonesia,” *Quaest. Geogr,* vol. 37, pp. 115 - 126, 2018.

[63] H. Jin, X. Qian, T. Chin and H. Zhang, “A Global Assessment of Sustainable Development Based on Modification of the Human Development Index via the Entropy Method,” *Sustainability,* vol. 12, p. 3251, 2020.

[64] S. Mohammed, S. H. Abdo, S. Szabo, Q. B. Pham, I. J. Holb, N. T. T. Linh, D. T. Anh, K. Alsafadi, A. Mokhtar, I. Kbibo, J. Ibrahim and J. Rodrigo-Comino, “Estimating Human Impacts on Soil Erosion Considering Different Hillslope Inclinations and Land Uses in the Coastal Region of Syria,” *Water,* vol. 12, p. 2786, 2020.

[65] A. Guneroglu, “Prioritising coastal zone management issues through fuzzy cognitive mapping approach,” *Ocean Coast Manag,* vol. 118, pp. 225-233, 2015.

[66] M. Wang, “Remote sensing of the ocean contributions from ultraviolet to near-infrared using the shortwave infrared bands: simulations,” *Appl Opt,* vol. 46, pp. 1535-1547, 2007.

[67] M. Nazeer, J. E. Nichol and Y. K. Yung, “Evaluation of atmospheric correction models and Landsat surface reflectance product in an urban coastal environment,” *Int J Remote Sens,* vol. 35, pp. 6271-6291, 2014.

[68] L. Congedo, “Semi-Automatic Classification Plugin: A Python tool for the download and processing of remote sensing images in QGIS,” *J Open Source Softw,* vol. 6, p. 3172, 2021.

[69] M. S. Hossain, M. Yasir, P. Wang, S. Ullah, M. Jahan, S. Hui and Z. Zhao, “Automatic shoreline extraction and change detection: A study on the southeast coast of Bangladesh,” *Marine Geology,* vol. 441, p. 106628, 2021.

[70] E. A. Himmelstoss, R. E. Henderson, M. G. Kratzmann and A. S. Farris, “Digital Shoreline Analysis System (DSAS) Version 5.1 User Guide,” Geological Survey Open-File Report 2021–1091, 2021.

[71] S. Weisberg, Applied linear regression, vol. 528, John Wiley & Sons, 2005.

[72] R. E. Kalman, “A New Approach to Linear Filtering and Prediction Problems,” *J Basic Eng,* vol. 82, pp. 35-45, 1960.

[73] J. W. Long and N. G. Plant, “Extended Kalman Filter framework for forecasting shoreline evolution,” *Geophys Res Lett,* vol. 39, 2012.

[74] M. A. Hearst, S. T. Dumais, E. Osuna, J. Platt and B. Scholkopf, “Support vector machines,” *IEEE Intelligent Systems and their applications,* vol. 13, pp. 18 - 28,

1998.

[75] M. A. Nanda, K. B. Seminar, D. Nandika and A. Maddu, “A Comparison Study of Kernel Functions in the Support Vector Machine and Its Application for Termite Detection,” *Information,* vol. 9, 2018.

[76] L. Breiman, “Random Forests,” *Machine Learning,* vol. 45, p. 5–32, 2001.

[77] A. Olawoyin and Y. Chen, “Predicting the Future with Artificial Neural Network,” *Procedia Computer Science,* vol. 140, pp. 383-392, 2018.

[78] X. Glorot and Y. Bengio, “Understanding the difficulty of training deep feedforward neural networks,” *roceedings of the Thirteenth International Conference on Artificial Intelligence and Statistics*, vol. 9, pp. 249-256, 2010.

[79] D. E. Kim and M. Gofman, “Comparison of shallow and deep neural networks for network intrusion detection,” *IEEE 8th Annual Computing and Communication Workshop and Conference (CCWC),* 2018.

[80] T. Fawcett, “An introduction to ROC analysis,” *Pattern Recognition Letters,* vol. 27, p. 861–874, 2006.

[81] D. Chicco and G. Jurman , “The advantages of the Matthews correlation coefficient (MCC) over F1 score and accuracy in binary classification evaluation,” *BMC Genomics,* vol. 21, 2020.

[82] Y. Ho and S. Wookey, “The Real-World-Weight Cross-Entropy Loss Function: Modeling the Costs of Mislabeling,” *IEEE Access,* vol. 8, pp. 4806 - 4813, 2019.

[83] B. H. Menze, B. M. Kelm, R. Masuch, U. Himmelreich, P. Bachert, W. Petrich and F. A. Hamprecht, “A comparison of random forest and its Gini importance with standard chemometric methods for the feature selection and classification of spectral data,” *BMC Bioinformatics,* vol. 10, 2009.

[84] N. Xu, Z. Gao and J. Ning, “Analysis of the characteristics and causes of coastline variation in the Bohai Rim (1980–2010),” *Environ Earth Sci,* vol. 75, p. 719, 2016.

[85] P. S. Mujabar and N. Chandrasekar , “Shoreline change analysis along the coast between Kanyakumari and Tuticorin of India using remote sensing and GIS,” *Arab J Geosci,* vol. 6, p. 647–664, 2013.

[86] A. Misra and R. Balaji, “A Study on the Shoreline Changes and LAND-use/ Land-cover along the South Gujarat Coastline,” *Procedia Eng,* vol. 116, pp. 381-389, 2015.

[87] M. Mishra, P. Chand, N. Pattnaik, D. B. Kattel, G. K. Panda, M. Mohanti and U. D. Baruah, “Response of long- to short-term changes of the Puri coastline of Odisha (India) to natural and anthropogenic factors: a remote sensing and statistical assessment,” *Environ Earth Sci,* vol. 78, p. 338, 2019.

[88] E. Foti, R. E. Musumeci and M. Stagnitti, “Coastal defence techniques and climate change: a review,” *Rend. Fis. Acc. Lincei,* vol. 31, p. 123–138, 2020.

[89] N. Rangel-Buitrago, A. T. Williams and G. Anfuso, “Hard protection structures as a principal coastal erosion management strategy along the Caribbean coast of Colombia. A chronicle of pitfalls,” *Ocean Coast Manag,* vol. 156, pp. 58-75, 2018.

[90] M. Haasnoot, J. Lawrence and A. K. Magnan, “Pathways to coastal retreat,” *Science,* vol. 372, pp. 1287-1290, 2021.

[91] Z. Zhu and Y. Zhang, “Flood disaster risk assessment based on random forest

algorithm," *Neural Computing and Applications*, 2021.

[92] U. Paudel, T. Oguchi and Y. Hayakawa, "Multi-Resolution Landslide Susceptibility Analysis Using a DEM and Random Forest," *International Journal of Geosciences,* vol. 7, pp. 726-743, 2016.

[93] U. Thampanya, J. E. Vermaat, S. Sinsakul and N. Panapitukkul, "Coastal erosion and mangrove progradation of Southern Thailand," *Estuarine, Coastal and Shelf Science,* vol. 68, pp. 75-85, 2006.

[94] S. Roy, M. Mahapatra and A. Chakraborty, "Mapping and monitoring of mangrove along the Odisha coast based on remote sensing and GIS techniques," *Modeling Earth Systems and Environment,* vol. 5, p. 217–226, 2019.

[95] H. M. Salem and A. A. Meselhy, "A portable rainfall simulator to evaluate the factors affecting soil erosion in the northwestern coastal zone of Egypt," *Natural Hazards,* vol. 105, p. 2937–2955, 2021.

[96] O. T. Magoon, B. L. Edge and K. E. Stone, "The Impact of Anthropogenic Activities on Coastal Erosion," in *27th International Conference on Coastal Engineering (ICCE),* Sydney, Australia, 2000.

[97] C. S. Pedersen, "The UN Sustainable Development Goals (SDGs) are a Great Gift to Business!," *Procedia CIRP,* vol. 69, pp. 21-24, 2018.

[98] F. Doni, A. Gasperini and J. T. Soares, "SDG13 – Climate Action: Combating Climate Change and its Impacts (Concise Guides to the United Nations Sustainable Development Goals)," *Emerald Publishing Limited,* pp. 21-30, 2020.

[99] S. Liu, J. Bai and J. Chen, "Measuring SDG 15 at the County Scale: Localization and Practice of SDGs Indicators Based on Geospatial Information," *ISPRS International Journal of Geo-Information,* vol. 8, p. 515, 2019.

[100] M. Oppenheimer, B. C. Glavovic, J. Hinkel, R. van de Wal, A. K. Magnan, A. Abd-Elgawad, R. Cai, M. Cifuentes-Jara, R. M. DeConto, T. Ghosh, J. Hay, F. Isla, B. Marzeion, B. Meyssignac and Z. Sebesvari, "Sea Level Rise and Implications for Low-Lying Islands, Coasts and Communities," IPCC Special Report on the Ocean and Cryosphere in a Changing Climate, 2019.

[101] A. K. Mohanty and V. V. G. Rao, "Hydrogeochemical, seawater intrusion and oxygen isotope studies on a coastal region in the Puri District of Odisha, India," *Catena,* vol. 172, pp. 558-571, 2019.

[102] K. Pierre-Louis, "How rising groundwater caused by climate change could devastate coastal communities," MIT technology review, 2021.

[103] I. D. Correa and J. L. Gonzalez, "Coastal erosion and village relocation: a Colombian case study," *Ocean & Coastal Management,* vol. 43, pp. 51-64, 2000.

[104] Y. Yan, Q. Dai, Y. Yuan, X. Peng, L. Zhao and J. Yang, "Effects of rainfall intensity on runoff and sediment yields on bare slopes in a karst area, SW China," *Geoderma,* vol. 330, pp. 30-40, 2018.

Appendix 1: Research Contributions

Publication accepted:

1. Mohanty Badal and Sarkar Raju, "**An assessment of historical and future coastal dynamic response along the Odisha coast**" in *Environmental Earth Sciences* (Accepted on 5th June 2022).

From: **Yan Zheng** <em@editorialmanager.com>
Date: Sunday, June 5, 2022
Subject: ENGE: Your manuscript entitled An assessment of historical and future coastal dynamic response along the Odisha coast - [EMID:62a7e5a3ed535c28]
To: Raju Sarkar <rajusarkar@dce.ac.in>

Ref.:
Ms. No. ENGE-D-21-02905R1
An assessment of historical and future coastal dynamic response along the Odisha coast
Environmental Earth Sciences

Dear Prof. Sarkar:

It is my pleasure to accept your manuscript entitled An assessment of historical and future coastal dynamic response along the Odisha coast for publication in Environmental Earth Sciences in its current state.

Publication under review:

1. Mohanty Badal, Sarkar Raju, and Saha Sunil, "**Preparing coastal erosion vulnerability index applying deep learning techniques in Odisha state of India**" in *International journal of disaster risk reduction* (Submitted after major revision on 20th May 2022).

From: **International Journal of Disaster Risk Reduction** <em@editorialmanager.com>
Date: Sun, 17 Apr 2022 at 1:54 PM
Subject: Decision on submission to International Journal of Disaster Risk Reduction
To: Raju Sarkar <rajusarkar@dce.ac.in>

Manuscript Number: IJDRR-D-22-00265

Preparing coastal erosion vulnerability index applying deep learning techniques in Odisha state of India

Dear Dr. Sarkar,

Thank you for submitting your manuscript to International Journal of Disaster Risk Reduction.

I have completed my evaluation of your manuscript. The reviewers recommend reconsideration of your manuscript following major revision. I invite you to resubmit your manuscript after addressing the comments below. Please resubmit your revised manuscript by Jun 16, 2022.

Appendix 2: Map Submitted to IITB-AICTE Mapathon 2022

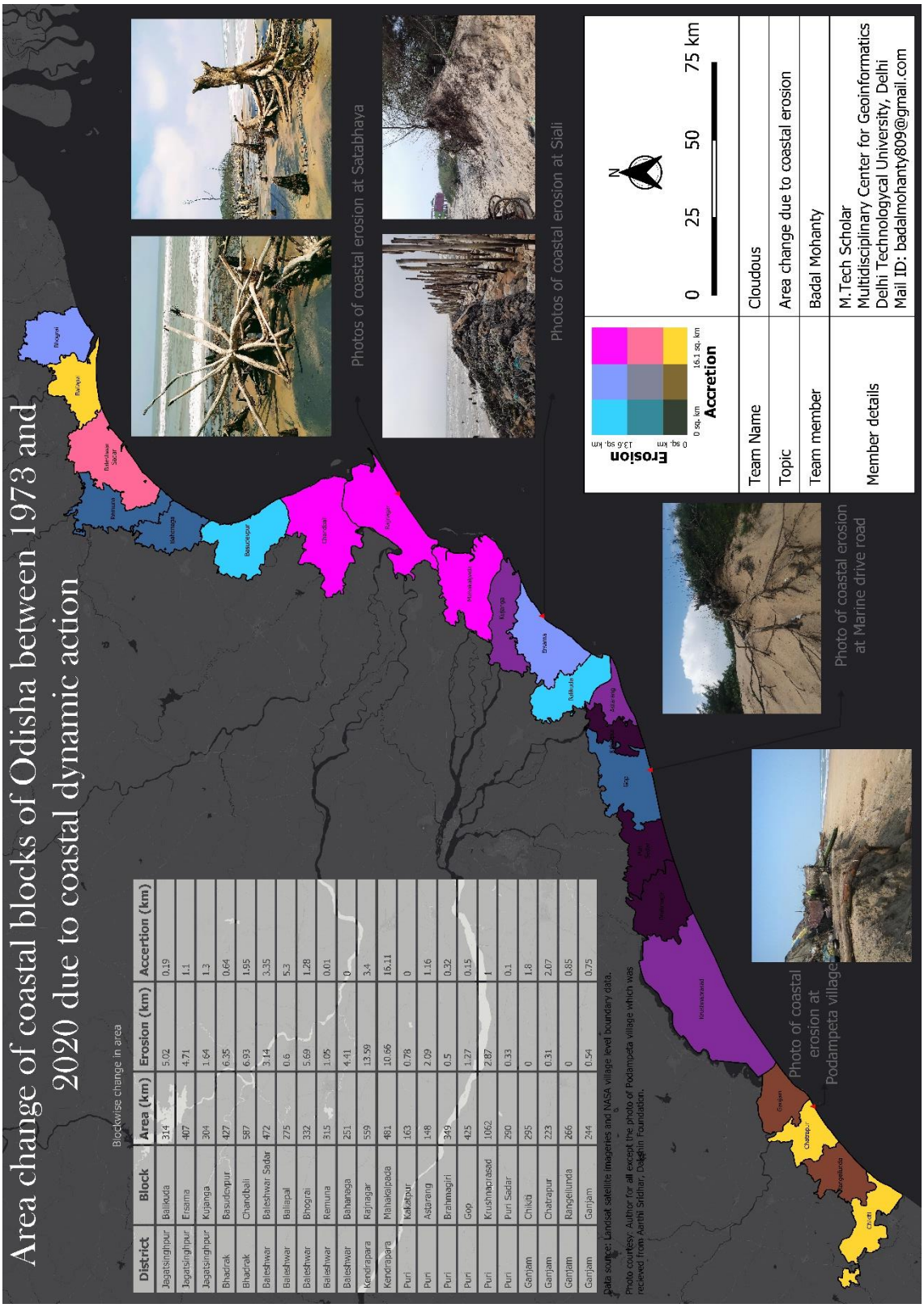

District	Block	Area (km)	Erosion (km)	Accretion (km)
Jagatsinghpur	Balikuda	314	5.02	0.19
Jagatsinghpur	Erasma	407	4.71	1.1
Jagatsinghpur	Kujanga	304	1.64	1.3
Bhadrak	Basudevpur	427	6.35	0.64
Bhadrak	Chandbali	587	6.93	1.95
Baleshwar	Baleshwar Sadar	472	3.14	3.35
Baleshwar	Baliapal	275	0.6	5.3
Baleshwar	Bhograi	332	5.69	1.28
Baleshwar	Remuna	315	1.05	0.01
Baleshwar	Bahanaga	251	4.41	0
Kendrapara	Rajnagar	559	13.59	3.4
Kendrapara	Mahakalpada	481	10.65	16.11
Puri	Kakatpur	163	0.78	0
Puri	Astarang	148	2.09	1.16
Puri	Brahmagiri	349	0.5	0.32
Puri	Gop	425	1.27	0.15
Puri	Krushnaprasad	1062	2.87	1
Puri	Puri Sadar	290	0.33	0.1
Ganjam	Chikiti	295	0	1.8
Ganjam	Chatrapur	223	0.31	2.07
Ganjam	Rangeilunda	266	0	0.85
Ganjam	Ganjam	244	0.54	0.75

Appendix 3: Photographs


Satabhaya, Kendrapara (Source: scroll)


Satabhaya, Kendrapara


Rajnagar, Kendrapara (Source: JD Pati) Siali, Jagatsinghpur


Siali, Jagatsinghpur

Siali, Jagatsinghpur

Siali, Jagatsinghpur

Marine drive, Puri